Linking land use with nitrate loading in receiving waters by integrating field experimentation and process-based modeling

by

Mohammad Amir Azimi

B.Sc., Razi University of Kermanshah, 2016

A Thesis Submitted in Partial Fulfillment
of the Requirements for the Degree of

Master of Science in Environmental Management

in the Graduate Academic Unit of Forestry and Environmental Management

Supervisor(s): Fan-Rui Meng, Ph.D., Forestry & Environmental Management
Yefang Jiang, Ph.D., Agriculture & Agri-Food Canada
Kang Liang, Ph.D., Earth System Science Interdisciplinary Center, University of Maryland

Examining Board: Paul Arp, Ph.D., Forestry & Environmental Management
Alexa Alexander Trusiak, Ph.D., Biology

This thesis is accepted by the Dean of Graduate Studies

THE UNIVERSITY OF NEW BRUNSWICK

August 2023

Abstract

Intensive agriculture in Atlantic Canada threatens aquatic ecosystems. To balance productivity with environmental conservation, farmers use best management practices (BMPs). Reliable data on BMP effects at field and watershed scales are crucial for decision-making. This study examined the impact of crop rotation and land use on nitrate loading. Objectives were: i.) studying field-scale nitrogen dynamics and potato yield under conventional (PBC) and alternative (PSB) rotations in PEI; ii.) refining baseflow estimation in PEI; iii.) assessing land use effects on nitrate loading via the Soil and Water Assessment Tool (SWAT); iv.) evaluating PSB rotation's effectiveness at a watershed scale. Results: i.) PSB rotation increased yields and reduced soil nitrate; ii.) incorporating groundwater level data improved baseflow estimation; iii.) potato rotation land contributed to 88% of nitrate loading in the Dunk River Watershed iv.) PSB rotation reduced nitrate load by 18.4%, showing red clover's significance. These findings aid Atlantic Canada's watershed management.

Acknowledgments

I am incredibly grateful to my supervisor, Dr. Fan-Rui Meng, and co-supervisor, Dr. Yefang Jiang, for consistently considering my best interests. I express my heartfelt appreciation for their invaluable assistance, encouragement, and mentorship, as this thesis would not have reached completion without them. I would like to thank my co-supervisor Dr. Kang Liang for his engagement and invaluable feedback on my research. I would like to thank Danielle Murnaghan and Ana Kostic for their field and lab support. This research was mainly funded by the Agriculture and Agri-Food (AAFC) Atlantic Living Laboratories collaborative projects "Using Living Laboratory approach to develop and transfer innovative soil and water quality BMPS in Prince Edward Island" (2019–2023) (J–002269) co-led by Drs. Yefang Jiang and Judith Nyiraneza, and "Collaborative program – Demonstrating BMPs to enhance soil health and water quality and crop productivity in PEI" (2019–2023) led by Andrea McKenna with the East Prince Agri-environmental Association. This research was also partly funded by the AAFC project "Reducing sediment, N and P loading from arable cropping systems to receiving waters in eastern Canada (PEI, NB, NS, QC) (J–001270).

Last but most certainly not least, I would like to express my endless love and appreciation to my mother, father, and brother for their unconditional love and support in every aspect of my life.

Table of Contents

List of Tables

List of Figures

List of Abbreviations

NPS	Non-Point Source Pollution
BMP	Best Management Practice
SWAT	Soil and Water Assessment Tool
TN	Total Nitrogen
PEI	Prince Edward Island
PSB	Potato-Soybean-Barley
PBC	Potato-Barley-Red Clover
GS	Growing Season
NGS	Non-Growing Season
ANOVA	Analysis of Variance
N_{min}	Soil Mineral Nitrogen Content
LSD	Least Significant Difference
BNF	Biological Nitrogen Fixation
DRW	Dunk River Watershed
HRU	Hydrologic Response Unit
WRW	Wilmot River Watershed
NSE	Nash-Sutcliffe Efficiency
PBIAS	Percent Bias
R^2	Coefficient of Determination
DEM	Digital Elevation Model
GW	Ground Water
SOL_AWC	Soil Available Water Content

SOL_BD	Soil Bulk Density
SOL_K	Saturated Hydraulic Conductivity
SUFI2	Sequential Uncertainty Fitting program

Chapter 1: Introduction

1.1 Water quality and non-point source pollution

Anthropogenic water pollution is the contamination of water bodies, including streams, groundwater, lakes, wetlands etc., occurring when human-sourced pollutants are released into the natural environment. Based on origin, water pollution can be classified as point or non-point source pollution, both presenting threats to aquatic ecosystems, especially for non-point source pollution with potentially complicated origins and consequently complicated monitoring and management strategies (FitzHugh and Mackay 2000; Leon et al. 2001). Non-point source water pollution results from the interaction of non-point source effluents with land cover (e.g., cropland, forest, prairie, urban), soil, land management practices (Giri et al. 2016; Giri and Qiu 2016; Jabbar and Grote 2019; Ouyang et al. 2019) with agricultural activities recognized as the dominant cause of non-point source pollution (Baker 1992; Xiang et al. 2017; Zhang et al. 2010). Increased nitrogen (N) loading to aquatic ecosystems is a significant cause of water quality impairment contributing to potential eutrophication globally (Hua et al. 2018; Vörösmarty et al. 2010). Nitrate is the predominant chemical contaminant found in groundwater aquifers worldwide (Ward et al. 2005), posing health risks when contaminating drinking water resources.

1.2 Excessive N loading in PEI

The southern Gulf of St. Lawrence is no exception to the environmental issues of excessive nitrogen loading. The estuaries of Prince Edward Island, with several dozens of anoxic events recorded from 2016 to 2021 (Government of Prince Edward Island 2022), have been more affected than New Brunswick or Nova Scotia estuaries.

Nitrate (NO_3^--N) is the predominant form of compound nitrogen in marine aquatic ecosystems owing to its highly stable and soluble properties (Goolsby and Battaglin 2001; Pellerin et al. 2014). Several studies demonstrated that nitrogen loads are considered equal to nitrate loads in PEI (Bugden et al. 2014; Jiang and Somers 2009; Savard et al. 2007), where nitrate constitutes more than 90% of total nitrogen in freshwaters (Danielescu and MacQuarrie 2011). Long-term monitoring of freshwater quality in PEI has shown significantly increasing nitrate concentration trends over the last several decades (Environment-Canada 2011). The elevation in the growing trend of nitrate was simultaneous to the significant agricultural land-use changes in PEI during the early to mid-1990s (Bugden et al. 2014) when potato farmlands increased from 11,982 ha in 1951 to 43,770 ha in 1996 (Grizard et al. 2020).

1.3 The role of agricultural activities and potato production

Agricultural non-point source pollution is the most significant source of nitrogen loading from watersheds to aquatic ecosystems (Green et al. 2004; Romanelli et al. 2020; Wade et al. 2005). PEI covers an area of 5,750 km^2, with agricultural land covering 40% and 20% of the island under potato production rotations (Grizard et al. 2020; Jiang and Somers 2009). Potatoes are mainly cultivated in the center and west of the island. Numerous studies have linked intensive potato production to the elevated nitrate concentrations in groundwater and surface water in PEI (Benson et al. 2006; Savard et al. 2007; Zebarth et al. 2015). Jiang et al. (2015) demonstrated that 75-98% of the nitrate in estuaries with elevated nitrate loads was sourced from potato rotation lands.

1.4 Nitrate loss pathways in PEI

Nitrate is mainly delivered to estuaries through groundwater discharge and surface runoff. However, the nitrate lost from agricultural lands via surface runoff is generally insignificant (Jackson et al. 1973; Logan et al. 1994; Ramos 1996). The reason is that with the assumptions of non-saturated soil conditions and good soil structure, the natural drainage will carry a predominant proportion of the nitrate to a depth where it will not be vulnerable to surface runoff (Baker 2001). In addition, as a common practice in PEI, the N fertilizer is banded with soil at planting. Furthermore, observations from multiple studies in PEI confirmed low nitrate concentrations in surface runoff (Dunn et al. 2011; Jiang et al. 2015).

On the other hand, agricultural farmlands are inherently leaky, and the loss of N from the systems through leaching is inevitable. Moreover, cropping systems in humid regions have been shown to have a high potential for nitrate leaching below the soil profile (Baker 2001; Jemison Jr and Fox 1994). In PEI, potato production with high N fertilization demands and low fertilizer recovery rate (40-60%) has been conducted on well-drained sandy soils (Jiang et al. 2015; Liang et al. 2019). The biophysical configuration of potato cultivation in PEI, accompanied by its humid maritime climate, creates a high risk for nitrate leaching.

1.5 Baseflow nitrate and summer eutrophication

A fractured, highly porous sandstone medium underlies most of the island (80-85%) with a relatively high hydraulic conductivity and low storage capacity (Bugden et al. 2014; Lamb et al. 2019; Paradis et al. 2016). The leached nitrate percolates through the vadose zone, reaches the aquifer, and discharges via baseflow into the streams and estuaries. Therefore, baseflow is the primary pathway of nitrate transport to estuaries and coastal

waters in PEI (Bugden et al. 2014; Danielescu and MacQuarrie 2011; Grizard et al. 2020; Jiang et al. 2015). In an analysis of water and nitrate oxygen isotope characteristics in PEI, Savard et a. (2010) suggested that the nitrate in stream water is principally derived from groundwater.

About 60-70% of the annual streamflow and nearly 100% of the summer streamflow consists of baseflow from groundwater in typical PEI streams (Bugden et al. 2014; Francis 1989; Grizard 2013; Jiang et al. 2004). Therefore, baseflow and associated nitrate mass are highly relevant to summer eutrophication and recurring anoxic events in the province (Jiang et al. 2015; Raymond et al. 2002; Schein et al. 2012). Bugden et al. (2014) demonstrated that most of the recorded anoxic events in PEI could be explained by the ratio of summer nitrate load to summer baseflow exceeding a critical threshold.

Several studies of agricultural watersheds in PEI have observed that nitrate concentrations in both stream water and groundwater exhibit low seasonal variability and remain relatively constant throughout the year (Bartlett 2014; Danielescu and MacQuarrie 2013; Jiang and Somers 2009; Somers et al. 2007). Therefore, the seasonal variation in nitrate loading is predominately a result of temporal variation in freshwater discharge, making the nitrate loading phenomena a transport-limited procedure rather than supply-limited (Bugden et al. 2014; Grizard et al. 2020). Jiang et al. (2015) predicted that the growing season (May-October) baseflow delivered 44% of the annual nitrate load in the Wilmot River watershed. Danielescu and MacQuarrie (2011) observed that the highest loads were delivered from November to March. A 3-year study of stream nitrate isotopes in the Wilmot River watershed unveiled that chemical fertilizers and soil organic matter contribute similarly to the growing season and summer load with 45 and 32% average contribution, respectively,

whereas soil organic matter is the dominant source of the non-growing season load, accounting for over 70% of the overall annual nitrogen mass (Savard et al. 2010). Similar observations were reported by Danielescu and MacQuarrie (2013) from McIntyre Creek watershed, a typical agricultural watershed located on the north shore of PEI.

1.6 Nitrate load mitigating strategies

Best management practices (BMPs) are designed to mitigate potential risks of groundwater NO3 contamination and improve soil and water quality without compromising crop production profitability. Since most potato farms in PEI are not irrigated, the BMPs to mitigate nitrate loss primarily rely on managing the quantity nitrate present in the soil. Generally, BMPs can be categorized as mitigating strategies through changes in N management of the potato crop (e.g., Split N application, Soil-based tests) or via modification of potato cropping systems (e.g., cover cropping, varying tillage practices) (Zebarth et al. 2015). Land use manipulation is one of the most effective practices for nitrate load reductions and improving surface and groundwater quality (Jha et al. 2010; Liang et al. 2019).

1.7 The process-based approach in modeling nitrate loading to streams

Due to resource (time and money) constraints, field evaluations of changes in land management strategies (e.g., alternative crop rotations) are less feasible to perform at a watershed scale. Thus, distributed and semi-distributed models are often used alternatively to simulate hydrological processes and the fate and transport of pollutants at watershed scale under different land use, management, and climate change scenarios (Liang 2020; Liang et al. 2020; Noori et al. 2020; Qi et al. 2018). The SWAT is a process-based semi-distributed model offering an alternative approach for simulating watershed processes and

predicting hydrological and water quality indicators (Arnold and Fohrer 2005; Arnold et al. 1998; Gassman et al. 2007). The SWAT model has been used extensively for evaluating the effectiveness BMPs in reducing nitrate and other pollutant loads from watersheds (Akhavan et al. 2010; Haas et al. 2017; Lee et al. 2017; Liang 2020).

1.8 Research objectives

The proposed research follows three key objectives: (1) Evaluate yield responses of four potato cultivars and soil N dynamic to an alternative potato rotation as a nitrate mitigating BMP through field experiment. (2) estimate the impact of land use on nitrate loading dynamics in the Dunk River Watershed using the SWAT model; (3) Assess the effectiveness of the alternative potato rotation in mitigating nitrate loading at watershed scale using the SWAT model. The field experiment is expected to provide reference information on the nitrogen sourced from potato cropping land for the SWAT.

1.9 Thesis overview

Chapter 1 provides an overview of the water quality issues induced by agricultural activities, with a particular focus on Atlantic Canada. This section reviews the various management tools implemented to mitigate these impacts, investigates the evaluation methods used to assess their effectiveness, and defines research objectives. Chapter 2 examines field observations to identify an alternative potato rotation's economic and environmental effects. Chapter 3 identifies a reliable methodology for estimating baseflow as the principal means of nitrate transportation from field to watershed outlet. Chapter 4 integrates field experiment results and watershed-specific variables, including results from Chapters 2 and 3, to model nitrate loading dynamics and land-use impact using SWAT. A watershed scale assessment of the proposed alternative rotation is carried out in this

chapter. Chapter 5. summarizes key conclusions and provides recommendations for future research. Figure 1.1 depicts the research subjects.

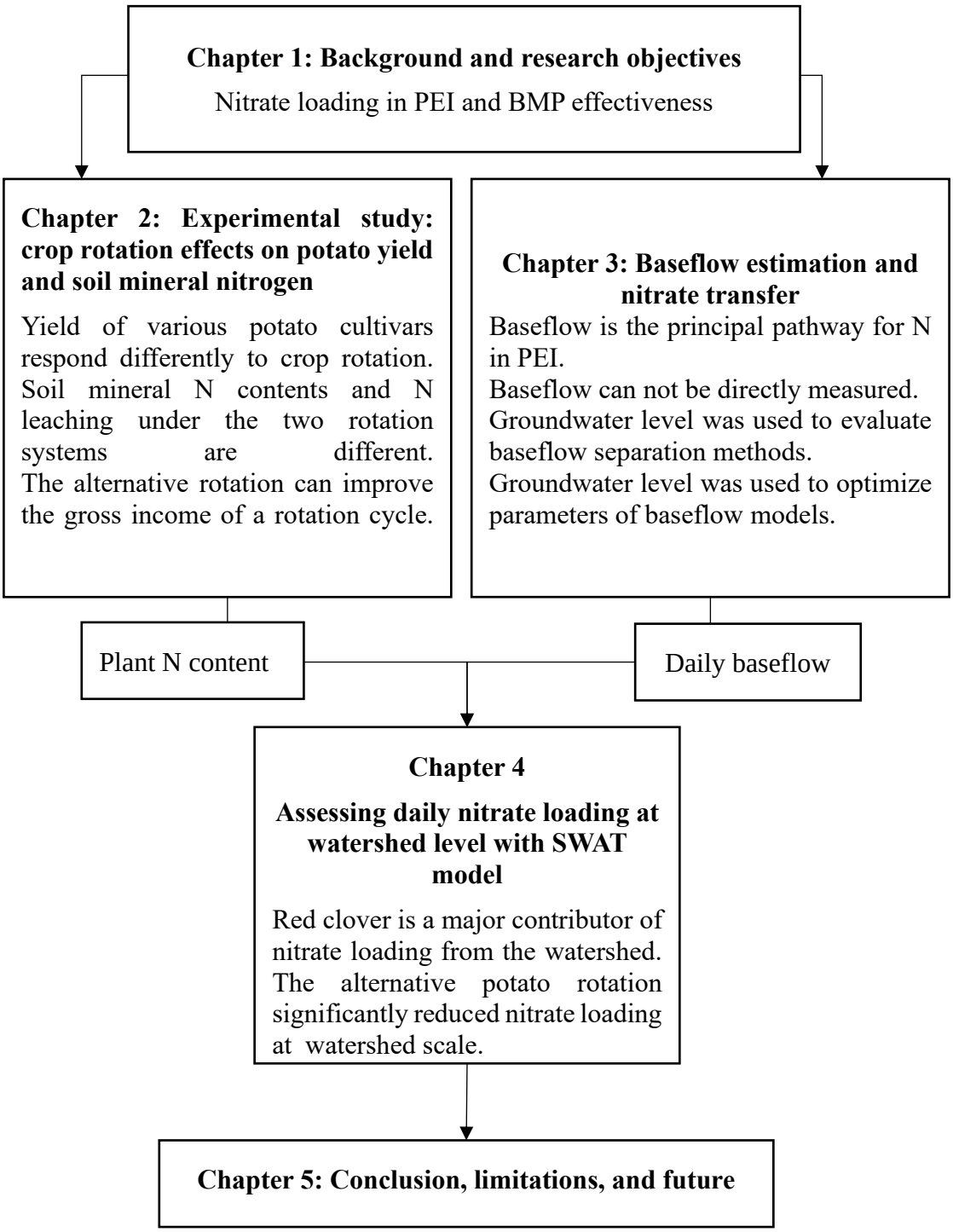

Figure 1.1 Flowchart of the study.

Bibliography

Afan, H.A., A. El-shafie, W.H.M.W. Mohtar, and Z.M. Yaseen. 2016. Past, present and prospect of an Artificial Intelligence (AI) based model for sediment transport prediction, *Journal of Hydrology*, 541: 902-13.

Ahmed, A.N., F.B. Othman, H.A. Afan, R.K. Ibrahim, C.M. Fai, M.S. Hossain, M. Ehteram, and A. Elshafie. 2019. Machine learning methods for better water quality prediction, *Journal of Hydrology*, 578: 124084.

Akhavan, S., J. Abedi-Koupai, S.-F. Mousavi, M. Afyuni, S.-S. Eslamian, and K.C. Abbaspour. 2010. Application of SWAT model to investigate nitrate leaching in Hamadan–Bahar Watershed, Iran, *Agriculture, ecosystems & environment*, 139: 675-88.

Arnold, J.G., and N. Fohrer. 2005. SWAT2000: current capabilities and research opportunities in applied watershed modelling, *Hydrological Processes: An International Journal*, 19: 563-72.

Arnold, J.G., R. Srinivasan, R.S. Muttiah, and J.R. Williams. 1998. Large area hydrologic modeling and assessment part I: model development 1, *JAWRA Journal of the American Water Resources Association*, 34: 73-89.

Baker, J.L. 2001. Limitations of improved nitrogen management to reduce nitrate leaching and increase use efficiency, *TheScientificWorldJOURNAL*, 1: 10-16.

Baker, L.A. 1992. Introduction to nonpoint source pollution in the United States and prospects for wetland use, *Ecological Engineering*, 1: 1-26.

Bartlett, G.L. 2014. Quantifying the temporal variability of discharge and nitrate loadings for intertidal springs in two Prince Edward Island estuaries. (MScE Thesis, Department of Civil Engineering, University of New Brunswick …).

Benson, V.S., J.A. VanLeeuwen, J. Sanchez, I.R. Dohoo, and G.H. Somers. 2006. Spatial analysis of land use impact on ground water nitrate concentrations, *Journal of environmental quality*, 35: 421-32.

Bugden, G., Y. Jiang, M. van den Heuvel, H. Vandermeulen, K. MacQuarrie, C. Crane, and B. Raymond. 2014. Nitrogen loading criteria for estuaries in Prince Edward Island. (Fisheries and Oceans Canada= Pêches et océans Canada).

Danielescu, S., and K.T. MacQuarrie. 2011. Nitrogen loadings to two small estuaries, Prince Edward Island, Canada: a 2-year investigation of precipitation, surface water and groundwater contributions, *Hydrological Processes*, 25: 945-57.

Danielescu, S., and K.T. MacQuarrie. 2013. Nitrogen and oxygen isotopes in nitrate in the groundwater and surface water discharge from two rural catchments: implications for nitrogen loading to coastal waters, *Biogeochemistry*, 115: 111-27.

Dunn, A., G. Julien, W. Ernst, A. Cook, K. Doe, and P. Jackman. 2011. Evaluation of buffer zone effectiveness in mitigating the risks associated with agricultural runoff in Prince Edward Island, *Science of the Total Environment*, 409: 868-82.

Environment-Canada. 2011. Water quality status and trends of nutrients in major drainage areas in Canada. Technical Summary.

FitzHugh, T.W., and D. Mackay. 2000. Impacts of input parameter spatial aggregation on an agricultural nonpoint source pollution model, *Journal of Hydrology*, 236: 35-53.

Francis, R.M. 1989. Hydrogeology of the Winter River Basin-Prince Edward Island. (Water Resources Branch, Department of the Island, Prince Edward Island).

Gassman, P.W., M.R. Reyes, C.H. Green, and J.G. Arnold. 2007. The soil and water assessment tool: historical development, applications, and future research directions, *Transactions of the ASABE*, 50: 1211-50.

Giri, S., A.P. Nejadhashemi, and S.A. Woznicki. 2016. Regulators' and stakeholders' perspectives in a framework for bioenergy development, *Land Use Policy*, 59: 143-53.

Giri, S., and Z. Qiu. 2016. Understanding the relationship of land uses and water quality in twenty first century: a review, *Journal of environmental management*, 173: 41-48.

Goolsby, D.A., and W.A. Battaglin. 2001. Long-term changes in concentrations and flux of nitrogen in the Mississippi River Basin, USA, *Hydrological Processes*, 15: 1209-26.

Green, P.A., C.J. Vörösmarty, M. Meybeck, J.N. Galloway, B.J. Peterson, and E.W. Boyer. 2004. Pre-industrial and contemporary fluxes of nitrogen through rivers: a global assessment based on typology, *Biogeochemistry*, 68: 71-105.

Grizard, P. 2013. 'Modeling nitrate loading from watersheds to coastal waters of the Northumberland Strait', University of New Brunswick.

Grizard, P., K.T. MacQuarrie, and Y. Jiang. 2020. Land-use based modeling approach for determining freshwater nitrate loadings from small agricultural watersheds, *Water Quality Research Journal*, 55: 278-94.

Haas, M.B., B. Guse, and N. Fohrer. 2017. Assessing the impacts of Best Management Practices on nitrate pollution in an agricultural dominated lowland catchment

considering environmental protection versus economic development, *Journal of environmental management*, 196: 347-64.

Hua, B., J. Yang, F. Liu, G. Zhu, B. Deng, and J. Mao. 2018. Characterization of dissolved organic matter/nitrogen by fluorescence excitation-emission matrix spectroscopy and X-ray photoelectron spectroscopy for watershed management, *Chemosphere*, 201: 708-15.

Jabbar, F.K., and K. Grote. 2019. Statistical assessment of nonpoint source pollution in agricultural watersheds in the Lower Grand River watershed, MO, USA, *Environmental Science and Pollution Research*, 26: 1487-506.

Jackson, W., L. Asmussen, E. Hauser, and A. White. 1973. Nitrate in surface and subsurface flow from a small agricultural watershed. In.: Wiley Online Library.

Jemison Jr, J.M., and R.H. Fox. 1994. Nitrate leaching from nitrogen-fertilized and manured corn measured with zero-tension pan lysimeters. In.: Wiley Online Library.

Jha, M.K., K. Schilling, P.W. Gassman, and C. Wolter. 2010. Targeting land-use change for nitrate-nitrogen load reductions in an agricultural watershed, *Journal of soil and water conservation*, 65: 342-52.

Jiang, Y., P. Nishimura, M.R. van den Heuvel, K.T. MacQuarrie, C.S. Crane, Z. Xing, B.G. Raymond, and B.L. Thompson. 2015. Modeling land-based nitrogen loads from groundwater-dominated agricultural watersheds to estuaries to inform nutrient reduction planning, *Journal of Hydrology*, 529: 213-30.

Jiang, Y., and G. Somers. 2009. Modeling effects of nitrate from non-point sources on groundwater quality in an agricultural watershed in Prince Edward Island, Canada, *Hydrogeology Journal*, 17: 707-24.

Jiang, Y., G. Somers, and J. Mutch. 2004. Application of numerical modeling to groundwater assessment and management in Prince Edward Island.

Lamb, K.J., K.T. MacQuarrie, K.E. Butler, S. Danielescu, E. Mott, M. Grimmet, and B.J. Zebarth. 2019. Hydrogeophysical monitoring reveals primarily vertical movement of an applied tracer across a shallow, sloping low-permeability till interface: Implications for agricultural nitrate transport, *Journal of Hydrology*, 573: 616-30.

Lee, S., A.M. Sadeghi, I.-Y. Yeo, G.W. McCarty, and W.D. Hively. 2017. Assessing the impacts of future climate conditions on the effectiveness of winter cover crops in reducing nitrate loads into the Chesapeake Bay watersheds using the SWAT model, *Transactions of the ASABE*, 60: 1939-55.

Leon, L., E. Soulis, N. Kouwen, and G. Farquhar. 2001. Nonpoint source pollution: a distributed water quality modeling approach, *Water Research*, 35: 997-1007.

Liang, K. 2020. 'Enhancing understanding of BMP effectiveness and land use change impacts on water quality, water quantity, and potato production in Atlantic Canada', University of New Brunswick.

Liang, K., Y. Jiang, J. Nyiraneza, K. Fuller, D. Murnaghan, and F.-R. Meng. 2019. Nitrogen dynamics and leaching potential under conventional and alternative potato rotations in Atlantic Canada, *Field Crops Research*, 242: 107603.

Liang, K., Y. Jiang, J. Qi, K. Fuller, J. Nyiraneza, and F.-R. Meng. 2020. Characterizing the impacts of land use on nitrate load and water yield in an agricultural watershed in Atlantic Canada, *Science of the Total Environment*, 729: 138793.

Logan, T., D. Eckert, and D. Beak. 1994. Tillage, crop and climatic effects of runoff and tile drainage losses of nitrate and four herbicides, *Soil and Tillage Research*, 30: 75-103.

Noori, N., L. Kalin, and S. Isik. 2020. Water quality prediction using SWAT-ANN coupled approach, *Journal of Hydrology*, 590: 125220.

Ouyang, W., X. Hao, L. Wang, Y. Xu, M. Tysklind, X. Gao, and C. Lin. 2019. Watershed diffuse pollution dynamics and response to land development assessment with riverine sediments, *Science of the Total Environment*, 659: 283-92.

Paradis, D., H. Vigneault, R. Lefebvre, M.M. Savard, J.-M. Ballard, and B. Qian. 2016. Groundwater nitrate concentration evolution under climate change and agricultural adaptation scenarios: Prince Edward Island, Canada, *Earth System Dynamics*, 7: 183-202.

Pellerin, B.A., B.A. Bergamaschi, R.J. Gilliom, C.G. Crawford, J. Saraceno, C.P. Frederick, B.D. Downing, and J.C. Murphy. 2014. Mississippi River nitrate loads from high frequency sensor measurements and regression-based load estimation, *Environmental Science & Technology*, 48: 12612-19.

Qi, J., S. Li, C.P.-A. Bourque, Z. Xing, and F.-R. Meng. 2018. Developing a decision support tool for assessing land use change and BMPs in ungauged watersheds based on decision rules provided by SWAT simulation, *Hydrology and Earth System Sciences*, 22: 3789-806.

Ramos, C. 1996. 'Effect of agricultural practices on the nitrogen losses to the environment.' in, *Fertilizers and environment* (Springer).

Raymond, B.G., C.S. Crane, and D.K. Cairns. 2002. Nutrient and chlorophyll trends in Prince Edward Island estuaries, *Can. Tech. Rep. Fish. Aquat. Sci./Rapp. Tech. Can. Sci. Halieut. Aquat.*: 142-53.

Romanelli, A., D.X. Soto, I. Matiatos, D.E. Martínez, and S. Esquius. 2020. A biological and nitrate isotopic assessment framework to understand eutrophication in aquatic ecosystems, *Science of the Total Environment*, 715: 136909.

Savard, M.M., D. Paradis, G. Somers, S. Liao, and E. van Bochove. 2007. Winter nitrification contributes to excess NO3− in groundwater of an agricultural region: A dual-isotope study, *Water Resources Research*, 43.

Savard, M.M., G. Somers, A. Smirnoff, D. Paradis, E. van Bochove, and S. Liao. 2010. Nitrate isotopes unveil distinct seasonal N-sources and the critical role of crop residues in groundwater contamination, *Journal of Hydrology*, 381: 134-41.

Schein, A., S.C. Courtenay, C.S. Crane, K.L. Teather, and M.R. van den Heuvel. 2012. The role of submerged aquatic vegetation in structuring the nearshore fish community within an estuary of the southern Gulf of St. Lawrence, *Estuaries and Coasts*, 35: 799-810.

Somers, G., M.M. Savard, and D. Paradis. 2007. Mass balance calculations to estimate nitrate proportions from various sources in the agricultural Wilmot watershed of Prince Edward Island. In *The 60th Canadian Geotechnical Conference and 8th Joint GCS/IAH-CNC Groundwater Conference, Ottawa*, 112-18.

Valiela, I., J.L. Bowen, and K.D. Kroeger. 2002. Assessment of models for estimation of land-derived nitrogen loads to shallow estuaries, *Applied Geochemistry*, 17: 935-53.

Vörösmarty, C.J., P.B. McIntyre, M.O. Gessner, D. Dudgeon, A. Prusevich, P. Green, S. Glidden, S.E. Bunn, C.A. Sullivan, and C.R. Liermann. 2010. Global threats to human water security and river biodiversity, *Nature*, 467: 555-61.

Wade, A., C. Neal, P. Whitehead, and N. Flynn. 2005. Modelling nitrogen fluxes from the land to the coastal zone in European systems: a perspective from the INCA project, *Journal of Hydrology*, 304: 413-29.

Weiskel, P.K., and B.L. Howes. 1991. Quantifying dissolved nitrogen flux through a coastal watershed, *Water Resources Research*, 27: 2929-39.

Xiang, C., Y. Wang, and H. Liu. 2017. A scientometrics review on nonpoint source pollution research, *Ecological Engineering*, 99: 400-08.

Zebarth, B.J., S. Danielescu, J. Nyiraneza, M.C. Ryan, Y. Jiang, M. Grimmett, and D.L. Burton. 2015. Controls on nitrate loading and implications for BMPs under intensive potato production systems in Prince Edward Island, Canada, *Groundwater Monitoring & Remediation*, 35: 30-42.

Zhang, X., X. Liu, M. Zhang, R.A. Dahlgren, and M. Eitzel. 2010. A review of vegetated buffers and a meta-analysis of their mitigation efficacy in reducing nonpoint source pollution, *Journal of environmental quality*, 39: 76-84.

Chapter 2: Yield responses of four common potato cultivars to an industry standard and alternative rotation in Atlantic Canada

Visual Abstract

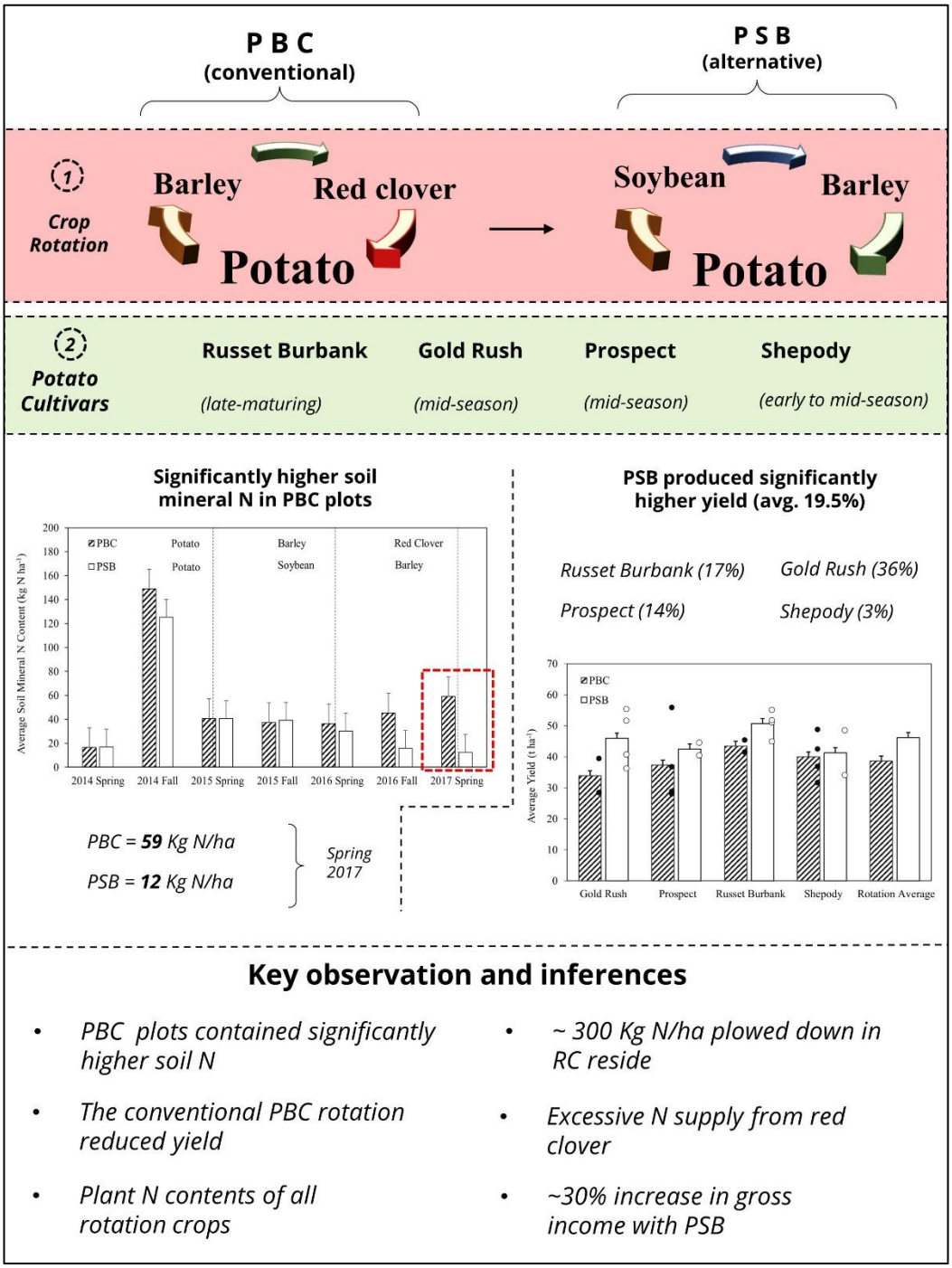

Abstract

This study was conducted to evaluate yield responses of four potato (*Solanum tuberosum* L.) cultivars ('Russet Burbank', 'Shepody', 'Gold Rush', and 'Russet Prospect') and soil N dynamic changes to two 3-year rotations in Prince Edward Island, Canada. The two rotations were the local industry standard potato–barley (*Hordeum vulgare L.*)–red clover (*Trifolium pratense* L.) rotation (PBC) and an alternative potato–soybean (*Glycine max* L.)–barley rotation (PSB). All potato cultivars received 170 kg N ha^{-1} input at planting without irrigation. Soil mineral N content before potato planting was significantly higher under the PBC rotation. However, the PBC rotation produced significantly lower yields, suggesting the possibility of excessive N supply from the plowed-down red clover. While cultivar and the interaction between cultivar and rotation did not show a significant difference in yield, yields of all cultivars were positively affected by the PSB rotation. The Gold Rush cultivar was affected the most (36%), followed by Russet Burbank (17%) and Prospect (14%) cultivars, with Shepody being the least affected (3%) by the alternative PSB rotation. Russet Burbank was the highest yielding cultivar under both rotations. With the three russet cultivars combined as a single russet cultivar, the PSB rotation significantly increased tuber yields, while the Shepody cultivar did not significantly benefit from the PSB rotation, suggesting that the russet cultivars responded more sensitively to the alternative rotation. Results demonstrate that adequately accounting for N supply from a preceding green manure crop is required for sustainable potato production in this humid temperate region.

Azimi, M.A., Jiang, Y., Meng, FR. et al. Yield responses of four common potato cultivars to an industry standard and alternative rotation in Atlantic Canada. Am. J. Potato Res. 99, 206–216 (2022). https://doi.org/10.1007/s12230-022-09873-4

Selected as the outstanding paper of 2022 in extension, production and management by the Editorial Board of the American Journal of Potato Research

2.1 Introduction

Potatoes are the third most important food crop in the world, after rice and wheat, and the predominant vegetable crop in Canada, representing 27% of all vegetable receipts (Agriculture and Agri-Food Canada 2020). Potatoes are the primary cash crop in Prince Edward Island (PEI), where 24% of Canada's potatoes are produced (Statistics Canada 2021). An average area of 34,500 ha is under potato cultivation in PEI each year, responsible for an annual average potato production of 36.2 t ha^{-1} (Statistics Canada 2021). In PEI, a province with a relatively short growing season (Jiang et al. 2012; Nyiraneza et al. 2021), Russet Burbank, Eva, HO2000, Gold Rush, Prospect, and Shepody are the top seven registered seed potato cultivars (Agriculture and Agri-Food Canada 2020).

Intensive potato production can result in undesirable environmental and economic consequences. Some of these negative consequences, especially in Atlantic Canada, include increased soil erosion (Edwards et al. 1998; Tiessen et al. 2009; Abolgasem 2014) and excessive nitrogen leaching into receiving waters (Jégo et al. 2008; Jiang et al. 2012). Liang et al. (2020) reported that 84.5% of the nitrate load in an agricultural watershed in PEI was sourced from lands under potato cultivation. Based on data from 27 watersheds in PEI, Jiang et al. (2015) estimated that potato field contributed 75–98% of the nitrate load in estuaries. In addition, high frequency and intensive potato cropping can reduce potato yield and quality due to increased soil-borne pathogenic organisms (Vos and Van Loon 1989), increased weed risk (Pawlonka et al. 2015), and incidences of harmful fungi (Grandy et al. 2002).

Crop rotation has been demonstrated to be an efficient Best Management Practice (BMP) for reducing the environmental impacts of intensive potato production while maintaining

soil quality and improving productivity. Wei et al. (2014) reported that coupling crop rotations with land closure treatments significantly reduced soil erosion on gentle slopes. Similarly, Freebairn et al. (1993) observed a potential yield increase and reduction in soil erosion after reducing tillage in combination with crop rotation. Moreover, crop rotation has been reported to influence soil quality and productivity, possibly by regulating soil microbial communities and reducing soil-borne diseases (Larkin and Honeycutt 2006; Qin et al. 2017; Gao et al. 2019). It has also been suggested that increased cropping frequency of potatoes in a crop rotation could increase incidences of diseases such as stem canker and black surf (Scholte 1992). Previous research has indicated that crop rotation directly or indirectly affects potato tuber yield through mediation of soil-borne diseases, microbial communities, fertility, and soil quality.

The effect of crop rotation on potato yield depends on rotation crop selection (Scholte 1990). In a study of 3-year rotations, soybean–canola–potato and soybean–barley/clover–potato rotations led to a 9–12% increase in total yield compared to continuous potato (Larkin and Honeycutt 2006). Nyiraneza et al. (2015) assessed the yield of potato rotated with barley–red clover (PBR), barley–sorghum Sudan grass/winter rape (PBSW), and barley–canola/winter rape (PBCW) in PEI from 2006 to 2013. They reported that PBSW and PBCW had higher yields than PBR due to noticeable residual effects of rotation.

The influence of rotation and cover crops on potato yield depends on potato cultivars as well as cover crop cultivars. Sturz et al. (2003) studied the influence of potato and red clover cultivar combinations in a potato–barley–red clover rotation in PEI. The study found that the yield of Shepody potato following AC Kingston red clover significantly increased compared to other red clover cultivars, while Russet Burbank and Kennebec yields were

not differently influenced by any preceding red clover cultivar. Sturz and Christie (1998) reported that root zone bacteria associated with red clover cultivar Marino led to the best performance of potato cultivar Russet Burbank while Shepody benefited from bacteria from 'Altaswede' root zones. These results indicate that there are potential interactions between cultivar and rotation cycles.

In PEI, potato growers commonly adopt the minimum length of 3-year rotation as mandated by the Province and follow local industry-standard management practices (Bernard et al. 1993). Traditionally, growers mainly planted barley and forages (e.g., red clover or a mix of red clover and one or two perennial grass species) as the rotation crops. In recent years, many potato growers have included soybean as a second cash crop in the rotation to increase farm profit (Government of Prince Edward Island 2019). Liang et al. (2019) compared the effects of an alternative potato–soybean–barley rotation (PSB) and conventional potato–barley–clover rotation on soil mineral N, N concentrations in soil leachate and potato yield in PEI. They demonstrated that replacing red clover with soybean in the rotation improved N utilization efficiency by as much as 1.6 times while increasing potato yield by 13.4% and farm income from soybean as a second cash crop (Liang et al. 2019). The alternative rotation provides a promising opportunity for farmers to increase farm income while reducing their environmental footprint. However, their results were derived from only the Russet Burbank cultivar. Whether the results are applicable to other common potato cultivars remains unknown. The objective of this study was to investigate the impacts of the PSB and PBC rotations on the yield of four common cultivars of potatoes and soil N dynamics.

2.2 Materials and Methods

2.2.1 Study Site

The experiment was conducted at the Harrington Research Farm of Agriculture and Agri-Food Canada from 2014 to 2017. The farm is located 12 km northwest of Charlottetown, PEI, Canada (46°20’31.045” N, 63°10’19.8” W, elevation of 57 m above sea level). The experimental field had a slope of about 1.5%. The soil was classified as Orthic humo-Ferric Podzols and Gleyed Eluviated Drystic Brunisols in the Canadian soil classification system (MacDougall et al. 1988). The sand, silt, and clay contents of the soil were 51%, 38%, and 11% (fine sandy loam) respectively based on tests using the hydrometer method presented by Gee and Bauder (1979). The total soil organic carbon content was 28 g kg^{-1}. The soil in the top 20 cm of the profile was well-drained with a bulk density ranging from 1.33 to 1.39 g cm^{-3}. The average soil pH was estimated to be 6.5 from measurements using 10 g soil/10 mL water. Tests conducted in this field showed low variability of soil organic carbon, soil fertility, C:N ratio, and bulk density in the top 45 cm ($p < 0.05$), indicating relatively uniform soil conditions (see Supplemental Table 1 for more details).

2.2.2 Weather

The mean annual precipitation was 1174 mm (25% as snow) based on historical data from 1988 to 2017 at the Charlottetown Airport (46°17'21.000" N, 63°07'09.000" W). The frost-free period ranged from 100 to 160 days. The site was characterized by a humid climate and cool to mild temperatures, with the growing season precipitation and mean air temperature being 437 mm and 14°C, respectively. Precipitation during the growing season of the 2017 potato year (May–September) was 515 mm, which was 17% more than the long-term average from 1988–2017 (Figure 2.1). The monthly precipitation during May

and August of 2017 was much higher than the long-term average (46% and 23% respectively). Precipitation in July and September of 2017 was lower than the long-term average (11% and 19%, respectively). Air temperatures during the 2017 growing season were similar to the long-term averages.

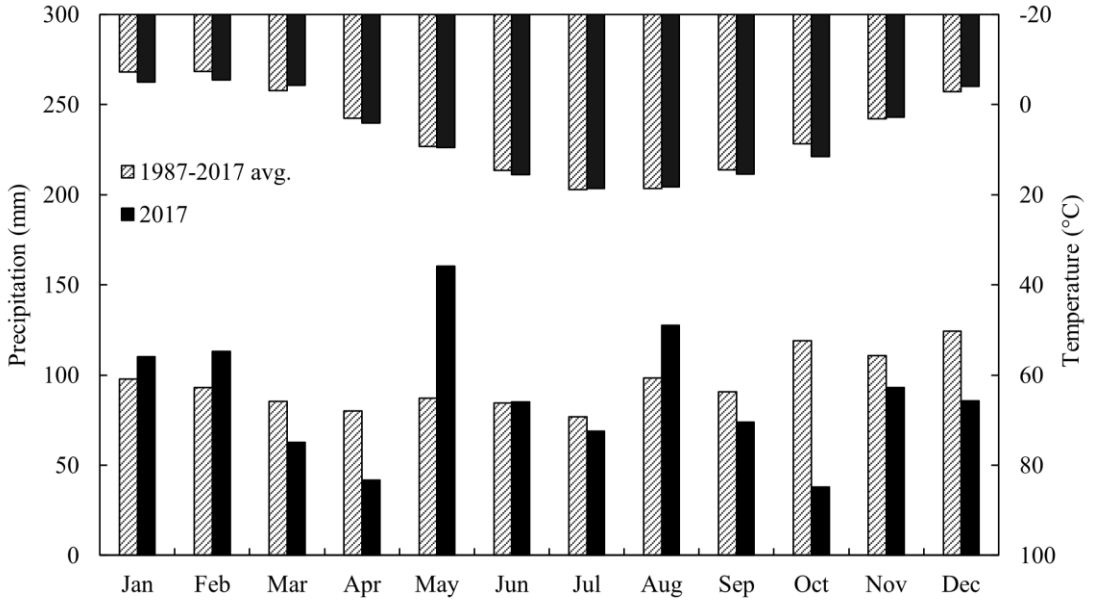

Figure 2.1 Monthly precipitation and temperature at the Environment and Climate Change Canada weather station at Charlottetown Airport.

2.2.3 Field Experiment

Russet Burbank, Shepody, Gold Rush, and Prospect cultivars were chosen for this study. These cultivars are widely grown in North America. Russet Burbank is a late-maturing cultivar with large tubers. Shepody is an early to mid-maturing cultivar with medium tubers mainly grown as an early french fry or baking potato. The Prospect is a mid-season cross-bred (Russette /Shepody) cultivar that produces large tubers and matures earlier than Russet Burbank. Gold Rush is a mid-season russet cultivar with average-sized tubers. Whole seeds with an average weight of 70g were used for Shepody and Gold Rush cultivars. For Prospect and Russet Burbank, whole seeds could not be found and therefore

hand-cut average 70g seed pieces were used. The seeds were obtained from the PEI Potato Board (Charlottetown, PEI). The experimental factors included two rotations and four cultivars. The two rotations were randomly assigned on 12 plots (six replications). Each plot was subdivided into two sub-plots in the final year (2017) to accommodate the four cultivars. Originally, the experiment was designed to include three replicates for each combination of cultivar and rotation levels. However, due to events beyond our control, the experiment was implemented by having two replications of Prospect and Shepody under PSB rotation and four replications under PBC rotation while having four replications of Russet Burbank and Gold Rush under PSB rotation and two replications under PBC rotation. The 12 main plots were distributed across four rows and three columns, with a row spacing of 6 m and a column spacing of 14 m acting as buffer zones. Each sub-plot accommodated six longitudinal rows (14 m long) of potatoes with row and plant spacing of 91 cm and 38 cm, respectively. Final field plan is presented in Figure 2.2.

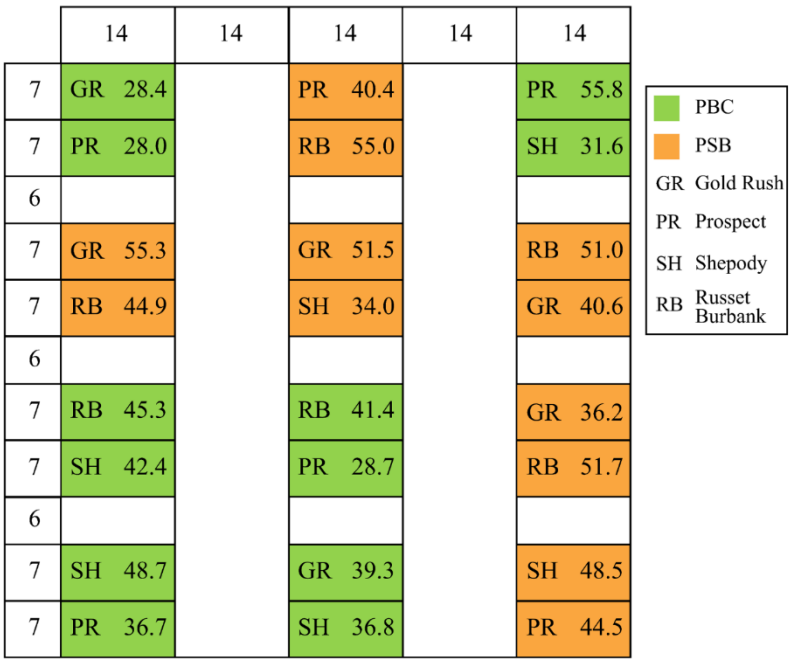

Figure 2.2 Field treatments layout and tuber yield (t ha–1) of each plot. Row and column spacing is in meters.

In the reference year of 2014, all plots were planted with the Russet Burbank cultivar and managed identically in order to create uniform fertility conditions before 2015. The PBC and PSB rotations were initiated in 2015 with barley and soybean, respectively. Red clover was the second crop in PBC and barley for PSB in 2016. The rotations were completed with potato cultivation in 2017. All plots were planted and harvested following standard production practices for potatoes at the commercial scale according to the Atlantic Canada Potato Guide (Bernard et al. 1993). The standard rate of N fertilizer application proposed for potatoes was 155 kg N ha^{-1} in PEI (PEI Analytical Laboratories, Department of Agriculture and Fisheries, PEI). The recommended rate of N fertilizer for different potato cultivars varies from 130 to 185 kg N ha^{-1}. In this study, the N application rate of 170 kg N ha^{-1} was banded to all treatments as Nitrogen–Phosphorus–Potassium (17–17–17)

compound fertilizer at planting time. Crop sequence and other rotation management operations are summarized in Table 2.1.

Table 2.1 Summary of field management practices

Season /year	Cultural practices
Spring 2014	Planted Russet Burbank on May 31; applied 170 kg N ha^{-1} (banded) Nitrogen–Phosphorus–Potassium (17–17–17) compound fertilizer at planting time.
Summer 2014	Followed standard local cultural practices to manage potato diseases; applied Admire[1] in furrow at a rate of 198 mL ha^{-1} to control insects; applied Sencor or Lorox 927 g ha^{-1} before potato emergence to control weeds; applied Manzate (1.98 kg ha^{-1}) or Bravo (2.47 L ha^{-1}) to control blight.
Fall 2014	Vine desiccation was facilitated using Reglone (1.98 L ha^{-1}) in September 15–16; Potatoes were harvested on October 12.
Spring 2015	PBC: Planted barley on May 29; applied 50 kg N ha^{-1} (banded) 17–17–17 compound fertilizer (ammonium nitrate) at planting time. PSB: Planted soybean on May 29 without fertilization.
Fall 2015	PBC: Harvested barley on August 8 and left straw in field. PSB: Harvested soybean with shoots left in the field on November 10.
Spring 2016	PBC: Planted red clover without fertilization on May 23. PSB: Planted barley on May 23; applied 50 kg N ha^{-1} (banded) 17–17–17 compound fertilizer (ammonium nitrate) at planting time.
Summer 2016	Red clover was clipped by flailing on June 15 with residues left in field; red clover regrew and was clipped by flailing on July 28 with residues left in field.
Fall 2016	PBC: Red clover regrew and was clipped by flailing on September 3 with residues left in field; killed red clover using Roundup on September 13; moldboard plowing was done on October 15. PSB: Harvested barley with straw returned to the field on September 17.
Spring 2017	Planted potato on May 31; applied 170 kg N ha^{-1} by banding Nitrogen–Phosphorus–Potassium (17–17–17) compound fertilizer at planting time.
Summer 2017	Followed standard local cultural practices to manage potato diseases; applied Admire in furrow at a rate of 198 mL ha^{-1} to control insects; applied Sencor or Lorox 927 g ha^{-1} before potato emergence to control weeds; applied Manzate (1.98 kg ha^{-1}) or Bravo (2.47 L ha^{-1}) as a means of late blight control.
Fall 2017	Reglone was used as Vine desiccation (i.e., topkill) at rate of 1.98 L ha^{-1} September 15–16; the potato crops were harvested on October 12.

2.2.4 Soil Sampling and Analysis

Soil samples were collected from all experimental plots at 15 cm increments from depths of 0–15, 15–30, and 30–45 cm with a handheld Dutch auger (5 cm diameter). Soil samples were collected in three random locations before planting in the spring and immediately following harvest in the fall. The collected soil samples were mixed to create a pooled soil sample for each plot and soil depth. Soil samples were stored at < 4°C prior to analysis (usually within two weeks after collection). Potassium chloride (KCl) extraction was carried out for each sample using 2 mol L^{-1} KCl. Concentrations of NO_3-N and NH_4-N in the extracts were determined using flow injection analysis on a Lachat QuikChem 8500 system (Lachat Instruments, USA). The concentrations of N in the extract were converted to kg N ha^{-1} based on a pre-determined bulk density, dry matter factor, as well as the specific depth of each layer.

2.2.5 Plant Sampling and Analysis

Four side-by-side specimens of potato plants in one row were obtained from each sub-plot before top kill application in mid-September. Potato tubers were cleaned, weighed, and converted into total potato yield in t ha^{-1} by multiplying a density factor based on the potato row and plant spacings. Six tubers from these four plants were subsampled, sliced and oven-dried at 60°C for 48 h to measure the dry matter content of tubers. Representative tubers were used to calculate specific gravity by recording the weight in air and weight in water using the following Equation 1 (Gould 1999). Calculation of starch content was carried out according to Equation 2 (Kawano et al. 1987).

$$\text{Specific gravity (g cm}^{-3}) = \frac{Weight\ in\ air}{Weight\ in\ air - Weight\ in\ water} \qquad (1)$$

Starch (%) = $(112.1 \times Specific\ Gravity) - 106.4$ (2)

2.2.6 Statistical Analysis

Normality and homogeneity of the dataset were confirmed using Shapiro-Wilk's and Levene's tests, respectively. All statistical analyses were performed using R 3.2.3. The significance level was set at a probability of < 5%. The differences in tuber yields among cultivars and rotations factors were tested with two-way Analysis of Variance (ANOVA). In addition, a Student's t-test was used to examine if the differences between yield and soil mineral N content under PBC and PSB rotations were statistically significant among the potato cultivars.

2.3 Results

2.3.1 Soil Mineral N Contents Before Planting in 2014

The variation of the historical mineral N content (Nm) of the soil in the top 45 cm before planting is plotted in Figure 2.3. Nm prior to the beginning of the rotation in the spring of 2014 in the PBC (=16.4 kg N ha^{-1}) and PSB (=16.8 kg N ha^{-1}) rotation plots did not have a significant difference ($p > 0.05$). This suggests relatively uniform fertility conditions due to similar field management before the experiment started. In the fall of 2014, after potato harvest, soil mineral N in the upper 45 cm soil layer increased to 149.0 and 125.3 kg N ha^{-1} in the PBC and PSB plots, which were significantly higher than spring N contents ($p < 0.001$). In the spring of 2015, however, soil mineral N in the upper 45 cm soil layer dropped by 72.6% for the PBC rotation and dropped by 62.4% for the PSB rotation. No significant difference in soil mineral N content was found between the PBC and PSB plots ($p > 0.05$).

Despite fertilization, only a slight decrease in Nm (3.3 kg N ha^{-1}) was observed in barley plots in the second year of the rotations in the fall of 2015. Similarly, the Nm in the soybean plots decreased slightly to 39.2 kg N ha^{-1}, and the difference between the two rotations was not significant ($p > 0.05$). Soil mineral N had a substantially lower reduction rate in the non-growing season between 2015 and 2016 compared to the previous non-growing season. The barely plots showed a 2.5% decline in soil Nm in the spring of 2016, and the soil Nm of the soybean plots decreased by 22%.

Soil Nm in PBC plots increased to 45.3 kg N ha^{-1} in the fall of 2016, following red clover, while soil Nm in PSB plots exhibited a further decline to 15.7 kg N ha^{-1} after barley in the fall of 2016. The difference in soil Nm between PBC and PSB rotations in the fall of 2016 was significant ($p < 0.05$).

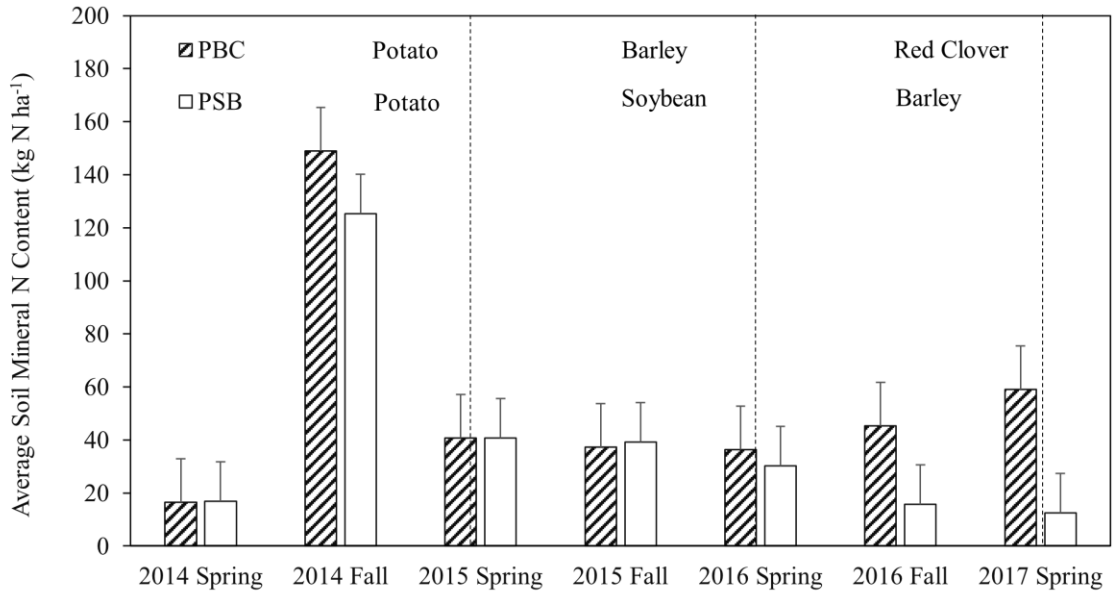

Figure 2.3 The variation of the historical mineral N content (Nm) of the soil in the top 45 cm before the planting. Error bar demonstrates standard error of mean.

2.3.2 Soil Mineral N Content Before Planting in the Spring of 2017

The PBC plots had a significantly higher soil mineral N content ($p < 0.001$; Table 2.2) in the spring of 2017 before planting. As demonstrated in Figure 2.4, the preceding red clover crop in the PBC plots led to significantly higher soil mineral N content after the completion of one rotation cycle from 2015 to 2017. On average, the PBC plots contained 59 kg N ha^{-1} compared to 12.5 kg N ha^{-1} in the PSB plots, representing 79% more soil Nm. Variations in N content of different treatments are shown in Figure 2.4. The standard deviation of soil mineral N content in the PBC plots was 25.2 kg N ha^{-1}, compared to 6.6 kg N ha^{-1} in the PSB plots. This indicates that the PBC plots demonstrated a considerably large spatial variation in soil mineral N content while the soil Nm in the PSB plots was relatively uniform. The PBC plots planted with Gold Rush and Shepody cultivars contained the lowest (37.3 kg N ha^{-1}), and highest (71 kg N ha^{-1}) mean soil Nm, respectively (Table 2.2). In order to assess the difference between cultivars within each rotation system, an analysis of variance was carried out separately for each group of the rotations. Results indicate that soil mineral N content was not significantly different between cultivars within the same rotation system for both PBC and PSB treatments (Table 2.3).

Table 2.2 Average tuber yields and soil mineral N content under different rotations and cultivars along with the results of Student's t-test.

Source of variation			Tuber yield				Pre-plant soil NO3			
Cultivar	Rotation	N	Mean (t ha^{-1})	Std. deviation	% Increase	Significance	Mean (Kg N ha^{-1})	Std. deviation	% Decrease	Significance
Gold Rush	PBC	2	33.9	7.7	35.6	0.18	37.3	15	75.8	0.01**
	PSB	4	45.9	9			9	3.3		
Prospect	PBC	4	37.3	12.9	13.8	0.62	54.3	15.7	71	0.03*
	PSB	2	42.5	2.9			15.7	8.7		
Russet Burbank	PBC	2	43.4	2.8	16.7	0.09	66.1	31.5	83.1	0.01**
	PSB	4	50.7	4.2			11.1	7		
Shepody	PBC	4	39.9	7.4	3.3	0.86	71	33	73.5	0.1
	PSB	2	41.3	10.2			18.8	6.7		
Rotation average	PBC	12	38.6	8.7	19.5	0.03*	59	25.2	78.8	<0.001
	PSB	12	46.2	7.2			12.5	6.5		
Russet cultivars	PBC	8	38	9.7	24.2	0.03*	53.0	20.1	78.9	<0.001
	PSB	10	47.2	6.7			11.2	5.9		

Table 2.3 Separated analysis of variance of pre-plant soil mineral N content for cultivars within each rotation.

		df	Sum sq.	Mean sq.	F-value	P-value
PBC	Cultivar	3	1708	569.3	0.865	0.498
	Residuals	8	5266	658.2		
PSB	Cultivar	3	158	52.8	1.402	0.311
	Residuals	8	301	37.6		

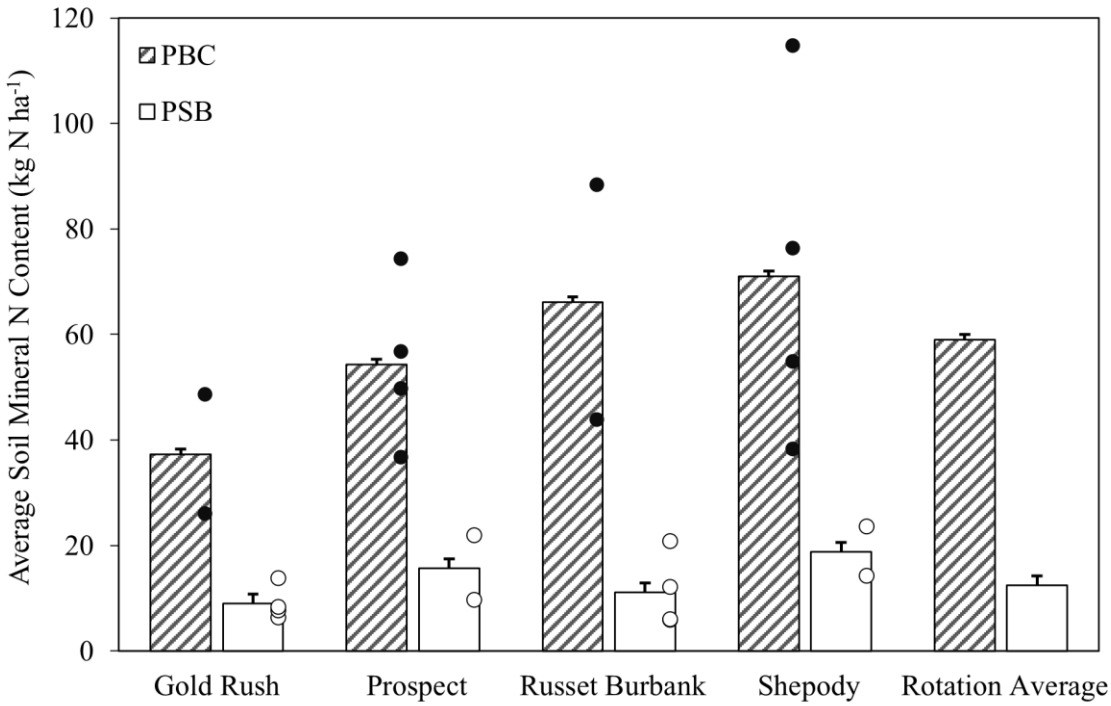

Figure 2.4 The variation of the soil mineral N content in the spring of 2017 before planting. Error bar represents standard error of mean**.**

2.3.3 Total Tuber Yield

Potato yields were significantly different between the PBC and PSB rotations ($p < 0.05$), while cultivar and the interaction between cultivar and rotation did not show significant differences (Table 2.4). Potato yields of different cultivars under the two different rotation systems are shown in Table 2.2. We found that the PSB rotation resulted in higher potato yields for all cultivars (Figure 2.5). On average, potato yields were 46.2 t ha^{-1} in the PSB plots, compared to 38.6 t ha^{-1} in the PBC plots (Table 2.2), representing a 19.5% difference.

Under the PSB rotation, Russet Burbank, Gold Rush, Prospect, and Shepody yielded 50.6, 45.9, 42.4 and, 41.2 t ha^{-1}, respectively. In contrast, 43.4 t ha^{-1} of tuber yield was produced by Russet Burbank, 33.8 t ha^{-1} by Gold Rush, 37.3 t ha^{-1} by Prospect and, 39.9 t ha^{-1} by Shepody under the PBC rotation. In comparison with the PBC rotation, the largest increase

in yield under the PSB rotation was observed for the Gold Rush cultivar (35.5%), followed by Russet Burbank (16.7%), then Prospect (13.7%). The yield of Shepody under the PSB rotation was only 3.3% higher than its yield under the PBC rotation. The differences in yield between cultivars under the two rotations were not statistically significant ($p > 0.05$), likely due to the relatively small sample size (two to four replicates for each treatment). However, increasing the sample size by combining the three russet cultivars (Russet Burbank, Gold Rush, and Prospect) into a single Russet group revealed that the PSB rotation significantly increased the yield ($p < 0.05$) (by 24% on average).

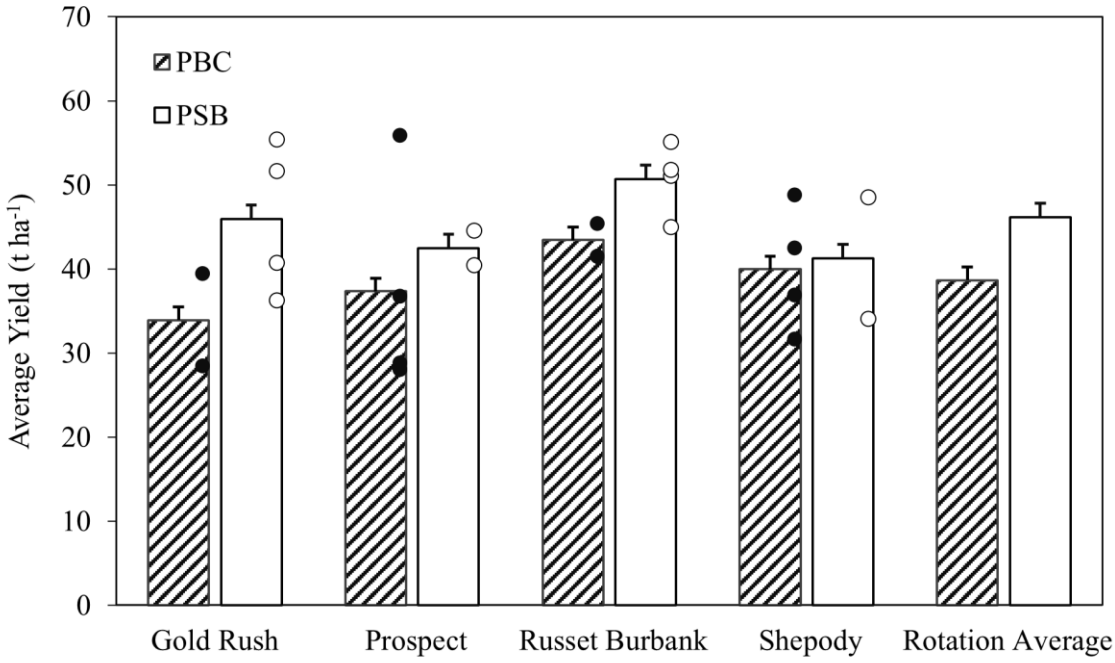

Figure 2.5 Average yield variation of all treatments. The yield of each plot is represented with a dot on the relative bar. Error bar represents standard error of mean.

Table 2.4 Separated analysis of variance of pre-plant soil mineral N content for cultivars within each rotation.

	df	Sum sq.	Mean sq.	F-value	P-value
Rotation	**1**	**339.7**	**339.7**	**4.76**	**0.044***
Cultivar	**3**	**181.7**	**60.6**	**0.848**	**0.487**
Rotation:Cultivar	**3**	**80.3**	**26.8**	**0.375**	**0.772**
Residuals	**16**	**1142**	**71.4**		

Table 2.5 Analysis of variance of tuber yields for cultivars within each rotation.

		df	Sum sq.	Mean sq.	F-value	P-value
PBC	**Cultivar**	**3**	**104.4**	**34.8**	**0.379**	**0.771**
	Residuals	**8**	**733.5**	**91.7**		
PSB	**Cultivar**	**3**	**157.6**	**52.5**	**1.029**	**0.43**
	Residuals	**8**	**408.4**	**51**		

2.3.4 Tuber Specific Gravity, Dry Matter and Starch Content

The PSB rotation resulted in higher specific gravity, starch, and dry matter for all cultivars combined (1.0898, 15.767%, and 10.7 t ha^{-1}, respectively). In comparison, the specific gravity and dry matter for the PBC rotation were 1.0868 and 8.8 t ha^{-1}, respectively. The estimated starch content of PBC plots averaged 15.425%. The PSB rotation increased the starch content and specific gravity in three cultivars only. However, under PSB, the Prospect cultivar demonstrated a decrease in specific gravity from 1.0865 to 1.0857 and in starch from 15.392% to 15.307%, compared with the values under PBC.

The highest specific gravity and starch content were 1.0923 and 16.05, respectively, both achieved by Russet Burbank under the PSB rotation. Gold Rush under the PSB rotation

had the second highest specific gravity (1.0901) and starch content (15.805%). Prospect had a specific gravity of 1.0857 and a starch content of 15.805% under the PSB rotation. The lowest measured specific gravity (1.0846) and estimated starch content (15.192%) in the experiment were produced by Russet Burbank under the PBC rotation. The highest specific gravity and starch content under the PBC rotation were 1.0884 and 15.614%, by the Gold Rush. The Shepody cultivar produced 15.481% and 1.0872 starch content and specific gravity respectively, under the PBC rotation and 15.601% and 1.0883, respectively, under the PSB rotation.

Dry matter content of all cultivars was positively affected by the PSB rotation. A higher tuber dry matter was produced by the PSB rotation with an average of 10.7 t ha^{-1} compared to that of PBC with 8.9 t ha^{-1}. Tuber dry matter of Gold Rush was affected the most, with a 41.7% increase from 7.3 to 10.4 t ha^{-1}, followed by Russet Burbank, which experienced a 16.7% increase in tuber dry matter under PSB compared to PBC. The Prospect was affected the least, with a 9.3% increase in dry matter. Statistically, the rotation factor had a significant increasing effect on specific gravity, starch and dry matter ($p < 0.05$), while cultivar and interaction effect did not lead to a significant difference (Table 2.6).

Table 2.6 Average dry matter, specific gravity, and starch content of tubers under various cultivars and rotations.

Rotation	Cultivar	Dry matter (t ha^{-1})	Specific gravity (g cm^{-3})	Starch (%)
PBC	**Gold Rush**	**7.3**	**1.0884**	**15.614**
	Prospect	**8.6**	**1.0865**	**15.392**
	Russet Burbank	**10.0**	**1.0847**	**15.193**
	Shepody	**9.4**	**1.0872**	**15.481**
	Average	**8.9**	**1.0868**	**15.425**
PSB	**Gold Rush**	**10.4**	**1.0901**	**15.805**
	Prospect	**9.4**	**1.0857**	**15.307**
	Russet Burbank	**11.7**	**1.0923**	**16.050**
	Shepody	**10.8**	**1.0883**	**15.601**
	Average	**10.7**	**1.0898**	**15.770**
Significant effects ($P < 0.05$)		**Rotation**	**Rotation**	**Rotation**

2.4 Discussion

2.4.1 N Contribution to Potato Crops from Red Clover

We found that the PBC plots had significantly higher potato pre-plant soil N content than the PSB plots. Nitrogen from the plowed-down red clover probably contributed to the elevated soil N content in the PBC plots. On average, red clover added almost 37 kg N ha^{-1} mineral N into the soil compared to the barley plots. In addition, in-season mineralization of the red clover can release more N into the soil. However, the additional soil N in the PBC rotation did not translate into higher potato yields compared to those of the PSB rotation (Figure 2.4 and Table 2.2). On the contrary, the PBC rotation consistently produced lower yields for all cultivars. This suppressed yield was likely the result of an

oversupply of N in soil from the red clover residue given the relatively short growing period.

Jiang et al. (2019) reported that higher levels of soil N from mineralization of plowed-down red clover and soil organic matter can lead to over-fertilization and yield suppression of the late-maturing Russet Burbank cultivar when accompanied with the shorter than ideal growing season of PEI. Similarly, in another study conducted in PEI, Nyiraneza et al. (2015) compared cultivating an early to mid-maturing cultivar (Shepody) in the PBC rotation with two alternative rotations in which red clover was substituted with cover crops from the grass and vegetable oil family. They observed that the PBC rotation produced a lower yield and suggested that the extra N supply from red clover didn't necessarily translate to higher yields. A number of studies have indicated that the soil N supply in cool, humid Atlantic conditions is primarily dominated by N mineralization during the growing season (Ojala et al. 1990; Zebarth et al. 2004; Sharifi et al. 2007; Zebarth and Rosen 2007), and is subject to great uncertainty in terms of timing and amount (Sharifi et al. 2007; Nyiraneza et al. 2012). The uncertain level of soil N supply from growing season mineralization of the preceding legume can result in a poor correlation of tuber yield and pre-planting N measurements (Belanger et al. 2000; 2001). Other researchers have also documented that excessive N fertilization leads to tuber yield reduction (Ojala et al. 1990; Griffin and Hesterman 1991). Many previous studies documented that the over-application of nitrogen in the form of mineral fertilizer or organic manure not only causes potato yield reduction, but also leads to the degradation of potato quality (Li et al. 1999; Zebarth et al. 2004a; Sincik et al. 2008).

In addition, excessive N supply early in growing season can also suppress yield as a result of delaying tuber initiation and bulking (Lynch and Tai, 1989; Sarkar and Naik, 1998; Thornton 2020; Jones et al. 2021) as well as reducing tuber dry matter and specific gravity (Millard and Marshall, 1986; Laboski and Kelling, 2007; Maltas et al., 2018). Our observations were consistent with these results. The tuber dry matter and specific gravity were significantly lower under the PBC rotation.

Potato producers should adequately account for N supply from preceding rotation crops, especially legumes like red clover. However, the relatively large spatial and temporal variation of soil N from the preceding red clover creates a practical challenge for growers to accurately account for soil N supply where spatiotemporally consistent N supply is the management goal. Applying the same amount of fertilizer N to potato crops under the PBC and PSB rotations would not only increase costs, but could also cause yield losses in the PBC fields and lead to water quality contamination as a result of excessive N leaching (Zebarth et al. 2012; Jiang et al. 2019; Liang et al. 2019).

2.4.2 N Supply from Soybean Residues

In this experiment it was evident that the leguminous soybean did not provide considerable N supply to the subsequent crop. In fact, the spring soil N content experienced a greater decrease from fall to spring after soybean compared to barley. This can be explained by two main factors. Firstly, about 66% of total soybean nitrogen was harvested in seeds. The remaining roots and shoots contained about 76 kg N ha^{-1}, while barley residues contained about 36.5 kg N ha^{-1} (data reported elsewhere, Liang et al. 2019). Secondly, soybean residues have low C:N ratios and tend to mineralize quicker after being incorporated into soil (Baggs et al. 2000; Dessureault-Rompré et al. 2013). Several studies have reported the

high leaching potential of these mineralized residues over winter in the climatic conditions of Atlantic Canada (Sanderson et al. 1999; Seneviratne, G. 2000; Zebarth et al. 2005). Therefore, the decline of soil N in PSB plots was likely a result of the quick mineralization of soybean residues and later loss through leaching during winter. In addition, the average non-growing season nitrate leaching of soybean plots was significantly higher than that of barley plots in 2016 (data reported elsewhere, Liang et al. 2019), which further supports this explanation.

2.4.3 Effects of Rotation and Cultivar on Tuber Yield, Dry Matter, Specific Gravity, and Starch Content

With all cultivars combined, the PSB rotation resulted in a significant increase (19.5%) in total tuber yield. In a study carried out in Maine, US, using the Russet Burbank cultivar, 224 kg N ha^{-1} fertilization and similar management conditions, it was reported that the soybean-barley/clover-potato rotation produced 9.7% higher yields than that the standard three-year barley/clover-clover-potato rotation, with yields of 28.7 t ha^{-1} and 31.5 ta ha^{-1}, respectively. However, the difference was not statistically significant (Larking and Honeycutt 2006). We found that PSB and PBC rotations considerably influenced potato yields for different cultivars. We observed that the PSB rotation led to higher yields for the Russet Burbank, Gold Rush, and Prospect (except for one sample of Prospect) cultivars. The Gold Rush cultivar was affected the most (36%), followed by Russet Burbank (17%) and Prospect (14%) cultivars, whereas Shepody was not affected as much (3%) under different rotations.

We found that Russet Burbank maintained a relatively high yield under both rotations with an average yield of 50.69 t ha^{-1} and 43.41 t ha^{-1} for PSB and PBC respectively. Zaeen et

al. (2020) reported that an increase of N fertilization from 168 kg N ha^{-1} to 228 kg N ha^{-1} resulted in a slight decrease in Shepody's tuber yield without influencing Russet Burbank yield. They reported an N fertilization rate of 168 kg N ha^{-1} as an optimal rate for both Shepody and Russet Burbank to maximize tuber yield and quality. These results indicated that Russet Burbank is able to maintain a relatively high yield within a wider range of N supply, although excessive N supply can still suppress the yield.

The PSB rotation led to a significant increase in specific gravity, starch content, and tuber dry matter with averages of 1.0898, 15.770%, and 10.7 t ha^{-1}, respectively, compared to the PBC averages of 1.0868, 15.425%, and 8.9 t ha^{-1}. While the cultivar effect didn't show statistical significance for these dependent variables, the studied cultivars responded differently to the alternate rotation. The highest and lowest specific gravity and starch content were observed in Russet Burbank under PSB and PBC rotation, respectively, making it the most affected cultivar. Shepody was the least positively affected cultivar and Prospect was the only cultivar that experienced a decrease in specific gravity and starch content under the PSB rotation. Tuber dry matter increased in all cultivars under the PSB rotation. Similar to tuber yield, Gold Rush benefited the most from the alternative rotation in dry matter with a 41.8% increase, followed by Russet Burbank (16.7%), Gold Rush (15.2%), and Shepody (9.3%).

2.4.4 Economic Implications of PSB Rotation

In the conventional rotation, the potato crop creates about 93.5% of the total gross income of a PBC rotation cycle, which approximated to be \$7496 ha^{-1} (Supplemental Table 2). Therefore, an increase in the potato yield along with the addition of a secondary cash crop to the rotation can translate into a significant economic benefit for potato farmers. It is

estimated that replacing red clover with soybean in potato rotation can increase the gross income of a rotation cycle by 30%. This increase is composed of about \$792 ha^{-1} from 2.2 t ha^{-1} soybean yield (yield results reported elsewhere, Liang et al. 2019) and \$1472 ha^{-1} from the 7.6 t ha^{-1} increase in average potato yield of the PSB rotation. Incomes are estimated based on the 2011–2019 average unit price of \$344.6 ton^{-1} and \$193.8 ton^{-1} for soybean and potato, respectively (Government of Prince Edward Island 2019; 2020). Note that these results are based on data from one cycle of a three-year rotation and more work is required to assess the long-term economic and environmental implications of the PSB rotation.

2.5 Conclusion

The PSB rotation had significantly higher yields than PBC rotation and positively influenced the yield of all cultivars. The russet cultivars were more sensitive to the alternative PSB rotation, with the Gold Rush being the most affected, followed by Russet Burbank and Prospect cultivars, whereas Shepody was not affected as much (3%) under the two different rotations. Russet Burbank had the highest yield under both PBC and PSB rotations. Although the differences in yields were numerically clear, an analysis of variance did not detect statistically significant differences between cultivars nor between rotations within each cultivar. This is likely because the sample sizes (two to four replications) were relatively small compared to the high variation in the dependent variables. However, increasing the sample size by treating the three russet cultivars as a single russet group, the PSB rotation significantly increased tuber yield. In addition, a preliminary economic analysis revealed that the average increase in potato yield along with the additional income from soybeans in the PSB rotation can increase gross income by as much as 30%. Soil

analyses showed that the PBC rotation had significantly higher pre-planting soil mineral N content than the PSB rotation. The elevated mineral N content in PBC plots was probably sourced from the decomposition of the plowed-down red clover biomass. The lower yield of the PBC rotation despite higher mineral N available at planting was likely caused by an oversupply of nitrogen from red clover residue decomposition. Results indicate that potato growers should adjust the N application rate based on pre-plant soil N concentration by taking into account extra N supply from residues of nitrogen-fixing cover crop such as red clover. This will produce higher yields and improve tuber quality while at the same time reducing nitrate leaching. It is important to stress that these are preliminary results concluded from a short-term field study. More comprehensive and longer term studies with increased replications are needed to further verify the results.

2.6 Acknowledgments

This study was funded by the Agriculture and Agri-Food Canada project “Reducing sediment, N and P loading from arable cropping systems to receiving waters in eastern Canada” (J–001270) and Agriculture and Agri-Food Canada’s Living Labs (J–002269) led by Dr. Yefang Jiang. We thank Danielle Murnaghan, Brian Murray, Sandy Jenkins, Taylor Main, Ana Kostic, the Harrington farm crew, and several co-op and summer students for their field/lab assistance.

Bibliography

Abolgasem, T.M.M. 2014. Effect of variety, fertilisation, rotation, crop protection and growing season on yield and nutritional quality of potato (Solanum tuberosum L.). http://theses.ncl.ac.uk/jspui/handle/10443/2551. Accessed 10 May 2021.

Agriculture and Agri-Food Canada. 2020. Potato Market Information Review – 2019–2020. https://agriculture.canada.ca/en/canadas-agriculture-sectors/horticulture/horticulture-sector-reports/potato-market-information-review-2019-2020. Accessed 10 May 2021.

Baggs, E., R. Rees, K. Smith, and A. Vinten. 2000. Nitrous oxide emission from soils after incorporating crop residues, *Soil use and management*, 16: 82–87.

Bélanger, G., J. Walsh, J. Richards, P. Milburn, and N. Ziadi. 2000. Yield response of two potato culivars to supplemental irrigation and N fertilization in New Brunswick, *American Journal of Potato Research*, 77: 11–21.

Bélanger, G., J. Walsh, J. Richards, P. Milburn, and N. Ziadi. 2001. Predicting nitrogen fertilizer requirements of potatoes in Atlantic Canada with soil nitrate determinations, *Canadian Journal of Soil Science*, 81: 535–44.

Belanger, G., J. Walsh, J. Richards, P. Milburn, and N. Ziadi. 2002. Nitrogen fertilization and irrigation affects tuber characteristics of two potato cultivars, *American Journal of Potato Research*, 79: 269–79.

Bernard, G., S. Asiedu, and P. Boswall. 1993. Atlantic Canada potato guide, *Atlantic Provinces Agriculture Services Coordinating Committee publication*, 1300: 93.

Bishop, E.C. 2015. Incentivizing Beneficial Management Practice Adoption to Improve Groundwater Quality in Prince Edward Island: An Economic-Hydrologic Modelling Approach.

Cavendish Farms. 2012. Our story. https://www.cavendishfarms.com/en/our–story/. Accessed 10 May 2021.

Cerdà, A., Ó. González-Pelayo, A. Giménez-Morera, A. Jordán, P. Pereira, A. Novara, E.C. Brevik, M. Prosdocimi, M. Mahmoodabadi, and S. Keesstra. 2016. Use of barley straw residues to avoid high erosion and runoff rates on persimmon plantations in Eastern Spain under low frequency-high magnitude simulated rainfall events, *Soil Research*, 54: 154–65.

Dessureault-Rompré, J., B.J. Zebarth, D.L. Burton, E.G. Gregorich, C. Goyer, A. Georgallas, and C.A. Grant. 2013. Are soil mineralizable nitrogen pools replenished during the growing season in agricultural soils?, *Soil Science Society of America Journal*, 77: 512–24.

Edwards, L., G. Richter, B. Bernsdorf, R.G. Schmidt, and J. Burney. 1998. Measurement of rill erosion by snowmelt on potato fields under rotation in Prince Edward Island (Canada), *Canadian Journal of Soil Science*, 78: 449–58.

Freebairn, D., R. Loch, and A. Cogle. 1993. Tillage methods and soil and water conservation in Australia, *Soil and Tillage Research*, 27: 303–25.

Gao, Z., Z. Ma, M. Han, C. Liu, Y. Hu, W. Jiao, J. Hu, Z. Li, L. Liu, and Q. Tian. 2019. Effects of continuous cropping of sweet potato on the fungal community structure in rhizospheric soil, *Frontiers in microbiology*, 10: 2269.

Gee, G., and J. Bauder. 1979. Particle size analysis by hydrometer: a simplified method for routine textural analysis and a sensitivity test of measurement parameters, *Soil Science Society of America Journal*, 43: 1004–07.

Gould, W. 1995. Specific gravity-its measurement and use, *Chipping Potato Handbook*, 18.

Government of Prince Edward Island. 2019. PEI Farm Cash Receipts. https://www.princeedwardisland.ca/sites/default/files/publications/fin_farmcash.pdf

Accessed 04 December 2020.

Government of Prince Edward Island Canada. 2020. The Prince Edward Island potato sector: An economic impact analysis. PEI Department of Agriculture and Land. www.princeedwardisland.ca/sites/default/files/publications/af_potato_econ_impact_study.pdf. Accessed 22 September 2021.

Grandy, A.S., G.A. Porter, and M.S. Erich. 2002. Organic amendment and rotation crop effects on the recovery of soil organic matter and aggregation in potato cropping systems, *Soil Science Society of America Journal*, 66: 1311–19.

Griffin, T., and O. Hesterman. 1991. Potato response to legume and fertilizer nitrogen sources, *Agronomy Journal*, 83: 1004–12.

Inglis, D., D. Johnson, D. Legard, W. Fry, and P. Hamm. 1996. Relative resistances of potato clones in response to new and old populations of Phytophthora infestans, *Plant disease (USA)*.

Jégo, G., M. Martinez, I. Antigüedad, M. Launay, J.M. Sanchez-Pérez, and E. Justes. 2008. Evaluation of the impact of various agricultural practices on nitrate leaching under the root zone of potato and sugar beet using the STICS soil-crop model, *Science of the Total Environment*, 394: 207–21.

Jiang, Y., J. Nyiraneza, M. Khakbazan, X. Geng, and B.J. Murray. 2019. Nitrate leaching and potato yield under varying plow timing and nitrogen rate, *Agrosystems, Geosciences & Environment*, 2: 1–14.

Jiang, Y., B.J. Zebarth, G.H. Somers, J.A. MacLeod, and M.M. Savard. 2012. 'Nitrate leaching from potato production in Eastern Canada.' in, *Sustainable potato production: Global case studies* (Springer).

Jones, C.R., T.E. Michaels, C. Schmitz Carley, C.J. Rosen, and L.M. Shannon. 2021. Nitrogen uptake and utilization in advanced fresh-market red potato breeding lines, *Crop Science*, 61: 878-95.

Kawano, K., W.M.G. Fukuda, and U. Cenpukdee. 1987. Genetic and environmental effects on dry matter content of cassava root 1, *Crop Science*, 27: 69–74.

Laboski, C.A., and K.A. Kelling. 2007. Influence of fertilizer management and soil fertility on tuber specific gravity: a review, *American Journal of Potato Research*, 84: 283-90.

Larkin, R.P., and C.W. Honeycutt. 2006. Effects of different 3–year cropping systems on soil microbial communities and Rhizoctonia diseases of potato, *Phytopathology*, 96: 68–79.

Li, W., K.A. Zarka, D.S. Douches, J.J. Coombs, W.L. Pett, and E.J. Grafius. 1999. Coexpression of potato PVYo coat protein and cryV-Bt genes in potato, *Journal of the American Society for Horticultural Science*, 124: 218–23.

Liang, K., Y. Jiang, J. Nyiraneza, K. Fuller, D. Murnaghan, and F.R. Meng. 2019. Nitrogen dynamics and leaching potential under conventional and alternative potato rotations in Atlantic Canada, *Field Crops Research*, 242: 107603.

Liang, K., Y. Jiang, J. Qi, K. Fuller, J. Nyiraneza, and F.-R. Meng. 2020. Characterizing the impacts of land use on nitrate load and water yield in an agricultural watershed in Atlantic Canada, *Science of the Total Environment*, 729: 138793.

Lynch, D.R., and G.C. Tai. 1989. Yield and yield component response of eight potato genotypes to water stress, *Crop Science*. 29: 1207-1211.MacDougall, J., C. Veer, and F. Wilson. 1988. Soils of Prince Edward Island: Prince Edward Island Soil Survey. (Agriculture Canada, Research Branch).

Maltas, A., B. Dupuis, and S. Sinaj. 2018. Yield and quality response of two potato cultivars to nitrogen fertilization, *Potato Research*, 61: 97-114.

Millard, P., and B. Marshall. 1986. Growth, nitrogen uptake and partitioning within the potato (Solatium tuberosum L.) crop, in relation to nitrogen application, *The Journal of Agricultural Science*, 107: 421-29.

Nyiraneza, J., N. Ziadi, B.J. Zebarth, M. Sharifi, D.L. Burton, C.F. Drury, S. Bittman, and C.A. Grant. 2012. Prediction of soil nitrogen supply in corn production using soil chemical and biological indices, *Soil Science Society of America Journal*, 76: 925–35.

Nyiraneza, J., R.D. Peters, V.A. Rodd, M.G. Grimmett, and Y. Jiang. 2015. Improving productivity of managed potato cropping systems in Eastern Canada: Crop rotation and nitrogen source effects, *Agronomy Journal*, 107: 1447–57.

Nyiraneza, J., D. Chen, T. Fraser, and L.P. Comeau. 2021. Improving Soil Quality and Potato Productivity with Manure and High-Residue Cover Crops in Eastern Canada, *Plants*, 10: 1436.

Ojala, J., J. Stark, and G. Kleinkopf. 1990. Influence of irrigation and nitrogen management on potato yield and quality, *American Potato Journal*, 67: 29–43.

Pawlonka, Z., K. Rymuza, K. Starczewski, and A. Bombik. 2015. Biodiversity of segetal weed community in continuous potato cultivated with metribuzin-based weed control, *Journal of Plant Protection Research*, 55.

Porter, G.A., and J.A. Sisson. 1991. Response of Russet Burbank and Shepody potatoes to nitrogen fertilizer in two cropping systems, *American Potato Journal*, 68: 425–43.

Prosdocimi, M., A. Jordán, P. Tarolli, S. Keesstra, A. Novara, and A. Cerdà. 2016. The immediate effectiveness of barley straw mulch in reducing soil erodibility and surface runoff generation in Mediterranean vineyards, *Science of the Total Environment*, 547: 323–30.

Qin, S., S. Yeboah, L. Cao, J. Zhang, S. Shi, and Y. Liu. 2017. Breaking continuous potato cropping with legumes improves soil microbial communities, enzyme activities and tuber yield, *PloS one*, 12: e0175934.

Sanderson, J., J. MacLeod, and J. Kimpinski. 1999. Glyphosate application and timing of tillage of red clover affects potato response to N, soil N profile, and root and soil nematodes, *Canadian Journal of Soil Science*, 79: 65–72.

Sarkar, D., and P.S. Naik. 1998. Effect of inorganic nitrogen nutrition on cytokinin-induced potato microtuber production in vitro, *Potato Research*, 41: 211-17.Seneviratne, G. 2000. Litter quality and nitrogen release in tropical agriculture: a synthesis, *Biology and fertility of soils*, 31: 60–64.

Scholte, K. 1990. Causes of differences in growth pattern, yield and quality of potatoes (Solanum tuberosum L.) in short rotations on sandy soil as affected by crop rotation, cultivar and application of granular nematicides, *Potato research*, 33: 181–90.

Scholte, K. 1992. Effect of crop rotation on the incidence of soil-borne fungal diseases of potato, *Netherlands Journal of Plant Pathology*, 98: 93–101.

Sharifi, M., B.J. Zebarth, D.L. Burton, C.A. Grant, G.A. Porter, J.M. Cooper, Y. Leclerc, G. Moreau, and W.J. Arsenault. 2007. Evaluation of laboratory-based measures of soil mineral nitrogen and potentially mineralizable nitrogen as predictors of field-based indices of soil nitrogen supply in potato production, *Plant and Soil*, 301: 203–14.

Sincik, M., Z.M. Turan, and A.T. Göksoy. 2008. Responses of potato (Solanum tuberosum L.) to green manure cover crops and nitrogen fertilization rates, *American Journal of Potato Research*, 85: 150–58.

Statistics Canada. 2021. Table 32-10-0358-01 Area, production and farm value of potatoes. www.princeedwardisland.ca/sites/default/files/publications/af_potato_econ_impact_study.pdf Accessed 07 October 2021.

Sturz, A., W. Arsenault, and B. Christie. 2003. Red clover–potato cultivar combinations for improved potato yield, *Agronomy Journal*, 95: 1089–92.

Sturz, A., and B. Christie. 1998. The potential benefits from cultivar specific red clover-potato crop rotations, *Annals of applied biology*, 133: 365–73.

Sturz, A., and B. Matheson. 1996. Populations of endophytic bacteria which influence host-resistance to Erwinia-induced bacterial soft rot in potato tubers, *Plant and Soil*, 184: 265–71.

Tiessen, K., S. Li, D. Lobb, G. Mehuys, H. Rees, and T. Chow. 2009. Using repeated measurements of 137Cs and modelling to identify spatial patterns of tillage and water erosion within potato production in Atlantic Canada, *Geoderma*, 153: 104–18.

Thornton, M. 2020. Potato growth and development, In *Potato Production Systems*, 19-33. Springer: Cham.

Tribouillois, H., J.P. Cohan, and E. Justes. 2016. Cover crop mixtures including legume produce ecosystem services of nitrate capture and green manuring: assessment combining experimentation and modelling, *Plant and Soil*, 401: 347–64.

Vos, J., and C. Van Loon. 1989. Effects of cropping frequency on potato production. In *Effects of crop rotation on potato production in the temperate zones*, 1-23. Springer: Dordrecht.

Wei, W., L. Chen, H. Zhang, L. Yang, Y. Yu, and J. Chen. 2014. Effects of crop rotation and rainfall on water erosion on a gentle slope in the hilly loess area, China, *Catena*, 123: 205–14.

Zaeen, A.A., L. K. Sharma, A. Jasim, S. Bali, A. Buzza, and A. Alyokhin. 2020. Yield and quality of three potato cultivars under series of nitrogen rates, *Agrosystems, Geosciences & Environment*, 3: e20062.

Zebarth, B., Y. Leclerc, and G. Moreau. 2004a. Rate and timing of nitrogen fertilization of Russet Burbank potato: Nitrogen use efficiency, *Canadian Journal of Plant Science*, 84: 845–54.

Zebarth, B., G. Tai, R.d. Tarn, H. De Jong, and P. Milburn. 2004b. Nitrogen use efficiency characteristics of commercial potato cultivars, *Canadian Journal of Plant Science*, 84: 589–98.

Zebarth, B., and C. Rosen. 2007. Research perspective on nitrogen BMP development for potato, *American Journal of Potato Research*, 84: 3–18. Zebarth, B., W. Arsenault, S. Moorehead, H. Kunelius, and M. Sharifi. 2009. Italian ryegrass management effects on nitrogen supply to a subsequent potato crop, *Agronomy Journal*, 101: 1573–80.

Supplementary Information

Table S1 Soil nitrate, carbon content, organic carbon to nitrogen ratio, and the bulk density measurements along with sampling dates. The number in parentheses are standard deviations. No significant differences between rotations detected

Rotation	NO_3 (kg N ha^{-1})	C (%)	C:N	Bulk Density (g cm^{-3})
	May, 2014	May, 2015	May, 2015	May, 2016
PBC	16.45 (0.44)	1.2 (0.25)	11.62 (1.44)	1.63 (0.1)
PSB	16.87 (0.56)	1.25 (0.25)	11.95 (0.88)	1.67 (0.13)
Average	16.66 (0.53)	1.22 (0.24)	11.79 (1.15)	1.65 (0.11)

Table S2 Provincial averages of total yield, harvested area and total farm cash receipts in Prince Edward Island (2011-2019)

Crop	Yield (ton)	Area (ha)	Farm cash receipts ($)	Unit price ($ ton^{-1})	Unit price ($ ha^{-1})
Potato	**1252440**	**34565**	**242,489,556**	**193.8**	**7,016.2**
Soybean	**47622**	**20457**	**16,364,000**	**344.6**	**803.3**
Barley	**85189**	**25143**	**11,365,667**	**133.9**	**454.7**
Hay	**207222**	**48305**	**1,242,333**	**6.2**	**25.8**

Chapter 3: Improving baseflow separation accuracy of Digital Filter methods with regional time series of groundwater level data

Visual Abstract

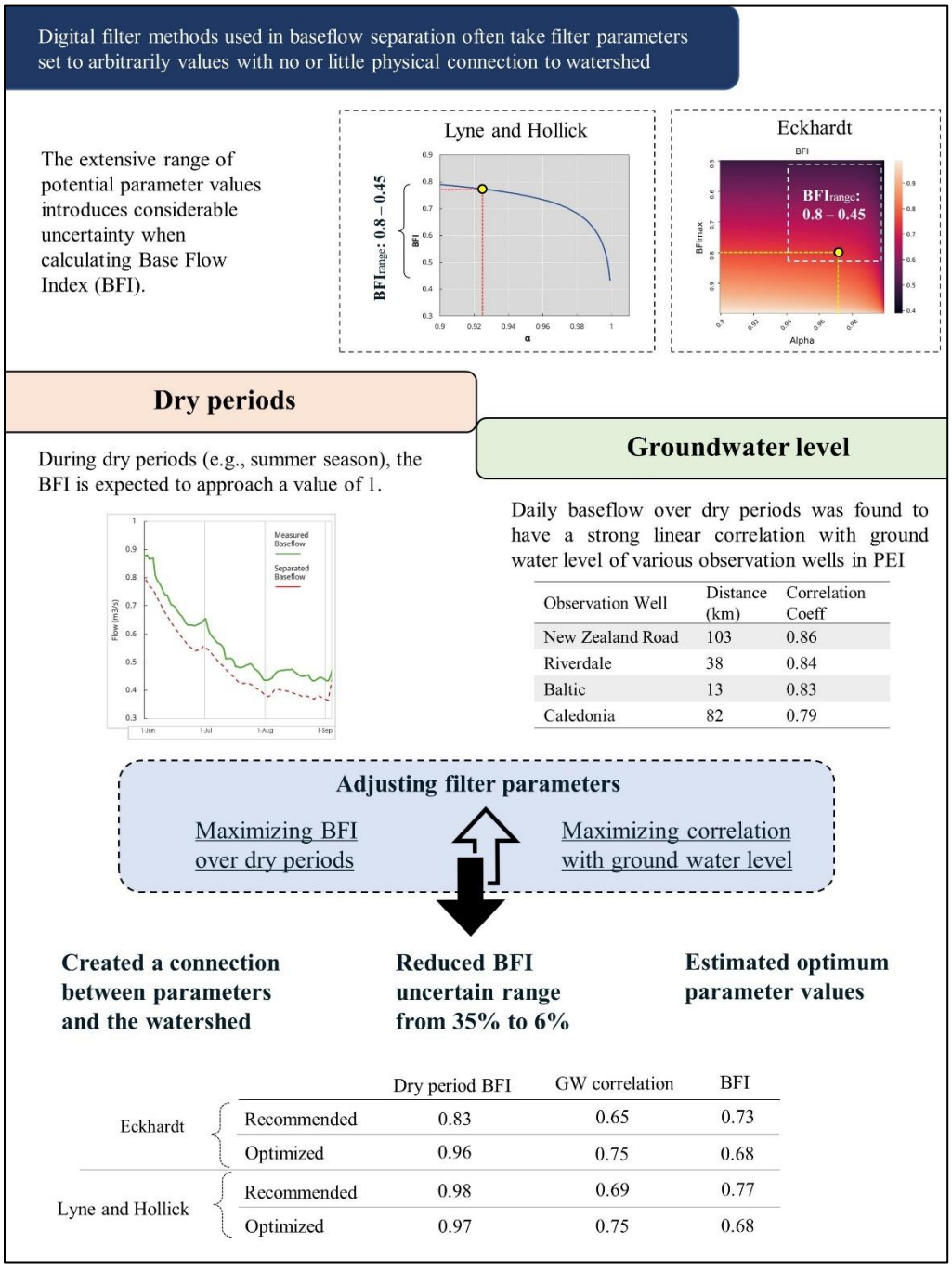

Abstract

Recommended filter parameters from literature are commonly utilized when applying digital filter methods to baseflow separation. However, the choices of the filter parameters can lead to significant uncertainties in baseflow separation because these parameters vary in relatively large ranges, and the digital filter methods are sensitive to the variations of these parameters. In this study, we explored using groundwater level data as an additional data source to constrain the filter parameters for reducing the uncertainties in baseflow separation. Firstly, we established the relationship between groundwater level and baseflow by analyzing dry periods when streamflow primarily came from groundwater discharge. Secondly, we evaluated the performance of recommended and alternative parameterization schemes of Lyne and Hollick (LH) and Eckhardt (EK) methods using a set of new evaluative measures based on: (a) the correlation between separated baseflow and groundwater level, and (b) the methods' ability to predict baseflow during dry periods. Thirdly, to minimize parameter uncertainty and improve baseflow separation, we introduced a new procedure based on maximizing the evaluative measures. The correlation coefficient between groundwater level and daily streamflow during dry periods was as high as 0.86, indicating a strong daily relationship. During baseflow-dominated periods, the EK method, with general and local recommended parameterization, underestimated baseflow by up to 17% and 27% respectively. In contrast, both recommended and alternative filter parameters of the LH method yielded a baseflow ratio close to 100% during dry periods, with relatively high correlation coefficients with groundwater level. The uncertain range of calculated Baseflow Indices (BFI) using LH or EK methods was significantly reduced from 0.45-0.88 to 0.64-0.70 after implementing our designated procedure. Estimating the

optimum LH and EK parameters yielded identical BFIs of 0.68 and nearly identical evaluative measures. The results showcased that the widely available groundwater level data can be used to greatly narrow the uncertainty in filter parameter estimation and improve the accuracy of baseflow separation while establishing a physics-based linkage to the watershed.

3.1 Introduction

Streamflow typically consists of multiple components, including surface runoff, groundwater discharge (i.e., baseflow), bank storage return flow, interflow, and water flushing out of wetlands or depressions by rainfall (Cartwright et al. 2014; Lin et al. 2007; McCallum et al. 2010; Schwartz 2007). These components are commonly characterized by varying residence times as well as isotopic and chemical signals (Cartwright and Morgenstern 2018). These components combinedly regulate a river's runoff process and water chemistry properties, affecting the river's ecosystem (Howcroft et al. 2019; Saraiva Okello et al. 2018). Knowing the dynamics of each component is important in watershed hydrology. Due to the difficulty of independently measuring the various streamflow components, they are typically estimated by separating the components from the hydrograph (Hagedorn 2020; Lin et al. 2007). The streamflow is commonly decomposed into surface runoff and baseflow (i.e., groundwater discharge) (Chapman 1999; Eckhardt 2005; Schwartz 2007; Tallaksen 1995). Surface runoff is considered the rapid flow component occurring on the watershed surface as a response to rainfall or snowmelt events, whereas baseflow represents the delayed flow from shallow and deep sub-subsurface water stores (Cartwright and Miller 2021; Nathan and McMahon 1990). Baseflow is generalized to be equivalent to the groundwater discharge to the stream (Graszkiewicz et al. 2011; Lott

and Stewart 2016; Lyu et al. 2020). Baseflow represents the discharge that can be sustained during little or no precipitation (including snow melt) periods. In addition, baseflow can be an important pathway of dissolved nutrient transport from watersheds. Many studies have shown that non-point source nitrogen is mainly delivered into streams with baseflow (Kang et al. 2008; Schilling and Zhang 2004; Schilling and Lutz 2004; Villarini et al. 2016). Due to its solubility and mobility, nitrate can infiltrate the soil profile, percolate to groundwater, and eventually discharge into receiving stream network via baseflow (Kang et al. 2008).

Accurately quantifying baseflow contributions to streamflow is critical for understanding the water budget in a watershed (Stewart et al. 2007), particularly where baseflow provides a critical water supply during the dry seasons (Smakhtin 2001; Werner et al. 2006) and acts as the principal means of nutrient transport. Baseflow separation is commonly conducted to estimate groundwater discharge for hydrological models and estimate nutrient loading in water quality assessments (Lott and Stewart 2016; Müller et al. 2003; Schilling and Zhang 2004; Tan et al. 2009; Yu and Schwartz 1999). Numerous methods for baseflow separation have been developed (Nathan and McMahon 1990; Nejadhashemi et al. 2003; Stewart et al. 2007). Baseflow separation methods can be classified into three categories: analytical, empirical, and mass balance (Zhang et al. 2013). Empirical methods are arguably the most extensively utilized methods for baseflow separation and are developed based on experience or calibration of a hypothetical model using field observations. The two primary forms of empirical approaches are low-pass filter methods and graphical methods (Stewart et al. 2007; Zhang et al. 2013). The United Kingdom Institute of Hydrology (UKIH) code (Piggott et al. 2005), hydrograph separation program (HYSEP)

(Sloto and Crouse 1996), and streamflow partitioning method (PART) (Rutledge 1998), are automated variants of the classic separation procedure. Most baseflow series produced by these techniques are broken lines that do not reflect baseflow's natural transition (Duncan 2019; Eckhardt 2008).

The low-pass filters separate the low-frequency component representing base flow from the high-frequency (runoff) component. The recursive digital filter is one form of low-pass filter extensively used in baseflow separation (Chapman 1991; Nathan and McMahon 1990). These filters are based on signal-processing theory and are purely analytical in the sense that they are not dependent on physical processes in a watershed. The operator determines the degree of filtering by modifying a filter coefficient and determining the number of passes the filter runs through the hydrograph (Mau and Winter 1997; Nathan and McMahon 1990). Since these filters are not derived from hydrologic processes, it is challenging to evaluate their accuracy objectively, and the filtering process is based on the operator's subjective judgments (Stewart et al. 2007). Although some filters have been developed based on Boussinesq (Huyck et al. 2005) or hillslope mass-balance equations (Furey and Gupta 2001), they often require defining or obtaining multiple difficult-to-obtain parameters specific to the studied watershed (Stewart et al. 2007). Eckhardt (2005) developed a two-parameter recursive filtering algorithm based on the linear reservoir theoretical framework, which includes two parameters: the recession coefficient (α), representing the recession features of baseflow, and the BFImax, representing the long-term baseflow to streamflow ratio. Although recession analysis may easily identify the recession coefficient (α), empirical estimation of BFImax (maximum value of the long-

term ratio of baseflow to total streamflow) is necessary (Eckhardt 2012). It has been repeatedly suggested that there is considerable uncertainty associated with the estimation of BFImax, which requires correction (e.g., calibration) using other methods, such as the mass balance method using environmental tracers (Lott and Stewart 2016; Rammal et al. 2018; Saraiva Okello et al. 2018; Zhang et al. 2013). Due to its clear physics and ease of use, the Eckhardt method has been widely implemented for baseflow separation (Guzmán et al. 2015; Hagedorn 2020; Li et al. 2014; Xie et al. 2020; Zhang et al. 2017).

While calibration is commonly required for hydrological modeling, calibration is rarely used in baseflow separation due to the challenge of data availability. In applying low-pass filters, it is common to implement standard filter parameterizations (i.e., previously recommended) to multiple watersheds, which may involve significant spatial and temporal variations in the filter coefficients. Examples of such recommended parametrization have been presented by Lyne and Hollick (1979), Eckhardt (2008); Ladson et al. (2013); Nathan and McMahon (1990). Due to the uncertainty involved in using previously recommended parametrization and the absence of calibration data, it has been suggested to perform sensitivity and uncertainty analysis (Ladson et al. 2013). Voutchkova et al. (2019) demonstrated that the uncertainty is significantly higher for snow-dominated watersheds than for rain-dominated watersheds. As a result, they deemed the uncertainty evaluation and reducing the range of possible filter parameters crucial for baseflow separation in snow-dominated watersheds, suggesting avoiding using BFI estimates obtained from heuristic baseflow separation methods altogether. However, the studies of both

Voutchkova et al. (2019) and Ladson et al. (2013) did not present any solution for reducing the range of filter parameters in the absence of calibration data.

Although baseflow is not directly measurable, baseflow has been observed to demonstrate similar dynamics with other hydrological variables. For example, Zhang et al. (2013) reported a strong similarity between the response of the groundwater table and streamflow to recharge events, suggesting that a more accurate baseflow separation could be evident from a more synchronized dynamics of separated baseflow and field-measured groundwater table. The close correlation between baseflow and water table fluctuation is mainly driven by the rapid pressure propagation within the soil-vadose zone-aquifer continuum. This process was documented by Warrick (1971), Bresler (1973), Pickens and Gillham (1980) and demonstrated in the field by Jiang et al. (2017). The correlation between baseflow and water table provides an opportunity to constrain baseflow separation using water table data. This study introduced a new procedure to optimize baseflow separation with the low-pass filter methods based on regional multiple time series of groundwater table data. Briefly, the parameters in the low-pass field methods were optimized using the linear correlation of daily separated baseflow with groundwater level and the ability of each baseflow separation method to predict the baseflow during dry periods when streamflow is entirely groundwater-fed. The procedure benefits from linking the arbitrary parameter values to measured hydrogeological responses of the watershed. Specific objectives were: (1) to evaluate two low-pass filter methods using multiple sets of recommended and alternative parametrization schemes and (2) to demonstrate a new

procedure for reducing the uncertainties of baseflow separation with low-pass filter methods.

3.2 Methods

3.3 Study site

PEI is located on the east coast of Canada and covers an area of 5670 km^2. A terrestrial sandstone formation with a thickness of 1200-1600m underlies the entire Island (1200–1600 m). The sandstone formation includes a series of 'red beds ranging from the Carboniferous to Middle Early Permian periods, consisting of primarily red-brown fine to medium-grained sandstone layers, with lesser amounts of siltstone and claystone lenses (Van de Poll 1981). The bedrock is either flat-lying or gently dipping to the north, northeast, or east at an average of 1–3 degrees showing insignificant structural deformation. A thin layer of sandy glacial deposits (0-10m) derived from the red beds overlies the bedrock. The topmost section (~150 m) of the bedrock formations along with the saturated till forms an unconfined fractured-porous aquifer, with fractures dominating the primary groundwater flow pathways and matrix pores defining the storage properties. These sandstones are characterized by relatively high hydraulic conductivity, between 10-6 and 10-4 m/s, but low storage capacity (1 to 3% under unconfined conditions). Below the aquifer depth of 30 m, permeability and flow drastically decrease (Paradis et al. 2006). The aquifer provides significant baseflow for the local aquatic ecosystems. The annual groundwater recharge represents approximately 37% of annual precipitation, averaging 410 mm yr^{-1} (Paradis et al. 2018). The island's land surface is rolling. The stream networks occur densely on the landscape and form about 260 watersheds/sub-watersheds with drainage areas ranging from 0.02 to 196 km^2 (mean = 22 km^2) (PEI government

unpublished data). The relatively small variations in geology, soil, and climate across the island make hydrology relatively similar from watershed to watershed.

The Wilmot River watershed is located in the west-central part of PEI and covers an area of 61 km^2 with watershed dimensions of approximately 17 km long by 5 km wide Figure 3.1. Farming activities occupy above 70% of the total land area, with potato being the main crop generally in rotation with cereals, hay, or leguminous plants (Liang et al. 2019). About 11% of the land surface remains forested. The watershed is relatively flat, with slopes generally ranging from 2 to 6%. The elevation ranges from 88.9 m in the eastern part of the watershed to −0.1 m at the outlet area, where the Wilmot River drains into the Summerside harbor. The Wilmot River and its tributaries occur as a stream network, with the width of the main stem of the Wilmot River varying from 0.5 m at the head during dry seasons to about 200 m at the tidal reach in high flow seasons. The Charlottetown (Orthic Humo-Ferric Podzol) and Alberry (Orthic Humo-Ferric Podzol) series soils dominate the watershed, with the former accounting for 72 percent and the latter for 14 percent (Liang et al. 2020). The Charlottetown series are moderately well-drained and moderately coarse; water is extracted slowly relative to supply. Water is removed from the soil readily but not rapidly in the Alberry series, which is moderately coarse and well-drained. The relatively high hydraulic conductivity of the basin's overburden and rock formations leads to a rapid water table response. The time lag between groundwater level rise and precipitation events is approximately five days (Liao et al. 2005; Paradis et al. 2006).

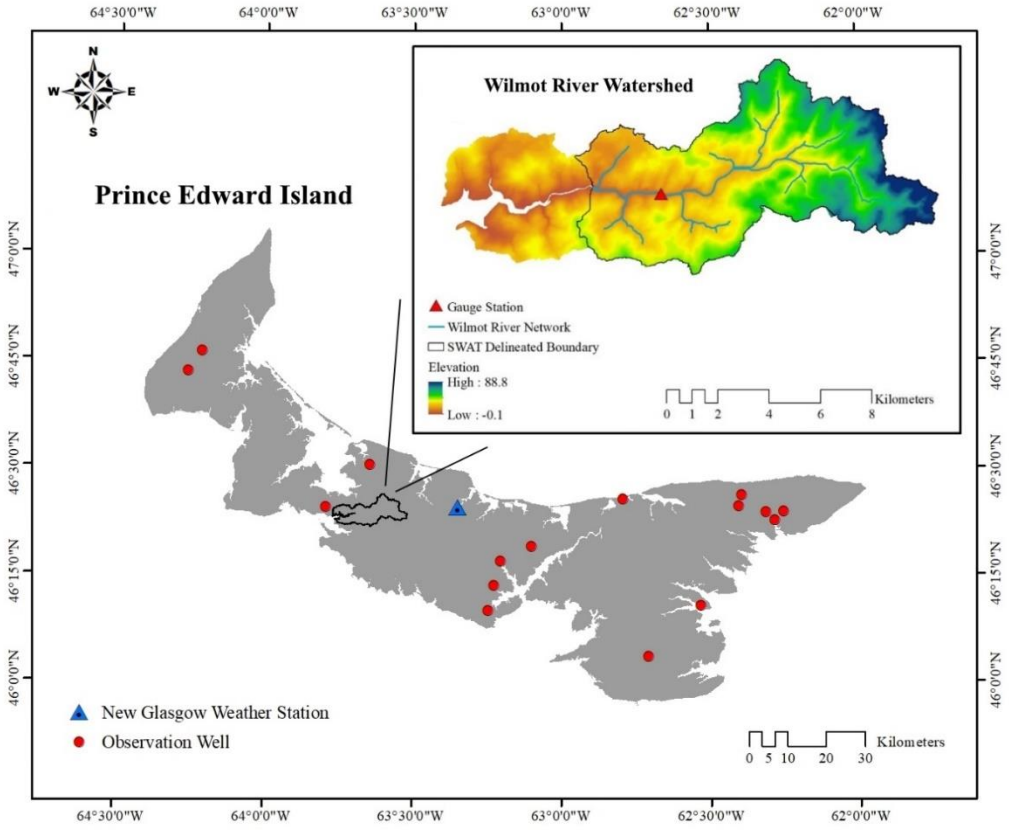

Figure 3.1 Wilmot River watershed, located in the central west of PEI. (replace gauge with gauging in the map)

The climate in this region is categorized as humid with a cool to mild temperature regime. Precipitation within the watershed ranges between 810 mm in 2006 and 1463 mm in 2002. Mean annual precipitation is 1225 mm (New Glasgow station; 1995–2019), most of which falls as rain (78%). Mean monthly precipitation ranges from 77.4 to 135.5 mm for July and October, respectively (Figure 3.2). The mean annual temperature is 6.5 °C, and monthly mean temperatures range from −6.4 °C in February to 19.5 °C in July (Environment Canada: https://climate.weather.gc.ca/historical_data/search_historic_data_e.html).

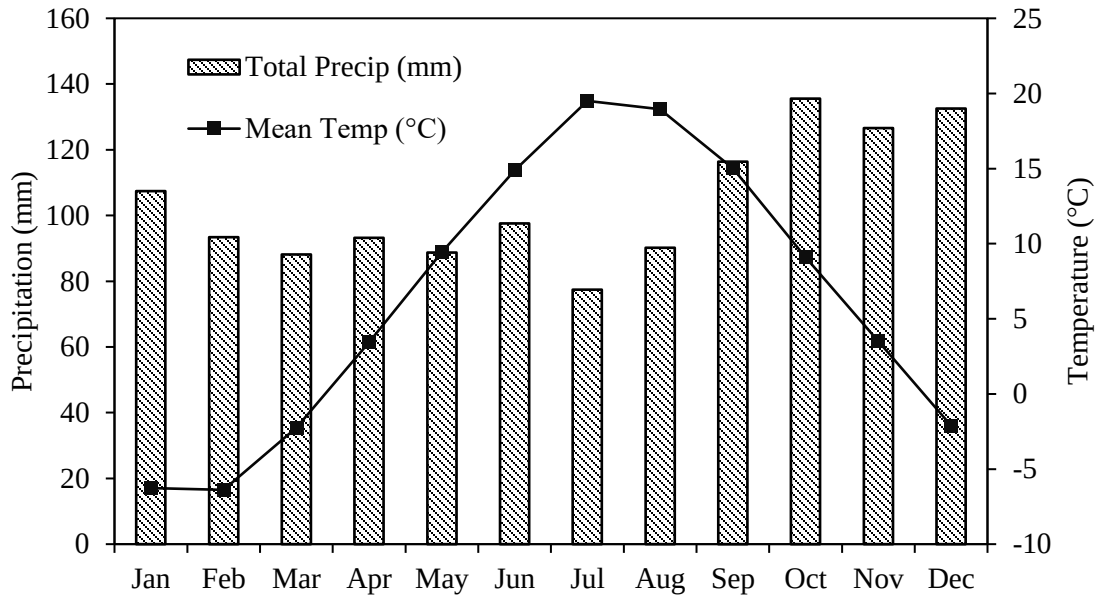

Figure 3.2 Long-term mean monthly temperature and precipitation over the watershed (New Glasgow station; 1995–2019).

3.3.1 Study period and data

Data for optimizing baseflow separation include precipitation, stream flow, and groundwater level data. The study covers the period of 1995 to 2019 as it produces the maximum overlap between the different data used in this study. Various sub-annual time frames are considered for periodic analyses based on the importance of each period in this region. The non-growing season indicates the first half of the water year, which begins on Oct 1st and ends on Apr 30th. Precipitation typically is in the form of snowfall within this period, and the major snowmelt event occurs in the last month, April. The growing season refers to the second half of the water year, beginning on May 1st and ending on September 30th. The summer season (June, July, and August) is the shortest time frame when streamflow is solely provided by groundwater. The precipitation data were obtained from the New Glasgow station (46.41, −63.35), which is 13 km northeast of the watershed since there are no Environment Canada weather stations located in the watershed. The Wilmot

gauge station maintained by Environment and Climate Change Canada is located near the outlet of the upper section of the watershed (Figure 3.1). Streamflow data show a mean annual discharge of 0.96 m3/s (station 01CB004) and a mean monthly discharge ranging from 0.43 m3/s in August to 1.94 m3/s in April during the spring freshet. Annual and seasonal streamflow in this study is represented as the accumulation of daily streamflow within each period. Water level data were accessed from the provincial long-term groundwater level monitoring network (http://www.gov.pe.ca/envengfor/groundwater/app.php?lang=E). A total of 16 observation wells have continuously monitored groundwater levels in PEI. However, none of the monitoring sites are located inside the Wilmot River watershed. The distance of observation wells from the gauge station at Wilmot River ranges from 10.6 to 108 km. The ground elevations of all observation wells (except the Caledonia) fall between the elevation range of the Wilmot watershed (0-88). Groundwater level data from all observation wells except the Bear River station cover over 40% of the entire period of the study (1995-2019). Table 3.1 summarizes the location, distance from the Wilmot watershed outlet, and percentage of data available from each well during the entire period of this study.

Table 3.1 Summary of the monitoring wells in PEI indicating the percentage of data coverage by each well and the distance from the watershed's gauging station.

Observation Well	Well head elevation (MASL)	Latitude	Longitude	Distance (km)	%obs. (1995-2019)
Baltic	**25.00**	**46.5100**	**-63.6481**	**13.03**	**82**
Bear River	**30.00**	**46.4389**	**-62.3914**	**97.32**	**26**
Bloomfield	**42.92**	**46.7717**	**-64.2200**	**60.08**	**90**
Caledonia	**99.99**	**46.0639**	**-62.7092**	**81.73**	**90**
Georgetown	**9.10**	**46.1825**	**-62.5322**	**89.70**	**95**
Knutsford	**30.48**	**46.7247**	**-64.2672**	**59.34**	**79**
Lakeside	**7.62**	**46.4311**	**-62.7928**	**66.55**	**59**
New Dominon	**19.93**	**46.1708**	**-63.2486**	**40.08**	**84**
New Zealand Road	**43.00**	**46.4000**	**-62.3100**	**103.47**	**41**
Riverdale	**40.00**	**46.2289**	**-63.2289**	**37.75**	**69**
Sleepy hollow	**12.20**	**46.2856**	**-63.2061**	**36.78**	**84**
Souris Line Road	**57.00**	**46.4000**	**-62.2500**	**108.07**	**45**
Souris River Road	**22.00**	**46.3800**	**-62.2800**	**105.79**	**40**
St. Charles	**51.26**	**46.4139**	**-62.4019**	**96.43**	**69**
Summerside GST	**30.48**	**46.4108**	**-63.7953**	**10.62**	**85**
York	**41.00**	**46.3197**	**-63.1006**	**43.64**	**61**

%obs represents the percentage of data covered by each observation well from 1995 to 2019.

3.3.2 Low-pass filter baseflow separation methods

Lyne and Hollick: The Lyne and Hollick (1979) filter (LH), as a low-pass filter, uses signal processing theory and is based on the hydrological reasoning that baseflow represents the low-frequency component of streamflow signal. The LH filter separates the total streamflow (Q) into two components, i.e., quick flow (Q_q) and baseflow (Q_b). It estimates the quick flow firstly as:

$$Q_{q(i)} = \alpha Q_{q(i+1)} + \frac{1+\alpha}{2}(Q_i - Q_{i-1}) \quad \text{(Eq. 1)}$$

where Q is total streamflow (mm/d), Q_q is quick flow (mm/d), i is the time step (day), and α is the filter parameter (dimensionless). The Lyne and Hollick method is widely used by

setting the recession constant α to a recommended value of 0.925 (Nathan and McMahon 1990). Baseflow (Q_b, mm/d) can subsequently be calculated by:

$$Q_{b(i)} = Q_i - Q_{q(i)} \quad \text{(Eq. 2)}$$

Eckhardt: The ECK filter is a two-parameter recursive digital filter, with the underlying assumption that aquifer outflow is directly proportional to groundwater storage. The equation is:

$$Q_{b(i)} = \frac{(1-BFI_{max})\alpha Q_{b(i-1)} + (1-\alpha)BFI_{max}Q_i}{1-\alpha BFI_{max}} \quad \text{(Eq. 3)}$$

Where *a* (dimensionless) is the baseflow recession constant, and BFI_{max} (dimensionless) is the maximum value of the baseflow index (the long-term average ratio of baseflow to total streamflow). Two parameters, α, and BFImax, need to be determined in equation 3. The baseflow recession constant was calculated as 0.97 using the Automated Master Recession Curve analysis (Arnold and Allen 1999). Generally, the BFImax value influences the magnitude of baseflow, whereas the α value influences the shape of the baseflow hydrograph (e.g., steep versus gentle slope of the hydrograph). Since the BFImax cannot be determined prior to baseflow separation, Eckhardt (2005) recommends a standard parametrization in which a value of 0.80 is chosen for perennial streams with porous aquifers, 0.50 for ephemeral streams with porous aquifers, and 0.25 for perennial streams

with hard rock aquifers. As an alternative, the BFImax can be set to the long-term BFI of the watershed obtained from other methods or reports from other studies of the watershed. The use of the BFI from literature avoids empirical judgments for the maximum baseflow index (Zhang et al. 2017; Zhang et al. 2013). Previous studies of the Wilmot River watershed have estimated a BFI value of 0.66 (Francis 1989; Grizard 2013; Jiang et al. 2004; Savard et al. 2010).

3.3.3 Parametrization schemes

We evaluated the performance of these three baseflow separation methods along with multiple parametrization schemes of the LH and the EK methods. For the Lyne and Hollick method, two filter parameters of 0.925 (LH(0.925)) as recommended by Nathan and McMahon (1990) and 0.97 (LH(0.97)), which represents the recession constant, are implemented. For the Eckhardt method, two combinations of the calculated α (0.97) with BFImax set to the recommended value (ECK(0.97,0.8)) and the BFI of the Wilmot in literature (ECK(0.97,0.66)) are considered.

3.3.4 Evaluative data preparation

In the absence of direct measurements for accurate tracer-based estimation of baseflow, alternative data sources that directly or indirectly represent the baseflow in the Wilmot watershed are used for the performance assessment of the baseflow separation methods.

3.3.4.1 Determining pure baseflow days

The annual snowmelt events in PEI occur from mid-March into mid-May (Danielescu and MacQuarrie 2011; Edwards et al. 2008; Jiang and Somers 2011; Zebarth et al. 2015) when the groundwater is recharged, followed by a recession during summer and early fall

months. In periods during the summer months (June, July, and August) where quick flow is normally not generated from rainfall events, the groundwater is the single source of stream flow. The drought periods when streamflow was completely fed by groundwater discharge were determined using the following criteria:

(1) There was no daily precipitation greater than the effective rainfall of 5 mm (Alberto et al. 2016; Jiang et al. 2021). The 5 mm threshold acts as a confidence limit for no runoff generation. Effective rainfall was adopted as a simple yet very safe alternative in order to prevent complications of extensive daily water balance calculations. In addition, it has been reported that under cold and humid climates, evapotranspiration tends to exceed precipitation in the summer (Devito et al. 1996; Liang et al. 2020). The average daily potential evapotranspiration for the Wilmot watershed during the summer months was calculated as 6.2 mm (Obtained from SWAT modeling; data not presented here).

(2) The drought period must continue for at least five consecutive days and occur within the summer months.

(3) No rainfall was recorded for at least two days prior to the beginning of the period (greater than 5 mm). The residence time of the stream water in the Wilmot River is as short as ~0.6 days (Jiang and Somers 2009). However, since the hourly observations are not available for the historical precipitation records, a two-day span is considered a safe window, ensuring no runoff from previous precipitation events exists in the stream flow.

The streamflow records are assumed to represent observed baseflow during these drought periods.

3.3.4.2 Selecting the driest summer seasons

A Z-score analysis is carried out to determine the driest summer seasons based on the total precipitation during each season. A threshold of -0.674 is considered for the z-score to represent years in which the total summer precipitation falls in the lowest 25% of the summer precipitation of the entire study period (1995-2019). A secondary z-score criterion was also considered for total summer streamflow, in which the z-score should not be larger than +0.674. This prevents selecting dry summer seasons in which the BFI is inevitably close to 100% because of exceptionally large groundwater recharge before the summer. Z-score is calculated using Equation 6.

$$Z = \frac{p-\mu_p}{\sigma_p} \qquad \text{(Eq. 6)}$$

Where Z represents the standard z-score, p is the total summer precipitation of each year, μ_p is the average of total summer precipitation (1995-2019), and σ_p is the standard deviation of summer precipitations.

The normality of total summer streamflow and precipitation as a criterion of the z-score analysis was confirmed using the Shapiro-Wilk test.

3.3.4.3 Assessing the correlation of groundwater level with baseflow

Groundwater levels are observed to respond rapidly to recharge events in PEI (Jiang et al. 2015). This rapid hydraulic response as affected by pressure propagation within the soil-vadose zone-aquifer continuum was demonstrated in field by Jiang et al. (2017). A correlation analysis will be conducted to test if the groundwater level can significantly explain the variations in the baseflow. For this purpose, the streamflow during pure

baseflow periods will be tested against groundwater level data from each observation well. The correlation coefficients are calculated using equation (4).

$$cc = \frac{\Sigma(Q_{pb(i)} - \overline{Q_{pb}})(WT_{(i)} - \overline{WT})}{\sqrt{\Sigma(Q_{pb(i)} - \overline{Q_{pb}})^2 \Sigma(WT_{(i)} - \overline{WT})^2}} \quad \text{(Eq. 4)}$$

Where cc is the correlation coefficient, $Q_{pb(i)}$ is the streamflow on the day i within the pure baseflow periods, $\overline{Q_{pb}}$ is the mean of pure baseflow records, $WT_{(i)}$ is water table and $\overline{WT}$ is the mean of the water table calculated over the detected pure baseflow periods.

Selecting representative observation wells

Although the 16 observation wells are located outside the Wilmot River watershed, groundwater level responses to recharge in these wells should be relevant to those in the Wilmot. This is because the two key factors (i.e., geology and precipitation) that influence groundwater level are either relatively uniform (geology) or precipitation rates among different weather stations were linearly correlated on the small island (Jiang et al. 2022). Therefore, a subset of wells will be selected from the total 16 long-term monitoring wells as representatives of groundwater in the Wilmot River Watershed by considering the following criteria: (1) A minimum correlation coefficient of 0.7 between groundwater level and streamflow during the pure baseflow period is required; (2) a minimum of 60% data coverage should exist for the selected observation wells; (3) no significantly large difference in elevation and distance from Wilmot must exist between the selected observation wells.

3.3.5 Evaluating the performance of baseflow separation methods

3.3.5.1 Short-term BFI during driest summer seasons

Baseflow Index (BFI) is the long-term ratio of total baseflow volume to total streamflow volume over a given period (one year or the entire observation period) (Beck et al. 2013; Smakhtin 2001). BFI is calculated using the following equation:

$$BFI = \frac{\sum Q_b}{\sum Q_{st}} \quad \text{(Eq. 5)}$$

Where Q_b is the separated daily baseflow, and Q_{st} represents the daily stream flow records.

The baseflow in PEI constitutes nearly 100% of streamflow during dry summer months (Francis 1989; Jiang et al. 2004; Savard et al. 2010). Respecting this baseflow domination during the summer season is a critical criterion for assessing the performance of each baseflow separation method. Several years with the driest summer seasons will be selected to represent the highest expected baseflow contribution. The short-term BFI over the selected summer seasons will be calculated to assess the percentage of the total summer streamflow contributed by baseflow. BFI values being close to 1 indicates the separation method respects the baseflow during the driest summer months the best.

3.3.5.2 Separated baseflow during pure baseflow days

We evaluate the methods by assessing how well each baseflow separation method can predict the baseflow during detected pure baseflow days where streamflow is assumed to be equal to the baseflow. The goodness-of-fit of the separated baseflow with the streamflow can be evaluated using the Root Mean Square Error (RMSE), percent bias (PBIAS), and the coefficient of determination (R^2). RMSE is the standard deviation of the prediction errors (residuals), where the residuals measure how far from the regression line

data points are. PBIAS calculates the average tendency of estimated values to be greater or less than observations. PBIAS, with a low magnitude, suggests better estimation, with zero being the optimum value (Gupta et al. 1999). Positive PBIAS values suggest an underestimation of the model, whereas negative values indicate an overestimation. The R^2 provides a statistical measure that assesses the ability of a model to explain the variation in observed data. The R^2 ranges from 0 as the worst performance to 1, representing the optimum performance.

$$RMSE = \sqrt{\sum \frac{\left(Q_{b(i)} - Q_{pb(i)}\right)^2}{N}} \qquad \text{(Eq. 6)}$$

$$PBIAS = 100 \times \frac{\sum\left(Q_{pb(i)} - Q_{b(i)}\right)}{\sum Q_{pb(i)}} \qquad \text{(Eq. 7)}$$

$$R^2 = \frac{\sum\left[\left(Q_{pb(i)} - \overline{Q_{pb}}\right)\left(Q_{b(i)} - \overline{Q_b}\right)\right]^2}{\sum\left(Q_{pb(i)} - \overline{Q_{pb}}\right)^2 \sum\left(Q_{b(i)} - \overline{Q_b}\right)^2} \qquad \text{(Eq. 8)}$$

Where Q_{pb} is the measured streamflow during pure baseflow periods, and Q_b is the separated baseflow.

3.3.5.3 Correlation analysis of separated baseflow with groundwater level over annual and seasonal periods

A correlation analysis of groundwater level and streamflow during pure baseflow periods was carried out to verify the strong intraday relationship between baseflow and water table. In the presence of a strong dependency within the two variables, the correlation coefficient between separated baseflow and groundwater level will be used to evaluate the performance of baseflow separation methods over annual and seasonal periods where no pure baseflow can be assumed or observed.

Statistical analysis, baseflow separation calculations, and drought period detections were performed in Python using multiple packages, i.e., scipy, sklearn, and pandas.

3.3.6 Sensitivity analysis

An extensive parameter adjustment covering the full range of possible values of all parameters was carried out to assess the sensitivity of BFI and evaluative measures, while quantifying the uncertainty in baseflow estimations.

3.3.7 Reducing uncertainty and optimizing baseflow separation

While there are recommendations for setting parameter values in both methods (i.e., α and BFImax), these values lack a measurable correlation with the watershed reality. Therefore, this arbitrary determination of filter values introduces uncertainty, which can lead to a wide possible range of BFI depending on the values of the filter parameters. To reduce the uncertainty, we utilized the evaluative measures to relate the input parameter values to measurable relevant hydrological responses. The fundamental rationale is that as the baseflow separation improves, the accuracy in predicting pure baseflow in dry days, baseflow domination over the driest summer months, and correlation with the water table should increase. However, a single set of parameter values may not simultaneously produce the best values of all three evaluative measures. In addition, since the parameter values are still not directly measured, a single optimal parameter may not produce the most reliable baseflow separation. Therefore, the 75^{th} percentiles of all the evaluative measures were considered as minimum requirements for producing the best baseflow separation. The steps to reduce the uncertainty are summarized as follows:

- 1. Calculating a single BFI and the relative evaluative measures (i.e., R^2 for pure baseflow and correlation with groundwater level) based on the recommended values of the filter parameters. This will serve as a minimum expectation of the method's performance.
- 2. Obtaining BFI and evaluative measures over the full range of possible filter parameter values.
- 3. Removing all the data points where at least one evaluative measure is lower than that obtained from the recommended parameters (step 1).
- 4. Calculating the 75^{th} percentile of each evaluative measure for the remaining data points.
- 5. Obtaining the new range of filter parameter values by removing all the data points where at least one evaluative measure is lower than the relevant 75^{th} percentile. This step provides a new range of filter parameter values in which all parameter values produce the evaluative measures equal to or greater than the fourth quartile.
- 6. Calculating the average BFI over the new set of separated baseflow as the optimized baseflow separation.

The uncertainty involved in selecting filter values was minimized by narrowing the range of filter parameter values to a range where all evaluative measures are maximized above the 75th percentiles.

3.4 Results

3.4.1 Evaluative measures

3.4.1.1 Driest summer seasons

Averages of total summer (June, July, and August) precipitation and total summer streamflow (cumulative) over the 1995-2019 period were 271 mm and 49 m^3/s, respectively. Based on total precipitation and the relevant z-score, six years were identified with the lowest precipitation during the summer season and a z-score below -0.674 (Table 3.2). The total streamflow during the summer seasons of 2001 and 1995 was above the long-term average, with z-scores greater than 0.674. Therefore, these two years were excluded due to significantly large baseflow sourcing from previous recharge events to prevent the inevitable omission of runoff influence on BFI. The final set of selected years consisted of 2012, 2005, 2013, and 2016. With the least precipitation and the summer evapotranspiration exceeding precipitation in the Wilmot, these selected summer seasons are expected to reflect the largest contribution of baseflow to streamflow(BFI~1).

Table 3.2 Summary of the total summer precipitation, streamflow, and z-score analysis.

Year	Total summer precipitation (mm)	Precipitation z-score	Total summer streamflow ($m^3/10^4$)	Streamflow z-score
2001	**141**	**-2.29**	**493**	**0.8**
2012	**165**	**-1.87**	**333**	**-1.2**
2005	**215**	**-0.99**	**414**	**-0.2**
2013	**222**	**-0.86**	**302**	**-1.5**
1995	**224**	**-0.82**	**510**	**1.0**
2016	**229**	**-0.74**	**366**	**-0.7**
1996	**236**	**-0.61**	**438**	**0.1**
…				
2009	**407**	**2.39**	**642**	**2.6**
Average	**271**	**-**	**427**	**-**
Std	**57**	**-**	**82**	**-**

The table is sorted in ascending order of precipitation z-score.

3.4.1.2 Drought periods with pure baseflow

A total of 95 periods, including 972 days within the summer seasons, were identified based on the three assumptions for the drought periods when streamflow is assumed to be purely provided by groundwater. Figure 3.3 depicts the detected periods within four typical water years. The numbers of periods in June, July, and August months were 34, 34, and 27, respectively. On average, each detected period included ten days. Among the detected periods, 62 were shorter than 10 days, 33 periods above 10, and 6 periods above 20 days.

Figure 3.4 represents the histogram of the selected periods indicating the frequency of the drought period durations. The average streamflow of the 972 detected pure baseflow days was 0.5 m3/s with a standard deviation of 0.14, indicating that the detected days exhibited low streamflow variations. Additionally, the average of 95 standard deviations of individual detected periods equaled 0.024, which confirms that the streamflow within the

detected periods was not subject to large fluctuations as naturally expected during a pure baseflow period. A summary of the pure baseflow periods is presented in Table 3.3.

Table 3.3 Summary of the detected pure baseflow periods.

Month	Periods count (days)	Avg. duration (days)	Total number (days)	Avg. Q (m^3/s)	Avg. SQP (m^3/s)
June	**34**	**10 (4.6)**	**285**	**0.63 (0.14)**	**0.031**
July	**34**	**11 (6.9)**	**320**	**0.48 (0.08)**	**0.023**
August	**27**	**9 (4.6)**	**367**	**0.42 (0.11)**	**0.016**
All	**95**	**10 (5.5)**	**972**	**0.5 (0.14)**	**0.024**

Numbers in parentheses indicate standard deviations. SQP: Standard deviation of streamflow within each period.

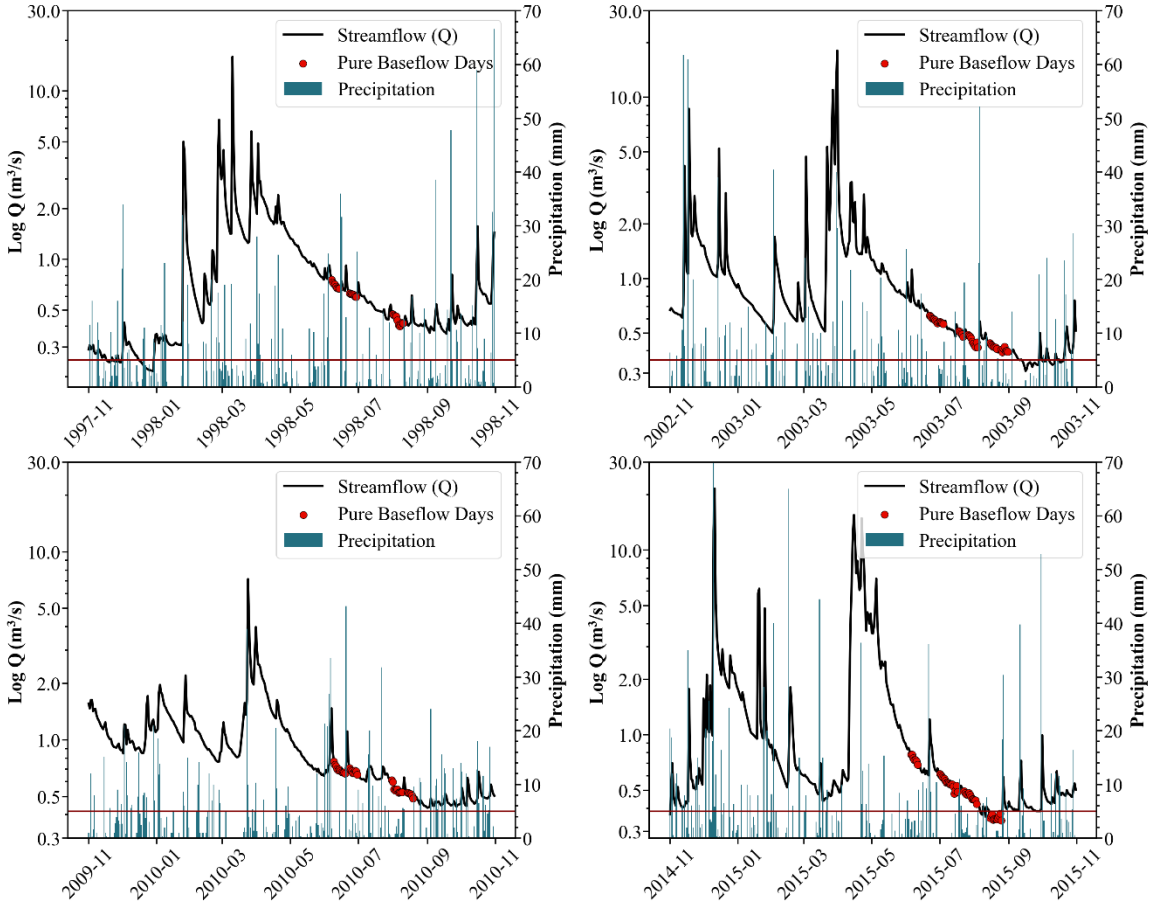

Figure 3.3 Detected drought periods within the summer months of 1998, 2003, 2010 and 2015. The red horizontal line represents the 5mm precipitation threshold.

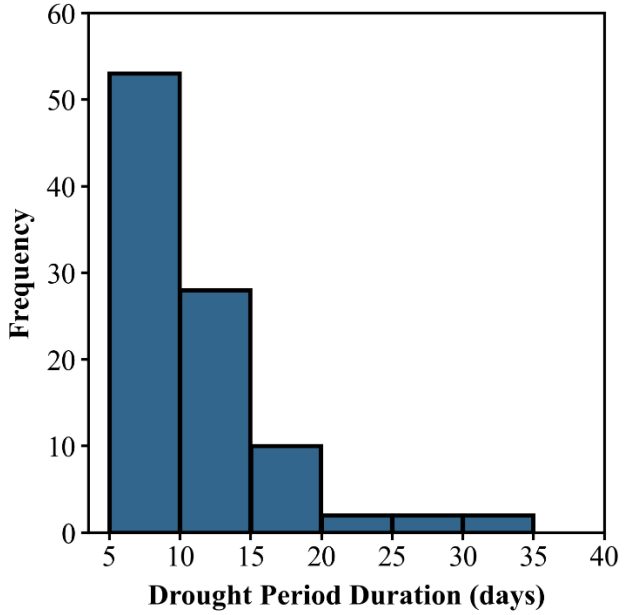

Figure 3.4 Frequency of pure baseflow drought period duration during 1995-2019.

3.4.1.3 Correlation of groundwater level with detected pure baseflow records

Groundwater levels of 13 observation wells had correlation coefficients larger than 0.5 with the streamflow during the pure baseflow periods. Four observation wells (New Zealand Road, Riverdale, Baltic, and Caledonia) demonstrated the highest correlation coefficients with 0.86, 0.84, 0.83, and 0.79, respectively. These indicate that daily baseflow in the Wilmot River Watershed is highly correlated with the same-day groundwater level in PEI. Table 3.4 reports the correlation coefficients calculated for each observation well and the data coverage over pure baseflow periods and the entire study period.

Table 3.4 Correlation coefficients of groundwater level with pure baseflow in PEI.

Observation Well	Elevation (MASL)	Distance (km)	% Obs. (1995-2019)	% Obs. (Pure baseflow)	Correlation Coeff
New Zealand Road	**43.00**	**103**	**41**	**38**	**0.86**
Riverdale	**40.00**	**38**	**69**	**68**	**0.84**
Baltic	**25.00**	**13**	**82**	**76**	**0.83**
Caledonia	**99.99**	**82**	**90**	**84**	**0.79**
Bloomfield	**42.92**	**60**	**90**	**90**	**0.73**
York	**41.00**	**44**	**61**	**63**	**0.73**
Summerside GST	**30.48**	**11**	**85**	**85**	**0.70**
Knutsford	**30.48**	**59**	**79**	**82**	**0.67**
Sleepyhollow	**12.20**	**37**	**84**	**82**	**0.66**
New Dominon	**19.93**	**40**	**84**	**87**	**0.64**
Georgetown	**9.10**	**90**	**95**	**94**	**0.59**
Souris Line Road	**57.00**	**108**	**45**	**43**	**0.56**
St Charles	**51.26**	**96**	**69**	**74**	**0.50**
Lakeside	**7.62**	**67**	**59**	**56**	**0.45**
Bear River	**30.00**	**97**	**26**	**24**	**0.25**
Souris River Road	**22.00**	**106**	**40**	**43**	**0.03**

% Obs. (Pure baseflow): Shows the percentage of data covered by each observation well during the pure baseflow periods.

In order to select a final set of observation wells for validating baseflow separation methods, a minimum correlation coefficient of 0.7 was considered to ensure a strong and meaningful linear correlation. Among all observation wells, seven showed correlation coefficients greater than the minimum. However, the New Zealand Road and Caledonia observation wells were removed from the selections due to their large distance from the Wilmot River gauge station, accompanied by either a high elevation difference or a low percentage of data coverage. Therefore, Riverdale, Baltic, Bloomfield, York, and Summerside GST were the five selected observation wells used to evaluate baseflow separation methods. The average correlation coefficient between streamflow and the five

final selected observation wells was 0.76. The distances between the Wilmot gauging station and the Summerside GST and Baltic wells were 11 and 13 km, which were reasonably close to the distance of 7.8 km between which soil moisture and tile drain were correlated with groundwater level in PEI (Jiang et al. 2011; 2019). Additionally, these monitoring wells reflect ambient water level fluctuations, as there is no intensive pumping within the adjacent vicinities.

3.4.2 Baseflow separation using standard parametrization

Figure 3.5 presents a summary of the calculated BFI (1995-2019) using the three baseflow separation methods and different filter parameters over the annual, growing season (GS), non-growing-season (NGS), and summer season periods. The long-term BFI varied from a maximum of 0.77, calculated using the LH(0.925), to a minimum of 0.62 obtained from the EK(0.97,0.66). The difference between the methods was more pronounced over the growing season. The long-term growing season BFI was as high as 0.92 for the LH(0.925), whereas the EK(0.97,0.66) calculated the smallest growing season BFI of 0.72. During the summer months, baseflow consisted of 95% and 94% of total streamflow at its highest calculated from LH(0.925) and LH(0.97), respectively, whereas the EK(0.97,0.66) and EK(0.97,0.8) estimated the baseflow to account for 74% and 84% of the total summer streamflow over the entire study period. Figure 3.6 demonstrates the streamflow and baseflow during four typical water years.

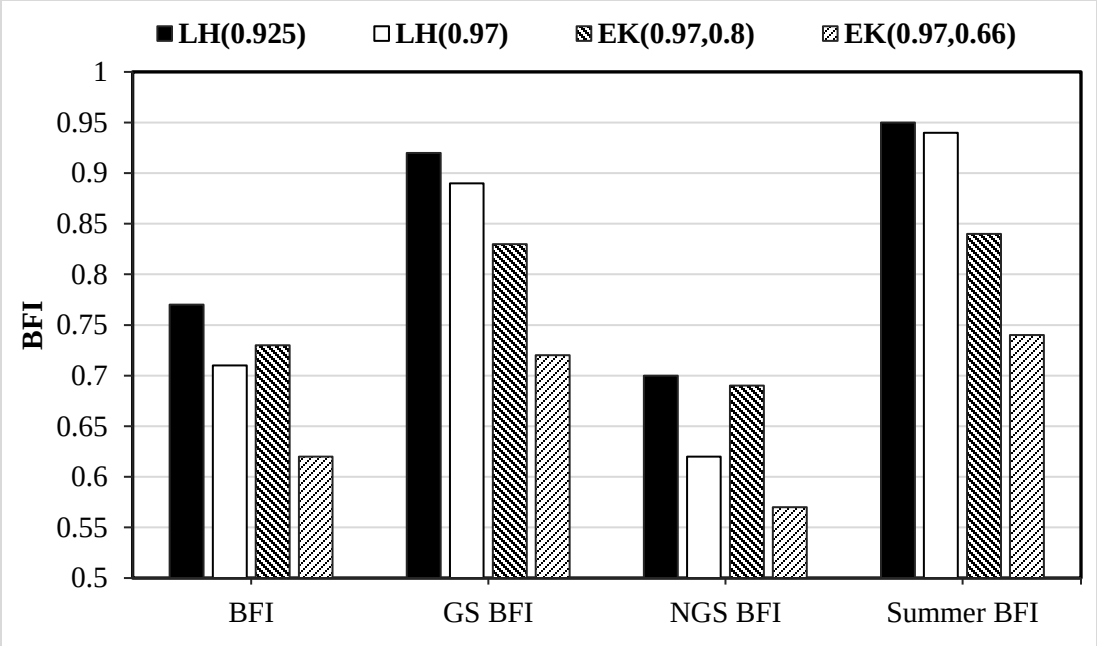

Figure 3.5 Seasonal and annual BFI, calculated over the entire study period (1995-2019).

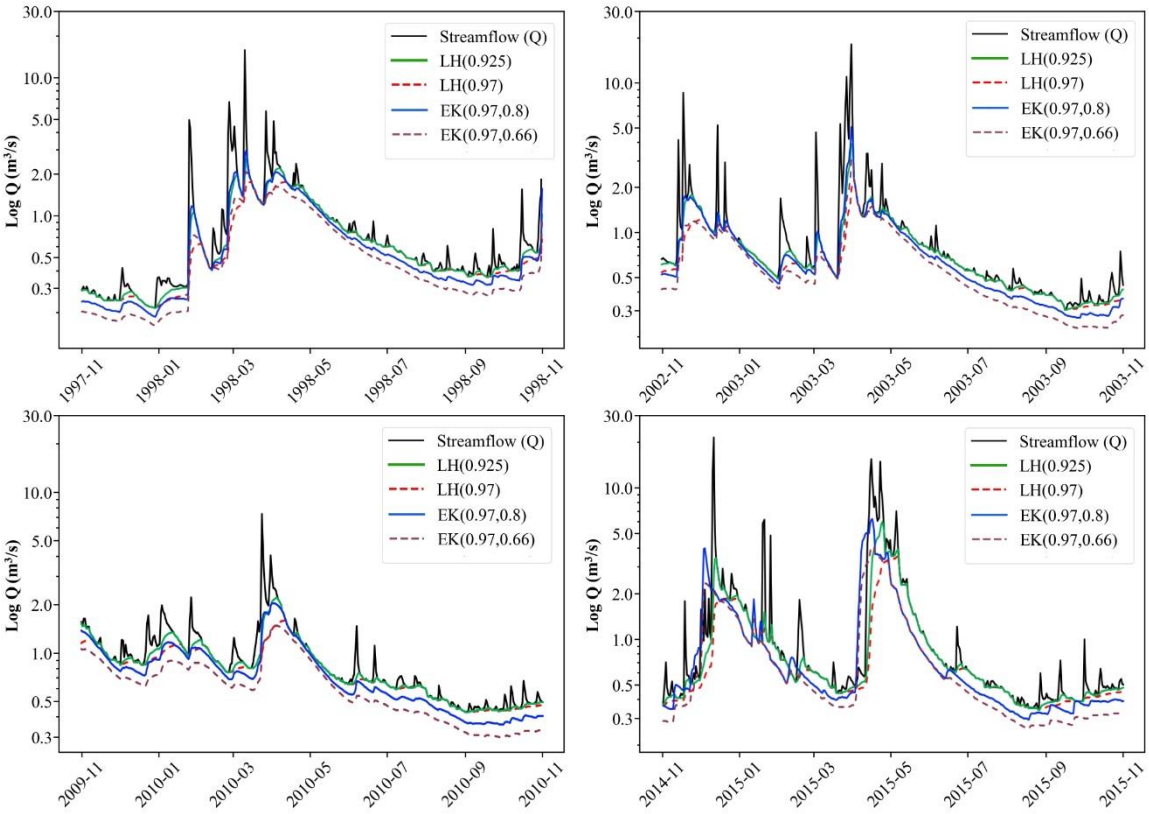

Figure 3.6 Hydrographs of Separated baseflow during four typical water years in the Wilmot River Watershed.

3.4.3 Evaluation of methods and parametrization schemes

3.4.3.1 Short-term BFI over the driest summer seasons

The Lyne and Hollick method with filter parameters of 0.925 and 0.97 produced the maximum short-term summer BFIs averaged over the four selected seasons with 0.98 and 0.97, respectively (Table 3.5). Regardless of the parameter values, the Eckard method produced lower summer BFI than the Lyne and Hollick. On average, the EK(0.97,0.8) estimated 83% of the streamflow being provided by groundwater discharge, followed by EK(0.97,0.66) with baseflow to streamflow ratios of 0.73 averaged over the four driest summer seasons. Figure 3.7 demonstrates the streamflow, separated baseflow, and monthly precipitation during the selected years with the driest summer seasons.

Table 3.5 Short-term summer BFI of the driest summer seasons.

Year	LH(0.925)	LH(0.97)	EK(0.97,0.8)	EK(0.97,0.66)
2005	**0.98**	**0.98**	**0.85**	**0.75**
2012	**0.97**	**0.97**	**0.82**	**0.72**
2013	**0.97**	**0.97**	**0.83**	**0.71**
2016	**0.98**	**0.95**	**0.83**	**0.74**
Avg.	**0.98**	**0.97**	**0.83**	**0.73**

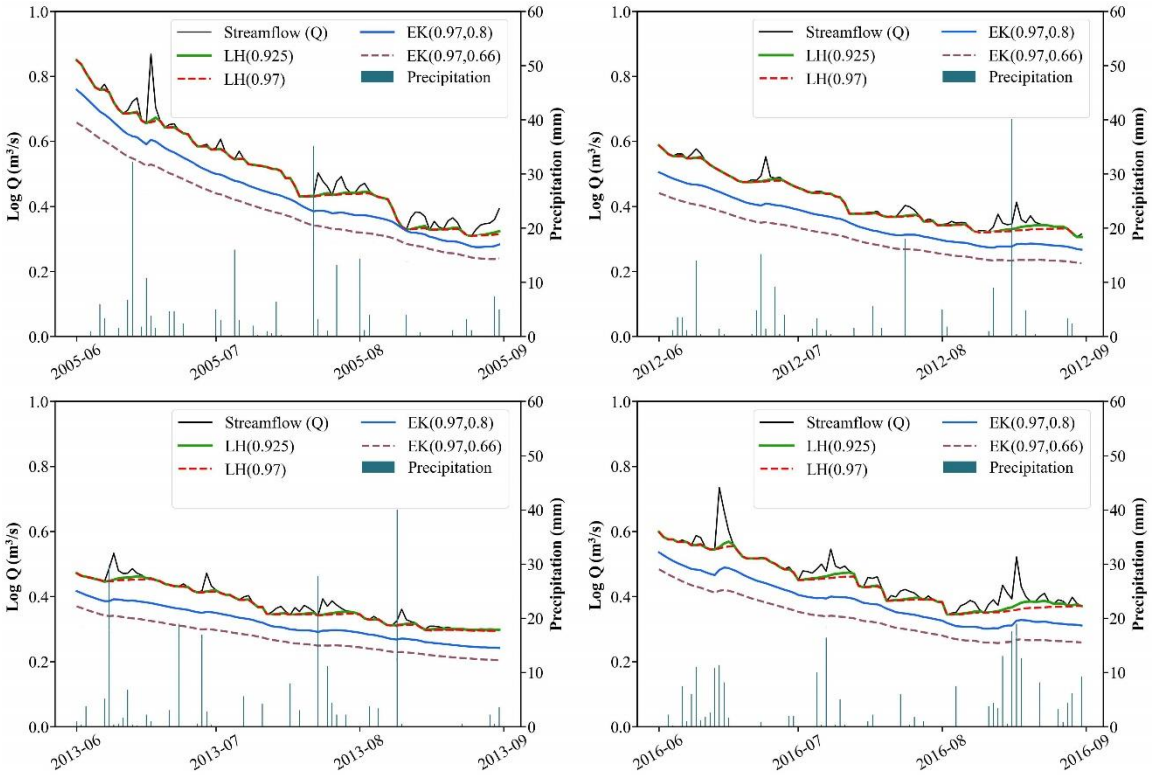

Figure 3.7 Streamflow and separated baseflow hydrographs during the driest summer seasons.

3.4.3.2 Separated baseflow during pure baseflow periods

Baseflow is expected to constitute 100% of the streamflow during the detected pure baseflow periods (i.e., BFI=1). Therefore, the streamflow records over the pure baseflow periods were used as observed baseflow, and various measures of goodness of fit were calculated to assess the performance of each method in estimating baseflow. Figure 3.8 demonstrates the linear relationship between separated baseflow and baseflow during pure baseflow periods. The separated baseflow from both LH(0.925) and LH(0.97) had the strongest linear relationship with pure baseflow records with coefficients of determination equaling 0.99 and 0.98. Both methods produced BFI values above 0.98 and percent biases below +2% indicating no tendency to over or under predicting the baseflow. The R^2,

PBIAS, and RMSE measures for the EK(0.97,0.8) were calculated as 0.79, +12%, and 0.06, respectively, corresponding to an underpredicted BFI of 0.87. The EK(0.97,0.66) baseflow estimation obtained significantly poor goodness of fit measures relative to the other methods. The R^2 and RMSE equaled 0.26 and 0.12, respectively, for the EK(0.97,0.66), with a significant underprediction of baseflow as indicated by PBIAS (+23%) and BFI (0.76). Table 3.6 represents the performance analysis results carried out for the pure baseflow periods.

Table 3.6 Evaluation results of the separated baseflow during the pure baseflow periods.

Method	**Avg. BF Q (m^3/s)**	**BFI**	**R^2**	**PBIAS**	**RMSE**
LH(0.925)	**0.495**	**0.992**	**0.995**	**0.816**	**0.010**
LH(0.97)	**0.492**	**0.985**	**0.985**	**1.465**	**0.017**
EK(0.97,0.8)	**0.438**	**0.877**	**0.792**	**12.258**	**0.064**
EK(0.97,0.66)	**0.384**	**0.769**	**0.264**	**23.143**	**0.120**

Avg. BF Q: Average daily separated baseflow of the pure baseflow days.

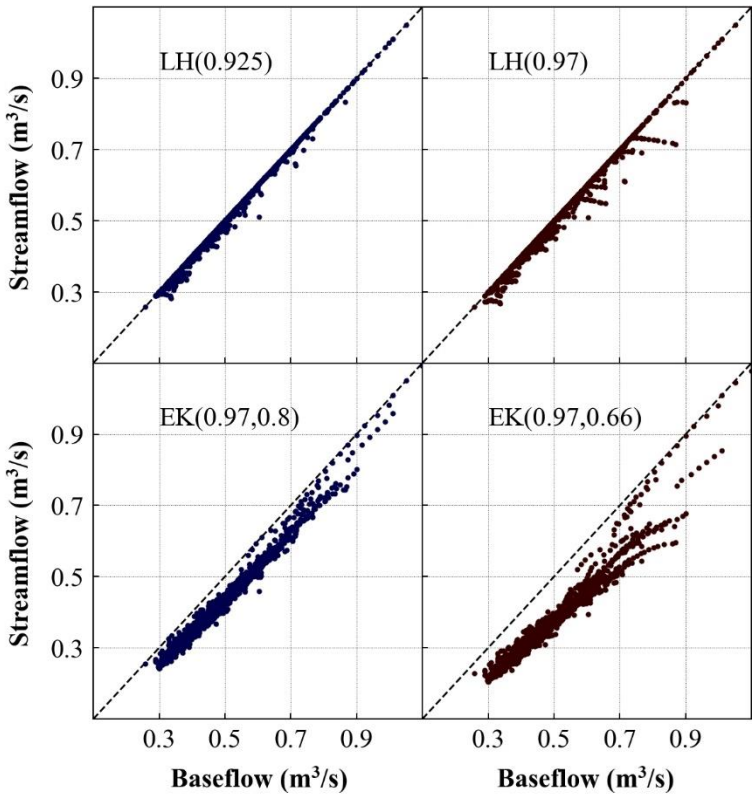

Figure 3.8 The one-on-one linear relationship between separated baseflow and streamflow during pure baseflow days.

3.4.3.3 Long-term annual and seasonal correlation of separated baseflow with groundwater level

The analysis of pure baseflow periods revealed that baseflow in the Wilmot watershed is strongly correlated to groundwater level, where the correlation coefficient was as high as 0.84 at the Riverdale well and averaged 0.77 (Table 3.4). Similarly, all baseflow separation methods demonstrated equally strong correlations (0.76 to 0.79) with groundwater level during pure baseflow periods (Table 3.7). Therefore, over the annual and seasonal periods when no baseflow observation or assumption of baseflow dominance exists, the correlation between groundwater level and separated baseflow was used to evaluate separation results. Table 3.7 shows the averaged daily correlation coefficients of the five observation wells

with separated baseflow over the entire study period (1995-2019). Correlation coefficients of baseflow separation methods with each selected observation well are reported in supplemental Table 1.

While streamflow and groundwater level were poorly correlated over the annual period (cc=0.33), the baseflow separation results produced strong annual correlations with groundwater levels. The LH(0.97) achieved the highest annual correlation coefficient of 0.75, averaged over the five observations wells, followed by LH (0.925), EK (0.97, 0.66), and EK (0.97, 0.8), with correlation coefficients being 0.7, 0.7 and 0.65, respectively. The non-growing season correlations with groundwater level followed the same order among methods as the annual period. The correlation coefficients for the LH (0.925) and LH (0.97) equaled 0.67 and 0.73, respectively, while the EK (0.97, 0.8) and EK (0.97, 0.66) separated baseflows showed to have correlation coefficients of 0.61 and 0.67. The difference in correlation with groundwater level decreased in the growing season. Growing season correlation coefficients ranged from 0.77 for LH (0.97) to 0.74 for EK(0.97, 0.8). The correlations of separated baseflow with groundwater level were consistently lower over the non-growing season for all methods. However, the Lyne and Hollick-based separation methods showed a smaller decrease. The LH(0.97) had the least difference between correlation coefficients of the growing season and non-growing season, with only a 4% difference, followed by LH(0.925) with 8%. The decrease of correlation coefficients from the growing season to the non-growing season was more pronounced for the Eckhardt methods, with EK(0.97, 0.8) and EK(0.97, 0.66) having 13 and 9% differences.

Table 3.7 Average correlation coefficients of the five selected observation wells with each baseflow separation method and parametrization scheme.

Period	LH (0.925)	LH (0.97)	EK (0.97,0.8)	EK (0.97,0.66)	Streamflow
Annual	**0.70**	**0.75**	**0.65**	**0.70**	**0.33**
NGS	**0.67**	**0.73**	**0.61**	**0.67**	**0.27**
GS	**0.75**	**0.77**	**0.74**	**0.76**	**0.52**
Pure BF	**0.77**	**0.78**	**0.78**	**0.79**	**0.76**

3.4.4 Reducing the uncertainty

3.4.4.1 Lyne and Hollick method

Both correlation of determination during pure baseflow periods and BFI over driest summers were insensitive to the filter parameter variation and were maximized almost over the entire range of the filter values (refer to Supplemental documents for more details). Therefore, the long-term annual correlation with groundwater level was the only measure considered for the LH method. The LH(0.925) produced a correlation coefficient of 0.69, considered a minimum for removing the rest of the filter parameters. Table 3.8 represents the results from each step of the uncertainty reduction procedure. The 75^{th} percentiles of the correlation coefficients were larger than 0.69 and equaled 0.74, creating a boundary to include the range filter parameters with correlation coefficients greater than the 75^{th} percentile. The new range covers all filter parameters between 0.964 and 0.991, corresponding to BFI values of 0.72 and 0.61, respectively. The average BFI over this period was calculated as 0.68. Figure 3. demonstrates the new filtered-out range with respect to the variations in BFI, correlation coefficients, and parameter values.

Table 3.8 Summary of the uncertainty reduction procedure for the Lyne and Hollick method at each step.

Step #	Step		α	BFI	DS-BFI	R^2	GWCC	count
1-2	LH(0.925)		0.925	0.774	0.975	0.994	0.698	-
3	Full range	min	0.925	0.56	0.965	0.932	0.698	71
		max	0.995	0.774	0.975	0.994	0.755	
4	75th percentile		-	-	-	-	0.747	-
5	New parameters	min	0.971	0.63	0.966	0.957	0.747	19
		max	0.989	0.711	0.97	0.984	0.755	

GWCC is the groundwater level correlation coefficient. α represents the recession constant. DS refers to the driest summer seasons.

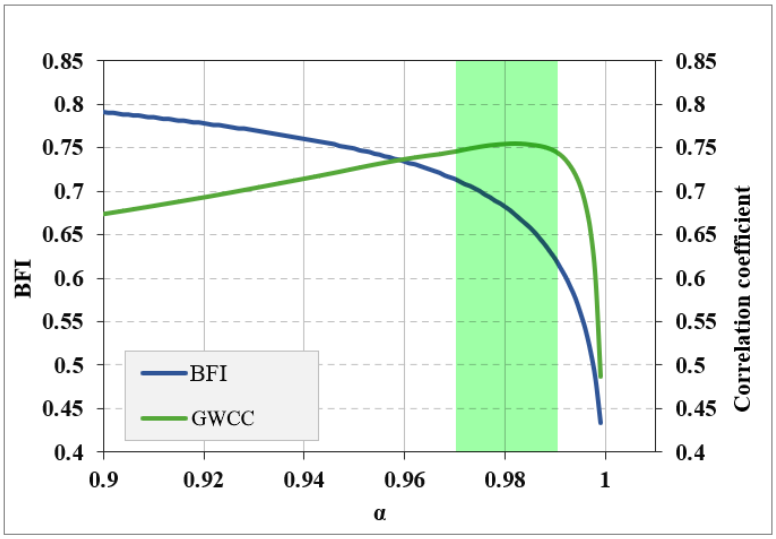

Figure 3.9 The new reduced range of likely filter parameter values (green shaded zone) for the Lyne and Hollick method and corresponding long-term annual BFI and correlation coefficient with groundwater level (GWCC).

3.4.4.2 The Eckhardt method

Although the recession constant is calculated, different methods of groundwater recession analysis (i.e., master recession analysis) can produce different values (Arnold et al. 1995;

Sujono et al. 2004; Tallaksen 1995; Whitaker et al. 2022). Therefore, both the estimated recession constant and the recommended BFImax are subject to uncertainty (refer to Supplemental documents for more details). Reducing this uncertainty is shown next. All combinations of the recession constant and BFImax that produced at least one evaluative measure lower than the EK(0.97,0.8) were removed. The 75th percentile of driest summer BFI, pure baseflow R^2, and correlation coefficient equaled 0.953, 0.955, and 0.744, respectively. In total, 42 unique combinations of BFImax and α separated the baseflow so that all evaluative measures were greater than the 75th percentiles. Figure 3.9 represents the appearance frequency of each parameter value within the remaining 42 parameter combinations. The selected BFImax ranged from 0.845 to 0.965, while the recession parameters varied from 0.995 to 0.999 at the extreme end of the initial α values. These final remaining parameters represent the new uncertain combination of filter parameters capable of achieving the highest evaluative measures, resulting in BFI ranging from 0.64 to 0.70 (Table 3.9).

Table 3.9 Summary of the uncertainty reduction procedure for the Eckhardt method at each step.

Step #	Step		a	BFImax	BFI	DS-BFI	R^2	GWCC	count
1-2	EK(0.97,0.8)		0.97	0.8	0.734	0.844	0.785	0.654	-
3	Full range	min	0.971	0.55	0.487	0.844	0.785	0.654	1135
		max	0.999	0.99	0.797	0.975	0.995	0.754	
4	75th percentile		-	-	-	0.953	0.955	0.744	-
5	New parameters	min	0.995	0.845	0.641	0.953	0.955	0.744	42
		max	0.999	0.965	0.705	0.967	0.98	0.754	

GWCC is the groundwater level correlation coefficient. α represents the recession constant.

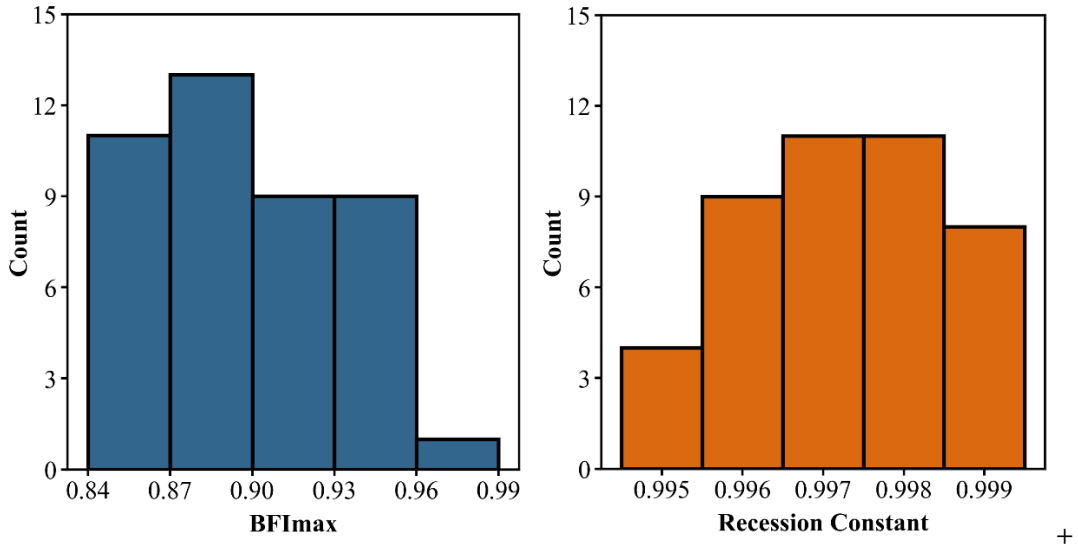

Figure 3.9 Frequency of each parameter value within the final reduced range of parameters for the Eckhardt method.

3.4.4.3 Optimizing baseflow separation

In order to achieve a single optimized estimation of baseflow, a daily average of baseflow separated using all the parameter values within the new reduced range were calculated. The optimized baseflow separations are denoted as EK(opt) and LH(opt). Table 3.10 compares the BFI and evaluative measures obtained from optimizing the two methods. Long-term BFI equaled 0.678 using both EK(opt) and LH(opt). Growing-season BFI was 0.869 for the LH(opt) and 0.863 for the EK(opt), and the non-growing season was estimated at 0.582 and 0.585 for the LH(opt) and EK(opt), respectively. The short-term BFI over the driest summer seasons, coefficient of determination for pure baseflow prediction, and long-term correlation coefficient with groundwater were calculated as 0.969, 0.975, and 0.757, respectively, for the LH(opt), and 0.961, 0.967, and 0.753, for the Ek(opt). Figure 3.10 depicts the optimized separated baseflow hydrograph during four typical water years in the Wilmot River Watershed.

Table 3.10 Baseflow and evaluative measures produced by the optimized methods.

Calculated measures		**LH (opt)**	**EK (opt)**
Baseflow index	**BFI**	**0.678**	**0.678**
	NGS-BFI	**0.582**	**0.585**
	GS-BFI	**0.869**	**0.863**
	DS-BFI*	**0.969**	**0.961**
Correlation with Groundwater	**GWCC***	**0.757**	**0.753**
	NGS-GWCC	**0.728**	**0.724**
	GS-GWCC	**0.793**	**0.791**
Pure baseflow estimation	**R^2***	**0.975**	**0.967**
	PBIAS	**1.836**	**2.422**
	BFI	**0.982**	**0.976**

***** Represents evaluative measures. DS refers to the driest summer seasons. GWCC is the groundwater level correlation coefficient.

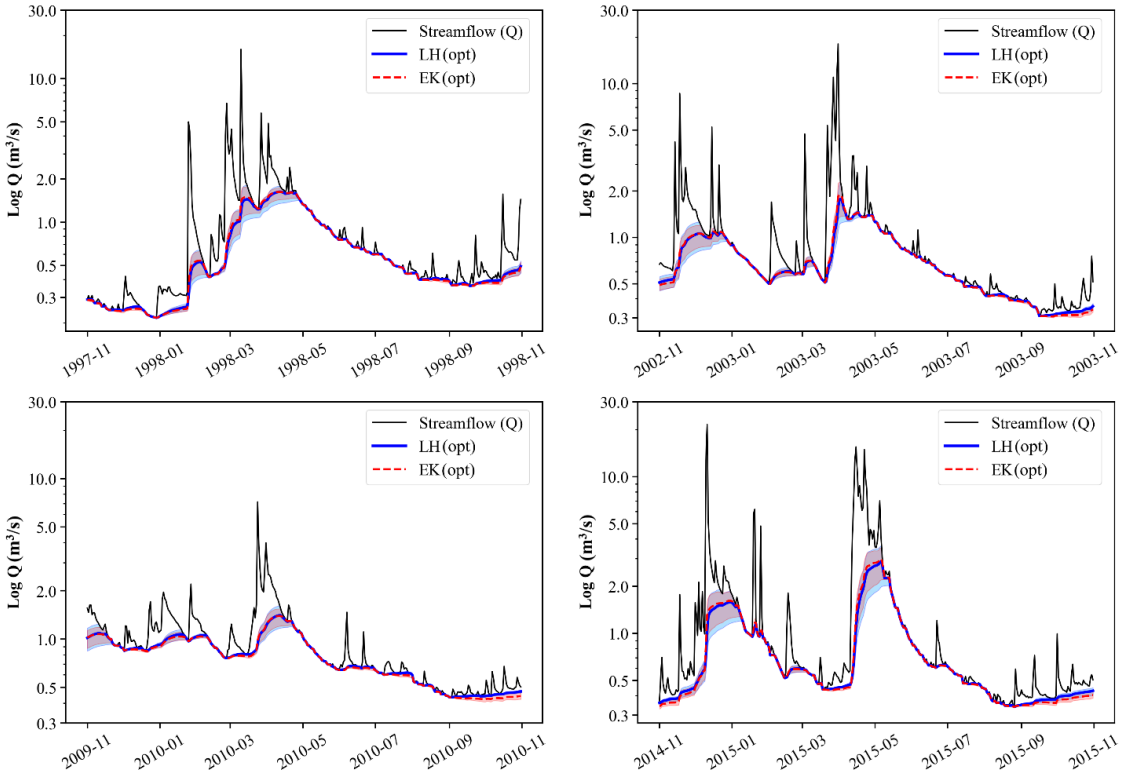

Figure 3.10 Hydrographs of separated baseflow during four typical water years obtained from the optimized parameters. The shaded areas demonstrate the maximum and minimum separated baseflow of the reduced parameter ranges.

3.5 Discussion

3.5.1 New evaluative measures

In the absence of direct baseflow measurements, three new evaluative measures were introduced to assess the performance of the baseflow separation methods. (1) The driest summer seasons: Streamflow in PEI is principally provided by ground water during dry summer months when evapotranspiration exceeds precipitation. The summer BFI, calculated over the years with the driest summer seasons, assesses baseflow separation methods and configurations at a seasonal scale. (2) Pure baseflow days: An algorithm was defined, using only precipitation data, to identify the days within summer months in which the streamflow was confidently all consisting of baseflow. A near-one coefficient of

determination indicates the performance of a baseflow separation approach on a daily scale over the entire span of the study. (3) A strong daily, linear relationship was verified between baseflow and water table using the detected drought period. The correlation between separated baseflow and water table creates a link between baseflow separation methods and the physics of the watershed. A higher correlation coefficient between separated baseflow and water table was considered as an indication of better performance in separating baseflow.

The algorithm for searching pure baseflow days detected 972 days within the summer months when streamflow was equal to baseflow. Identifying the pure baseflow periods is a critical step for optimizing baseflow separation in addition to determining the evaluative measures. The pure baseflow days enabled us to examine the credibility of groundwater fluctuations in explaining baseflow variation as the third evaluative measure as well as selecting the most relevant observation wells. Using correlation analysis between pure baseflow measurements and groundwater level readings from 16 observation wells in PEI, seven wells were strongly correlated with baseflow with correlation coefficients from 0.7 to 0.86. The analysis identified a strong daily linear relationship between the water level and baseflow. As such, the long-term correlation coefficient with the water level was used as the third measure for evaluating the performance of the methods irrespective of seasonality. Although there were no long-term observation wells in the Wilmot watershed during the study period, several monitoring wells located outside the watershed demonstrated correlation coefficients above 0.7. This strong correlation presents an opportunity to implement this methodology even if the groundwater levels within a specific watershed are not monitored. The unique opportunity is resulted from the combination of

relatively uniform geology and precipitation and negligible impacts of groundwater pumping in most watersheds across the island (Jiang et al. 2004).

3.5.2 Sensitivity and uncertainty analysis

The sensitivity analysis revealed that using a full range of possible filter parameters, the long-term BFI can range from 0.88 to 0.45 for the LH method and 0.39 to 0.99 for the EK method. The significant variation of BFI associated with parameter uncertainty in the LH and EK methods was also reported by Voutchkova et al. (2019) in a study of four snowmelt-dominated watersheds in Wyoming, US. They reported the long-term median BFI to vary as much as 0.25 to 0.84 for Buffalo Fork.

The sensitivity of BFI obtained from the LH method to the filter parameter gradually increased with the increase of parameter value and significantly steepened when the α increased over 0.96. A very similar sensitivity trend of the LH method was also reported by Voutchkova et al. (2019) in the study of snow-dominated watersheds, and by Ladson et al. (2013) in a study of rain-dominated watersheds in Australia, where the BFI gradually decreased with the increase in a and the reduction intensified significantly for parameter values greater than 0.96. Although the BFImax is generally considered less critical than α (Eckhardt 2012), in this study, the EK method was relatively insensitive to the recession constant parameter while it was lower than 0.98 the BFImax critically defined BFI over this range. For example, the BFI ranged from 0.75 to 0.73 when the recession constant varied from 0.9 to 0.98, and BFImax was set to 0.8. These observations were in agreement with the reports of Voutchkova et al. (2019), who demonstrated a significant sensitivity only for recession constants values above 0.98 when a BFImax of 0.8 was used.

Applying both LH and EK methods, the standard values of α based on recommendation (0.925) or Recession Curve analysis (0.97) did not overlap with the range in which the BFI was significantly sensitive to α, nor did they result in the highest evaluative measures. These two observations indicate parametrization errors and that the standard values not representing the most appropriate values for our studied watershed. Ladson et al. (2013) discussed that BFI estimates from the LH method are equally likely to range from 0.12 to 0.41 for a uniformly distributed selection of α between 0.987 and 0.90, respectively. They suggested that in the presence of some additional information to narrow down the range to select the α from, the uncertainty can be reduced. Similarly, Voutchkova et al. (2019) demonstrated that the BFI could be highly sensitive to parameter values and subjected to great uncertainty in snow-dominated watersheds. Therefore, the single BFI obtained from standard parametrization does not necessarily reflect the best solution. They concluded that uncertainty evaluation and reducing the range of possible filter parameters is critical in applying these methods for snowmelt-dominated systems.

3.5.3 Reducing the uncertainty

In order to reduce the uncertain range of parameter values and optimize the selection of parameters, we proposed a new procedure. This method obtains the information required to reduce the variation of possible parameter values from maximizing the new evaluative measures.

Evaluative measures that reflect baseflow-dominated periods (i.e., the pure baseflow periods and driest summer BFI) are not helpful for evaluating and adjusting the LH method. This is because baseflow days constantly increase with the decrease of the filter parameter value. In other words, the smallest filter parameter value (near zero) will always result in

the highest BFI during baseflow-dominated periods. The groundwater level correlation with baseflow was significantly responsive to over and under adjustment of the filter parameter and, therefore, appropriate for evaluation and reducing the uncertainty of the LH method. However, each evaluative measure was maximized over a wide range of parameter values for the EK method. Hence, to reduce the uncertain combination of parameters, all three measures needed to be used to constrain the variation in both parameters of the EK method.

The 75th percentile value of each evaluative measure was proposed as a minimum requirement for removing the parameters with poor performance and separating a smaller range of more possible parameter values. As a result, the range of possible BFI values was narrowed from 0.56-0.77 to 0.63-0.71 for the LH method and reduced from 0.48-0.79 to 0.64-0.7 for the EK method. The procedure led to a considerably larger reduction of the uncertainty range of BFI for the EK method than for the LH. This can be attributed to two reasons. Firstly, the three evaluative measures were applied to the EK method, whereas the LH method only benefited from the correlation coefficient with groundwater level. Therefore, more information was available to identify the better-performing parameters of the Ek method. Secondly, the reduced set of parameters by the 75th percentiles was composed of 4% of the full range that they were filtered out from for the EK method, which was much lower than the LH method by 27%.

Although selecting the 75th percentile is somehow an arbitrary choice and can introduce some levels of uncertainty, it at least maximizes the evaluative measures that represent meaningful linkages to the responses of a specific watershed instead of presumed or recommended parameter values.

3.5.4 Optimizing baseflow separation

While the optimized separated baseflow (the daily average of the baseflow separated by the reduced range of parameters) demonstrated significant improvements over the recommended parameterization of these methods, both LH(opt) and EK(opt) produced almost identical BFI and evaluative measures.

The driest summer BFI and R^2 of pure baseflow predictions for the EK(opt) equaled 0.96 and 0.97, respectively, which demonstrates a great improvement compared to those obtained from the EK(0.97,0.8) as 0.83 and 0.79 (Table 12). The long-term correlation with groundwater level was also improved from 0.65 to 0.75 for EK(0.97,0.8) and EK(opt), respectively. While the correlation coefficient with groundwater level improved from 0.7 by LH(0.925) to 0.75 from LH(opt), the other evaluative measures showed little change. The optimization of both methods suggested lower long-term baseflow estimations than the recommended parametrization of these methods. The EK(opt) demonstrated a lower long-term BFI of 0.68 compared to the recommended EK(0.97,0.8), with BFI equaling 0.73. The reduction was more significant for the LH method, in which the optimization reduced the BFI from 0.77 to 0.68 for LH(0.925) and LH(opt), respectively.

These results suggest that while the recommended parameterization of the Lyne and Hollick method (i.e., LH(0.925)) produced much more reliable evaluative measures compared to those of the Eckhardt method (i.e., EK(0.97,0.8)), which may be susceptible to overestimation of BFI. In addition, the results indicate that among all the initially tested methods and parameters, the Lyne and Hollick method with the recession constant as its filter parameter produced the most similar results to the optimized methods. Hence, it is the most reliable method to separate baseflow in the absence of optimization or calibration

techniques. Moreover, our results demonstrated the extreme sensitivity of the Eckhardt method to the recession constant over a narrow range (0.98 to 1) and BFImax, introducing significant uncertainty. The results suggest that applying the Eckhardt method with recommended parametrization schemes may be unreliable in this hydrogeological setup and should only be used when strict evaluative data is unavailable. Figure 3.11 compares the optimized separated baseflow hydrograph with the standard parametrization schemes during four typical water years.

Table 12. Comparison of long-term annual BFI, seasonal BFI, and evaluative measures of the optimized methods with initial parameterization schemes

	BFI	**DS-BFI**	**GWCC**	**R^2**
LH(opt)	**0.68**	**0.97**	**0.753**	**0.97**
LH(0.925)	**0.77**	**0.98**	**0.698**	**0.99**
LH(0.97)	**0.71**	**0.97**	**0.748**	**0.98**
EK(opt)	**0.68**	**0.96**	**0.757**	**0.97**
EK(0.97,0.8)	**0.73**	**0.83**	**0.654**	**0.79**
EK(0.97,0.66)	**0.62**	**0.73**	**0.701**	**0.26**

DS refers to the driest summer seasons. GWCC is the groundwater level correlation coefficient.

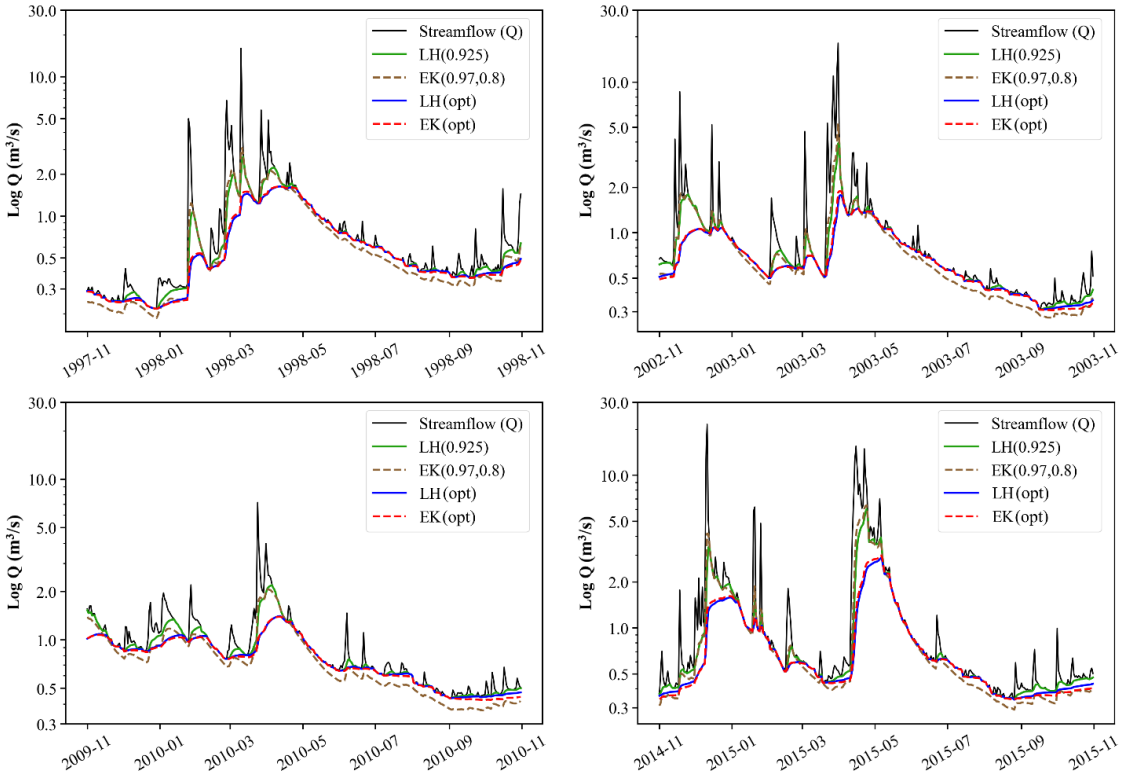

Figure 3.11 Hydrographs of separated baseflow during four typical water years obtained from the optimized parameters compared to standard parametrization.

3.5.5 Seasonal performance of the optimized methods

Both optimized methods produced identical growing season and non-growing season correlation coefficients and BFI. Both LH(0.97) and EK(0.97,0.8), as recommended parametrizations, were over-predicting the BFI during the wet periods by 12 and 11%, respectively (Table 3.11). However, the difference during the growing season was less pronounced, with an overestimation of 6% by LH(0.925) and an underestimation of 3% made by EK(0.97,0.8). Simultaneously, the recommended parametrization schemes lead to lower correlations with groundwater level over both growing and non-growing seasons, with the latter having more difference than the optimized methods. Two of the three evaluative measures solely control for the driest periods of the year. These observations in

the non-growing season may suggest that a higher correlation with groundwater level could also verify a more accurate baseflow separation over the wet seasons.

Table 3.11 Comparison of seasonal BFI and groundwater correlation coefficient produced by optimized methods with initial parameterization schemes.

	GS-GWCC	GS-BFI	NGS- GWCC	NGS-BFI
LH(opt)	**0.79**	**0.86**	**0.73**	**0.58**
LH(0.925)	**0.75**	**0.92**	**0.67**	**0.70**
LH(0.97)	**0.77**	**0.89**	**0.73**	**0.62**
EK(opt)	**0.79**	**0.86**	**0.72**	**0.58**
EK(0.97,0.8)	**0.74**	**0.83**	**0.61**	**0.69**
EK(0.97,0.66)	**0.76**	**0.72**	**0.67**	**0.57**

GS-GWCC and NGS-GWCC are the groundwater level correlation coefficient over growing and non-growing seasons, respectively.

3.6 Conclusion

Automated baseflow separation techniques are commonly applied to multiple watersheds with significant spatio-temporal variations based on previously recommended parameters. Here we implemented three low-pass filter methods using various recommended and alternative standard parameterization schemes, aiming to evaluate their performance and suggest the most suitable methods and parameters for the hydrogeological setting in PEI. In the absence of calibration data (e.g., conductivity), we proposed a new approach to evaluate the performance of each method. The approach includes two criteria: (a) the linear correlation of the daily separated baseflow with groundwater level and (b) the ability of each method to predict maximum baseflow during dry periods when streamflow is entirely

fed by groundwater discharge. The results demonstrated that the recommended and alternative parameterization of the Eckhardt method significantly under-predicted the baseflow during dry, baseflow-dominated periods. However, the Lyne and Hollick method produced excellent near-1 BFI during dry periods and high correlation coefficients of greater than 0.7 with groundwater level, with filter parameter set to the recommended value (0.925) or set to groundwater recession constant (0.97).

Finally, we introduced a new procedure in which the evaluative measures are used to reduce the uncertain range of parameters and optimize baseflow separation. The optimization of each method was to maximize the relevant evaluative criteria. LH(opt) and EK(opt) estimated identical BFI values of 0.68 and nearly identical evaluative measure values. Hence, both methods can produce accurate baseflow separation if it is optimized. This study demonstrated the ability of readily available data to identify and minimize inaccurate baseflow estimates resulting from inadequate parametrization. Our approach enables efficient optimization of baseflow separation even when direct calibration data is not at hand.

While the LH method with recommended filter parameter of 0.925 tended to overestimate BFI (0.77), the filter parameter of 0.97 produced the closest BFI (0.71) and evaluative measures to the optimized separated baseflow. Therefore, the Lyne and Hollick method with recession constant set as its filter parameter was the most suitable among the tested standard methods for separating baseflow in the Wilmot River Watershed. On the other hand, the optimum parameters for the Eckhart were all within the very extreme end of values for each parameter and did not overlap with any of the obtained parameter values based on recommendations. Therefore, we suggest that applying the Eckhardt method

without optimization should be avoided in the hydrogeological setting of PEI. While this study optimized the parameters of the digital filter methods, it also demonstrated a new framework that can be used to optimize baseflow separation using other methods with variable input parameters.

Bibliography

Alberto, A., A. St-Hilaire, S.C. Courtenay, and M.R. Van Den Heuvel. 2016. Monitoring stream sediment loads in response to agriculture in Prince Edward Island, Canada, *Environmental monitoring and assessment*, 188: 1-15.

Arnold, J., P. Allen, R. Muttiah, and G. Bernhardt. 1995. Automated base flow separation and recession analysis techniques, *Groundwater*, 33: 1010-18.

Arnold, J.G., and P.M. Allen. 1999. Automated methods for estimating baseflow and ground water recharge from streamflow records 1, *JAWRA Journal of the American Water Resources Association*, 35: 411-24.

Beck, H.E., A.I. van Dijk, D.G. Miralles, R.A. De Jeu, L.S. Bruijnzeel, T.R. McVicar, and J. Schellekens. 2013. Global patterns in base flow index and recession based on streamflow observations from 3394 catchments, *Water Resources Research*, 49: 7843-63.

Cartwright, I., B. Gilfedder, and H. Hofmann. 2014. Contrasts between estimates of baseflow help discern multiple sources of water contributing to rivers, *Hydrology and Earth System Sciences*, 18: 15-30.

Cartwright, I., and M.P. Miller. 2021. Temporal and spatial variations in river specific conductivity: Implications for understanding sources of river water and hydrograph separations, *Journal of Hydrology*, 593: 125895.

Cartwright, I., and U. Morgenstern. 2018. Using tritium and other geochemical tracers to address the “old water paradox” in headwater catchments, *Journal of Hydrology*, 563: 13-21.

Cey, E.E., D.L. Rudolph, G.W. Parkin, and R. Aravena. 1998. Quantifying groundwater discharge to a small perennial stream in southern Ontario, Canada, *Journal of Hydrology*, 210: 21-37.

Chapman, T. 1999. A comparison of algorithms for stream flow recession and baseflow separation, *Hydrological Processes*, 13: 701-14.

Chapman, T.G. 1991. Comment on “Evaluation of automated techniques for base flow and recession analyses” by RJ Nathan and TA McMahon, *Water Resources Research*, 27: 1783-84.

Danielescu, S., and K.T. MacQuarrie. 2011. Nitrogen loadings to two small estuaries, Prince Edward Island, Canada: a 2-year investigation of precipitation, surface water and groundwater contributions, *Hydrological Processes*, 25: 945-57.

Devito, K., A. Hill, and N. Roulet. 1996. Groundwater-surface water interactions in headwater forested wetlands of the Canadian Shield, *Journal of Hydrology*, 181: 127-47.

Duncan, H.P. 2019. Baseflow separation–A practical approach, *Journal of Hydrology*, 575: 308-13.

Eckhardt, K. 2005. How to construct recursive digital filters for baseflow separation, *Hydrological Processes: An International Journal*, 19: 507-15.

Eckhardt, K. 2008. A comparison of baseflow indices, which were calculated with seven different baseflow separation methods, *Journal of Hydrology*, 352: 168-73.

Eckhardt, K. 2012. Analytical sensitivity analysis of a two parameter recursive digital baseflow separation filter, *Hydrology and Earth System Sciences*, 16: 451-55.

Edwards, L., J.R. Burney, M. Brimacombe, and A.H. MacRae. 2008. Potato Land Use and Nitrate Runoff Characteristics of Two Subcatchments of the Wilmot River Watershed, Prince Edward Island (PEI), Canada, *Water Quality Research Journal*, 43: 121-28.

Francis, R.M. 1989. Hydrogeology of the Winter River Basin-Prince Edward Island. (Water Resources Branch, Department of the Island, Prince Edward Island).

Furey, P.R., and V.K. Gupta. 2001. A physically based filter for separating base flow from streamflow time series, *Water Resources Research*, 37: 2709-22.

Graszkiewicz, Z., R. Murphy, P. Hill, and R. Nathan. 2011. Review of techniques for estimating the contribution of baseflow to flood hydrographs. In *Proceedings of the 34th World Congress of the International Association for HydroEnvironment Research and Engineering: 33rd Hydrology and Water Resources Symposium and 10th Conference on Hydraulics in Water Engineering. Engineers Australia*, 138.

Grizard, P. 2013. 'Modeling nitrate loading from watersheds to coastal waters of the Northumberland Strait', University of New Brunswick.

Gupta, H.V., S. Sorooshian, and P.O. Yapo. 1999. Status of automatic calibration for hydrologic models: Comparison with multilevel expert calibration, *Journal of Hydrologic Engineering*, 4: 135-43.

Guzmán, P., O. Batelaan, M. Huysmans, and G. Wyseure. 2015. Comparative analysis of baseflow characteristics of two Andean catchments, Ecuador, *Hydrological Processes*, 29: 3051-64.

Hagedorn, B. 2020. Hydrograph separation through multi objective optimization: Revealing the importance of a temporally and spatially constrained baseflow solute source, *Journal of Hydrology*, 590: 125349.

Halford, K.J., and G.C. Mayer. 2000. Problems associated with estimating ground water discharge and recharge from stream-discharge records, *Groundwater*, 38: 331-42.

Howcroft, W., I. Cartwright, and D.I. Cendón. 2019. Residence times of bank storage and return flows and the influence on river water chemistry in the upper Barwon River, Australia, *Applied Geochemistry*, 101: 31-41.

Huyck, A.A., V.R. Pauwels, and N.E. Verhoest. 2005. A base flow separation algorithm based on the linearized Boussinesq equation for complex hillslopes, *Water Resources Research*, 41.

Jiang, Y., M. Ramsay, F. Meng, and T. Stetson. 2021. Characterizing potato yield responses to water supply in Atlantic Canada's humid climate using historical yield and weather data: Implications for supplemental irrigation, *Agricultural Water Management*, 255: 107047.

Jiang, Y., and G. Somers. 2009. Modeling effects of nitrate from non-point sources on groundwater quality in an agricultural watershed in Prince Edward Island, Canada, *Hydrogeology Journal*, 17: 707-24.

Jiang, Y., and G. Somers. 2011. Watershed evaluation of beneficial management practices (WEBs) in the Souris River Watershed, Prince Edward Island: Site hydrogeology. In *Proceedings of Joint Conference of the Canadian Quaternary Association (CANQUA)*. Canadian Chapter of the International Association of Hydrogeologists Quebec City.

Jiang, Y., G. Somers, and J. Mutch. 2004. Application of numerical modeling to groundwater assessment and management in Prince Edward Island.

Kang, S., H. Lin, W.J. Gburek, G.J. Folmar, and B. Lowery. 2008. Baseflow nitrate in relation to stream order and agricultural land use, *Journal of environmental quality*, 37: 808-16.

Ladson, A.R., R. Brown, B. Neal, and R. Nathan. 2013. A standard approach to baseflow separation using the Lyne and Hollick filter, *Australasian Journal of Water Resources*, 17: 25-34.

Li, L., H.R. Maier, D. Partington, M.F. Lambert, and C.T. Simmons. 2014. Performance assessment and improvement of recursive digital baseflow filters for catchments with different physical characteristics and hydrological inputs, *Environmental Modelling & Software*, 54: 39-52.

Liang, K., Y. Jiang, J. Qi, K. Fuller, J. Nyiraneza, and F.-R. Meng. 2020. Characterizing the impacts of land use on nitrate load and water yield in an agricultural watershed in Atlantic Canada, *Science of the Total Environment*, 729: 138793.

Liao, S.L., M. Savard, G. Somers, D. Paradis, and Y. Jiang. 2005. Preliminary results from water-isotope characterization of groundwater, surface water, and precipitation in the Wilmot River watershed, Prince Edward Island. (Natural Resources Canada, Geological Survey of Canada).

Lim, K.J., B.A. Engel, Z. Tang, J. Choi, K.S. Kim, S. Muthukrishnan, and D. Tripathy. 2005. Automated web GIS based hydrograph analysis tool, WHAT 1, *JAWRA Journal of the American Water Resources Association*, 41: 1407-16.

Lin, K., S. Guo, W. Zhang, and P. Liu. 2007. A new baseflow separation method based on analytical solutions of the Horton infiltration capacity curve, *Hydrological Processes: An International Journal*, 21: 1719-36.

Lott, D.A., and M.T. Stewart. 2016. Base flow separation: A comparison of analytical and mass balance methods, *Journal of Hydrology*, 535: 525-33.

Lyne, V., and M. Hollick. 1979. Stochastic time-variable rainfall-runoff modelling. In *Institute of Engineers Australia National Conference*, 89-93. Institute of Engineers Australia Barton, Australia.

Lyu, H., C. Xia, J. Zhang, and B. Li. 2020. Key challenges facing the application of the conductivity mass balance method: a case study of the Mississippi River basin, *Hydrology and Earth System Sciences*, 24: 6075-90.

Mau, D.P., and T.C. Winter. 1997. Estimating ground-water recharge from streamflow hydrographs for a small mountain watershed in a temperate humid climate, New Hampshire, USA, *Groundwater*, 35: 291-304.

McCallum, J.L., P.G. Cook, P. Brunner, and D. Berhane. 2010. Solute dynamics during bank storage flows and implications for chemical base flow separation, *Water Resources Research*, 46.

Müller, K., M. Deurer, H. Hartmann, M. Bach, M. Spiteller, and H.-G. Frede. 2003. Hydrological characterisation of pesticide loads using hydrograph separation at different scales in a German catchment, *Journal of Hydrology*, 273: 1-17.

Nathan, R.J., and T.A. McMahon. 1990. Evaluation of automated techniques for base flow and recession analyses, *Water Resources Research*, 26: 1465-73.

Nejadhashemi, A.P., A. Shirmohammadi, and H.J. Montas. 2003. Evaluation of streamflow partitioning methods. In *2003 ASAE Annual Meeting*, 1. American Society of Agricultural and Biological Engineers.

Paradis, D., J.-M. Ballard, R. Lefebvre, and M.M. Savard. 2018. Multi-scale nitrate transport in a sandstone aquifer system under intensive agriculture, *Hydrogeology Journal*, 26: 511-31.

Paradis, D., J. Ballard, M. Savard, R. Lefebvre, Y. Jiang, G. Somers, S. Liao, and C. Rivard. 2006. Impact of agricultural activities on nitrates in ground and surface water in the Wilmot Watershed, PEI, Canada. In *59th Canadian Geotechnical Conference and the 7th joint CGS/IAH-CNC Conference, Vancouver*, 1-4.

Partington, D., P. Brunner, C. Simmons, A. Werner, R. Therrien, H. Maier, and G. Dandy. 2012. Evaluation of outputs from automated baseflow separation methods against simulated baseflow from a physically based, surface water-groundwater flow model, *Journal of Hydrology*, 458: 28-39.

Piggott, A.R., S. Moin, and C. Southam. 2005. A revised approach to the UKIH method for the calculation of baseflow/Une approche améliorée de la méthode de l'UKIH pour le calcul de l'écoulement de base, *Hydrological sciences journal*, 50.

Pinder, G.F., and J.F. Jones. 1969. Determination of the ground-water component of peak discharge from the chemistry of total runoff, *Water Resources Research*, 5: 438-45.

Rammal, M., P. Archambeau, S. Erpicum, P. Orban, S. Brouyère, M. Pirotton, and B. Dewals. 2018. An Operational Implementation of Recursive Digital Filter for Base Flow Separation, *Water Resources Research*, 54: 8528-40.

Rutledge, A. 2005. The appropriate use of the Rorabaugh model to estimate ground water recharge, *Ground Water*, 43: 292-94.

Rutledge, A.T. 1998. Computer programs for describing the recession of ground-water discharge and for estimating mean ground-water recharge and discharge from streamflow records: Update. (US Department of the Interior, US Geological Survey).

Saraiva Okello, A.M.L., S. Uhlenbrook, G.P. Jewitt, I. Masih, E.S. Riddell, and P. Van der Zaag. 2018. Hydrograph separation using tracers and digital filters to quantify runoff components in a semi-arid mesoscale catchment, *Hydrological Processes*, 32: 1334-50.

Savard, M.M., G. Somers, A. Smirnoff, D. Paradis, E. van Bochove, and S. Liao. 2010. Nitrate isotopes unveil distinct seasonal N-sources and the critical role of crop residues in groundwater contamination, *Journal of Hydrology*, 381: 134-41.

Schilling, K., and Y.-K. Zhang. 2004. Baseflow contribution to nitrate-nitrogen export from a large, agricultural watershed, USA, *Journal of Hydrology*, 295: 305-16.

Schilling, K.E., and D.S. Lutz. 2004. RELATION OF NITRATE CONCENTRATIONS TO BASEFLOW IN THE RACCOON RIVER, IOWA 1, *JAWRA Journal of the American Water Resources Association*, 40: 889-900.

Schwartz, S.S. 2007. Automated Algorithms for Heuristic Base-Flow Separation 1, *JAWRA Journal of the American Water Resources Association*, 43: 1583-94.

Sloto, R.A., and M.Y. Crouse. 1996. HYSEP: A computer program for streamflow hydrograph separation and analysis, *Water-resources investigations report*, 96: 4040.

Smakhtin, V.U. 2001. Low flow hydrology: a review, *Journal of Hydrology*, 240: 147-86.

Stewart, M., J. Cimino, and M. Ross. 2007. Calibration of base flow separation methods with streamflow conductivity, *Groundwater*, 45: 17-27.

Sujono, J., S. Shikasho, and K. Hiramatsu. 2004. A comparison of techniques for hydrograph recession analysis, *Hydrological Processes*, 18: 403-13.

Tallaksen, L. 1995. A review of baseflow recession analysis, *Journal of Hydrology*, 165: 349-70.

Tan, S.B., E.Y.-M. Lo, E.B. Shuy, L.H. Chua, and W.H. Lim. 2009. Hydrograph separation and development of empirical relationships using single-parameter digital filters, *Journal of Hydrologic Engineering*, 14: 271-79.

Van de Poll, H. 1981. Report on the geology of Prince Edward Island, PEI Department of Tourism, Industry and Energy, Charlottetown, PEI, Canada.

Villarini, G., C.S. Jones, and K.E. Schilling. 2016. Soybean area and baseflow driving nitrate in Iowa's Raccoon River, *Journal of environmental quality*, 45: 1949-59.

Voutchkova, D.D., S.N. Miller, and K.G. Gerow. 2019. Parameter sensitivity of automated baseflow separation for snowmelt-dominated watersheds and new filtering procedure for determining end of snowmelt period, *Hydrological Processes*, 33: 876-88.

Werner, A.D., M.R. Gallagher, and S.W. Weeks. 2006. Regional-scale, fully coupled modelling of stream–aquifer interaction in a tropical catchment, *Journal of Hydrology*, 328: 497-510.

Whitaker, A.C., S.N. Chapasa, C. Sagras, U. Theogene, R. Veremu, and H. Sugiyama. 2022. Estimation of baseflow recession constant and regression of low flow indices in eastern Japan, *Hydrological sciences journal*, 67: 191-204.

Xie, J., X. Liu, K. Wang, T. Yang, K. Liang, and C. Liu. 2020. Evaluation of typical methods for baseflow separation in the contiguous United States, *Journal of Hydrology*, 583: 124628.

Yu, Z., and F.W. Schwartz. 1999. Automated calibration applied to watershed-scale flow simulations, *Hydrological Processes*, 13: 191-209.

Zebarth, B.J., S. Danielescu, J. Nyiraneza, M.C. Ryan, Y. Jiang, M. Grimmett, and D.L. Burton. 2015. Controls on nitrate loading and implications for BMPs under intensive potato production systems in Prince Edward Island, Canada, *Groundwater Monitoring & Remediation*, 35: 30-42.

Zhang, J., Y. Zhang, J. Song, and L. Cheng. 2017. Evaluating relative merits of four baseflow separation methods in Eastern Australia, *Journal of Hydrology*, 549: 252-63.

Zhang, R., Q. Li, T.L. Chow, S. Li, and S. Danielescu. 2013. Baseflow separation in a small watershed in New Brunswick, Canada, using a recursive digital filter calibrated with the conductivity mass balance method, *Hydrological Processes*, 27: 2659-65.

3.7 Supplementary documents

Supplemental table 1. Correlation coefficients of each selected observation well with each baseflow separation method and parametrization schemes.

Period	Obs. Well	LH (0.925)	LH (0.97)	EK (0.970.8)	EK (0.970.66)	Q
Annual	**Baltic**	**0.78**	**0.83**	**0.74**	**0.79**	**0.39**
	Bloomfield	**0.71**	**0.75**	**0.67**	**0.71**	**0.34**
	Riverdale	**0.80**	**0.78**	**0.78**	**0.79**	**0.46**
	SummersideGST	**0.50**	**0.60**	**0.45**	**0.51**	**0.17**
	York	**0.69**	**0.79**	**0.63**	**0.71**	**0.27**
NGS	**Baltic**	**0.76**	**0.81**	**0.71**	**0.76**	**0.34**
	Bloomfield	**0.65**	**0.67**	**0.59**	**0.63**	**0.26**
	Riverdale	**0.76**	**0.72**	**0.74**	**0.75**	**0.41**
	SummersideGST	**0.59**	**0.70**	**0.51**	**0.59**	**0.19**
	York	**0.60**	**0.73**	**0.52**	**0.62**	**0.16**
GS	**Baltic**	**0.79**	**0.81**	**0.79**	**0.79**	**0.50**
	Bloomfield	**0.76**	**0.79**	**0.76**	**0.76**	**0.57**
	Riverdale	**0.83**	**0.82**	**0.84**	**0.82**	**0.65**
	SummersideGST	**0.59**	**0.65**	**0.58**	**0.62**	**0.39**
	York	**0.76**	**0.79**	**0.77**	**0.79**	**0.50**
Pure BF	**Baltic**	**0.83**	**0.84**	**0.84**	**0.86**	**0.83**
	Bloomfield	**0.73**	**0.74**	**0.73**	**0.72**	**0.73**
	Riverdale	**0.84**	**0.85**	**0.85**	**0.85**	**0.84**
	SummersideGST	**0.69**	**0.70**	**0.71**	**0.73**	**0.70**
	York	**0.73**	**0.76**	**0.76**	**0.81**	**0.73**

3.7.1 Parameter sensitivity and uncertainty analysis

In order to quantify the uncertainty of baseflow separation and relate it to the uncertainty of the parameters, a sensitivity analysis was conducted over the entire study period (1995-2019). For this purpose, the products of baseflow separation such as BFI and evaluative measures, were calculated using uniform parameter distribution spanned over a full range of what we considered reasonable.

3.7.1.1 Lyne and Hollick

Sensitivity analysis was carried out by generating 500 uniformly distributed filter parameters (α) with values between 0.5 to 1 and an increasing step of 0.001. Figure 3.13 plots the BFI response to the variations of the filter parameter. BFI was highest (0.88) when the lowest value was assigned to the filter parameter (α =0.5). BFI decreased gradually with the increase of α before 0.9, where BFI equaled 0.79 and started declining at a higher rate. Once the α increased above 0.98, BFI dropped rapidly until it reached the minimum of 0.45, resulting from the maximum filter value (α = 0.999). Growing-season and nongrowing-season BFI demonstrated a similar trend in response to the variation of the filter parameter.

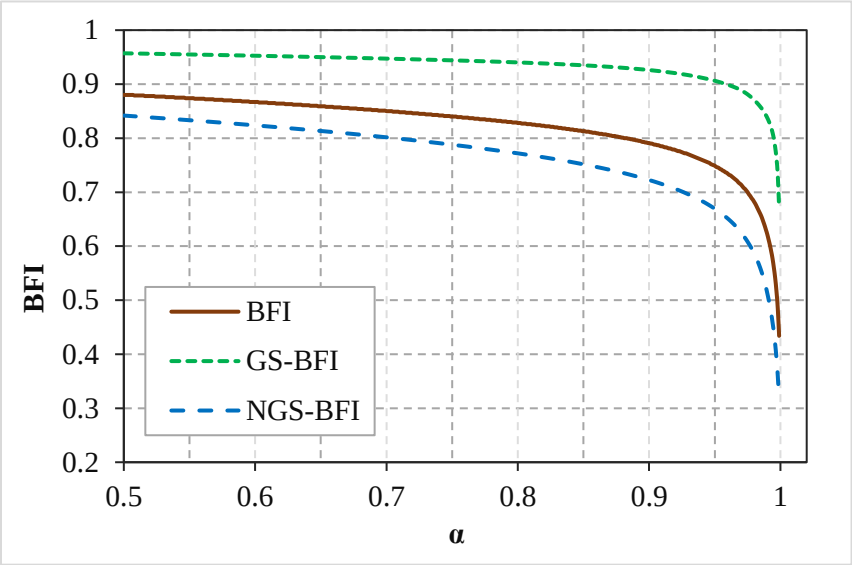

Figure 3.12 Long-term BFI, GS-BFI, and NGS-BFI in response to variations in the filter parameter of the Lyne and Hollick methods.

Figure 3.12 demonstrates the sensitivity of the evaluative measures to the Lyne and Hollick's filter parameter. The long-term annual correlation with groundwater level increased from 0.52 produced by LH(0.5) and maximized to 0.76 at α =0.982 before plummeting to 0.49, where the filter parameter equaled 0.999. of the evaluative measures, i.e., the annual correlation with groundwater and coefficient of determination. The coefficient of determination calculated for the pure baseflow periods was greater than 0.99 for most of the parameter range. A neglectable decrease was observed from 0.998 to 0.990, corresponding to LH(0,5) and LH(0.96), respectively. The R^2 decreased to 0.92 at α =0.996 and dropped to 0.3 at the end of the range. The seasonal BFI over the driest summer months showed a similar behavior where it started at 0.988 (α =0.5) and reached no lower than 0.96 at α =0.997.

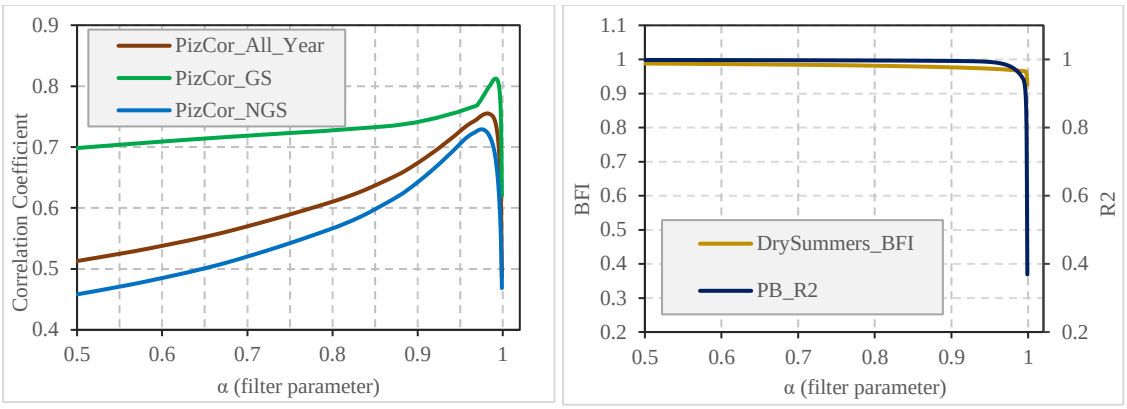

Figure 3.13 Response of evaluative measures to variations in the filter parameter of the Lyne and Hollick method.

3.7.1.2 Eckhardt

The parameter sensitivity of the Eckhardt method is illustrated using heatmaps representing the BFI values in response to variations in BFImax and the groundwater recession constant (Figure 3.13). The BFImax ranged from 0.5 to 1 with an increasing step of 0.05, and the recession constant (α) increased by 0.001 from 0.9 to 1, creating a grid of 100 by 100. The BFI showed to be relatively insensitive to the recession constant values from 0.9 to 0.98 and was principally determined by BFImax. This was evident from the lack of horizontal change of color over this span, where BFI was as low as 0.49 (BFImax=0.5) and as high as 0.99 (BFImax=0.999). When the recession constant increased over 0.98, BFI was sensitive to both parameters and significantly decreased as the recession constant increased. As an example, given a fixed BFImax of 0.8, and any α value between 0.9 and 0.98, the BFI was relatively constant, varying from 0.75 to 0.73. Whereas, by adopting a value of 0.997 for the recession constant, the BFI decreased to 0.61. In addition, it was evident that as the BFImax increased, the sensitivity of BFI to the α values larger than 0.98 was increased. In other words, one step of increase in the recession constant had more

impact on the BFI when the BFImax was closer to 0.8 compared to when BFImax was closer to 0.5.

During the growing season, the separated baseflow was sensitive to both parameters. Similarly, the sensitivity of the GS-BFI to recession constant significantly increased for values larger than 0.98. For the BFImax values between 0.5 and about 0.85, both parameters positively influenced the GS-BFI, with BFImax being more influential before the recession, increasing over 0.98. Over the range of 0.85 to 1 for BFImax, the GS-BFI was not sensitive to recession constants lower than 0.98. However, the recession parameter worked to decrease the GS-BFI past this point. The heatmap of non-growing season BFI showed almost identical characteristics to long-term BFI.

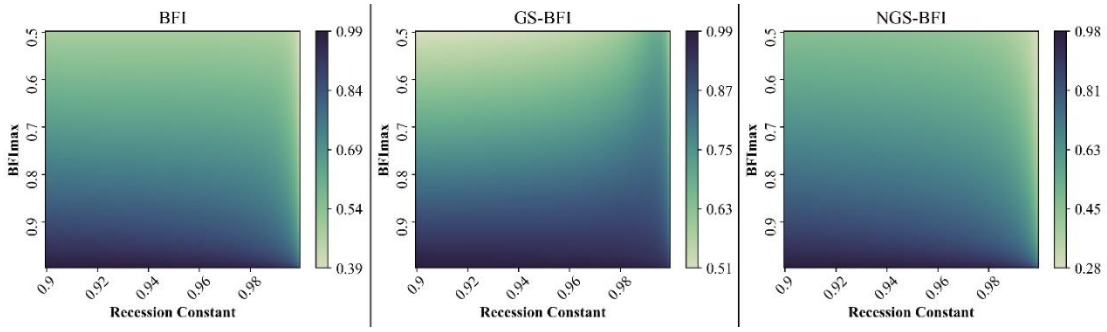

Figure 3.14 Long-term BFI, GS-BFI (growing season), and NGS-BFI (non-growing season) in response to variations in the parameters of the Eckhardt method.

Heatmaps demonstrating the response of evaluative measures to the parameters of the Eckhardt method were obtained similarly to assess the sensitivity (Figure 3.14). The short-term BFI over the driest summer seasons corresponding to different combinations of the parameter values was as low as 0.52 and as high as 0.99. In the driest summers, BFI was maximized regardless of the recession factor whenever the BFImax was greater than 0.95.

However, with BFImax below 0.95, only the recession constant values over 0.98 could reflect the domination of baseflow. As the BFImax decreased from 0.9, the Eckhard method required larger values for the α to maximize the driest summer BFI. For example, with a BFImax of 0.7, only recession constants between 0.99 and 0.999 could produce the driest summer BFI values greater than 0.9. For the prediction of baseflow during the pure baseflow period, the coefficient determination showed an almost identical response pattern with the difference that for any BFImax below 0.8, the R^2 was maximized and insensitive to the recession constant. Similarly, to maximize the R^2, the recession constant values needed to be increased above 0.98 after the decrease in BFImax. The best and worst prediction of pure baseflow using the Eckhardt method produced coefficients of determination equaling 0.99 and -1.98, respectively.

The sensitivity of the correlation between groundwater level and Eckhardt's parameters followed a different pattern than the other products of baseflow separation. For any fixed value of one parameter, an increase in BFImax decreased the correlation coefficient, and the increase in the recession constant positively influenced the correlation coefficient. The lower correlations were produced when the recession constant was below 0.98, and BFImax was increased over 0.9. The higher correlation coefficients were produced when the recession constant was greater than 0.98 and less sensitive to BFImax. However, the correlation was maximum when BFImax was larger than 0.9, and the recession factor was selected from a narrow range of values between 0.995 and 0.999.

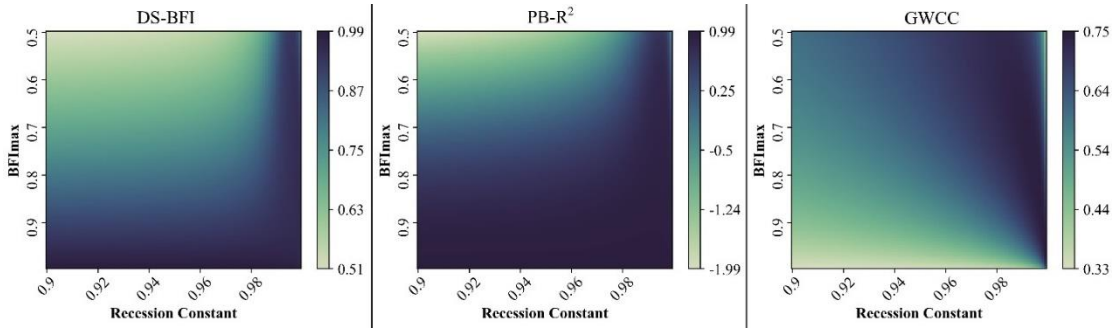

Figure 3.15 Driest summer seasons BFI (DS-BFI), coefficient determination during pure baseflow periods (PB-R^2), and correlation between groundwater level and separated baseflow (GWCC) in response to variations in the filter parameters of the Eckhardt method.

Chapter 4: Assessing the importance of red clover in nitrate loading and the mitigating potential of an alternative potato rotation in Atlantic Canada

Visual Abstract

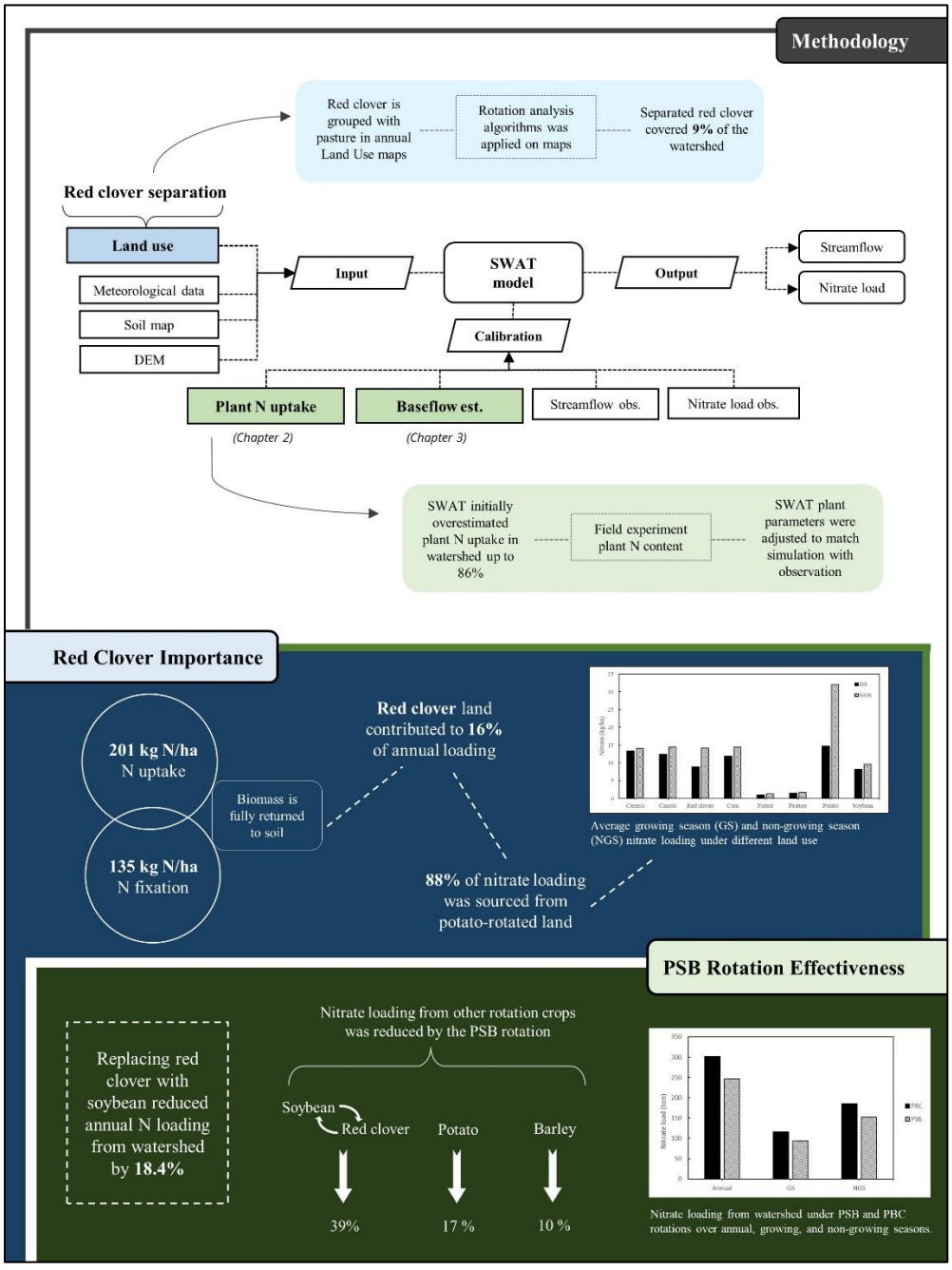

Abstract

The health of water bodies worldwide is at risk due to excessive nitrate loading from agricultural non-point sources. To develope effective mitigation strategies, it is crucial to quantify the sources and drivers of nitrate flux in watersheds and relate them to temporal and spatial land uses. Farmlands under potato rotation were identified as the principal contributor to nitrate loading in Prince Edward Island (PEI), Canada. This study was conducted in the Dunk River Watershed as an example of typical agricultural watersheds in PEI. The comprehensive hydrological model Soil and Water Assessment Tool (SWAT) was developed to simulate nitrogen loading dynamics in the watershed in order to follow three key objectives. (A) evaluating the impact of various land use on nitrate loading to surface water, (B) assessing the importance of accounting for organic N from red clover, and (C) evaluating the effectiveness of replacing red clover with soybean as a best management practice (BMP) in mitigating nitrate loading from potato rotation land use. The SWAT model was set up using historical streamflow, water quality, and annually updated land use records from 2011 to 2020. The SWAT model performed well in predicting daily streamflow, baseflow and nitrate load. Annual nitrate load ranged from 2.3 to 46.5 kg N ha^{-1} for forest and potato lands, respectively. Red clover, cereals, soybean, and pasture lands provided 23.2, 27.3, 17.9, and 3.2 N ha^{-1}, respectively. Potato-rotated land contributed 88% of the annual nitrate load to the watershed. Red clover was estimated to cover 9.3% of the watershed on an annual basis throughout the study. Red clover had an annual N fixation rate of 134 kg N $ha^{-1,}$ a significant additional source of nitrogen input compared to the previously unseparated pasture in the land use maps. Replacing the conventional potato-barley-red clover (PBC) with the alternative potato-soybean-barley

(PSB) rotation resulted in a substantial 18.4% reduction of annual nitrate load into the watershed. Furthermore, red clover replacement decreased nitrate loading from other rotation crops, potato, and barley, by 17.4% and 10%, respectively. The results of this study provided valuable insights into the importance of accounting for organic N from red clover for watershed management in PEI.

4.1 Introduction

Non-point source water pollution is a result of the interaction between non-point source effluents and land cover, soil, and land management practices (Giri et al. 2016; Giri and Qiu 2016; Jabbar and Grote 2019; Ouyang et al. 2019) with agricultural activities recognized as the dominant cause of non-point source pollution (Baker 1992; Xiang et al. 2017; Zhang et al. 2010). Agricultural operations may introduce sediments, nutrients (nitrogen or phosphorus), herbicides, and other pollutants into water bodies. Nitrogen, for instance, is one of the most essential nutrients for crop development. On the other hand, the low usage efficiency of nitrogen fertilizer causes a considerable amount of nitrogen to be lost to the environment, primarily through leaching and runoff events. This phenomenon has been frequently documented in the literature (De Notaris et al. 2018; Jiang et al. 2011; Peralta and Stockle 2002; Prunty and Greenland 1997; Torstensson et al. 2006; Zebarth et al. 2009). Increased nitrogen (N) loading to aquatic ecosystems is a significant cause of water quality impairment contributing to potential eutrophication globally (Hua et al. 2018; Vörösmarty et al. 2010).

Environmental issues stemming from excessive nitrogen loading are pervasive, and the southern Gulf of St. Lawrence is no exception. Compared to estuaries in New Brunswick or Nova Scotia, the estuaries of Prince Edward Island have experienced a greater impact,

with several dozens of anoxic events documented from 2016 to 2021 (Government of Prince Edward Island, 2021). Nitrate is the primary form of combined nitrogen in marine aquatic ecosystems, thanks to its high stability and solubility (Goolsby and Battaglin 2001; Pellerin et al. 2014). Over the past few decades, continuous freshwater quality monitoring in PEI has revealed notable upward trends in nitrate levels (Environment-Canada 2011). The rise in nitrate concentration coincided with significant transformations in agricultural land use during the early to mid-1990s when potato farmlands increased from 11,982 ha in 1951 to 43,770 ha in 1996 (Bugden et al. 2014; Grizard et al. 2020).

PEI covers an area of 5,750 km^2, with agricultural land covering 40% and 20% of the island under potato production rotations (Grizard et al. 2020; Jiang and Somers 2009). Several studies have linked intensive potato production to high nitrate levels in groundwater and surface water on the island (Benson et al. 2006; Savard et al. 2007; Zebarth et al. 2015). Jiang et al. (2015) reported that potato rotation lands were responsible for 75-98% of the nitrate in estuaries with elevated nitrate loads. Previous studies have shown that organic N is a significant contributor to nitrate loading in agricultural watersheds in PEI. Savard et al. (2010) conducted a 3-year study of stream nitrate isotopes in the Wilmot River watershed, revealing that chemical fertilizers and soil organic matter contributed equally to the growing season and summer load, with an average contribution of 45% and 32%, respectively. Meanwhile, soil organic matter was identified as the primary source of the non-growing season load, accounting for more than 70% of the total annual nitrogen mass. Danielescu and MacQuarrie (2013) reported similar findings in the McIntyre Creek watershed, a typical agricultural watershed situated on the north shore of PEI.

Conventionally, farmers plow down the legumes in fall as green manures for the many expected benefits of fall plowing (Myrbeck 2014; Vos et al. 2012). Multiple studies have demonstrated the magnitude of organic N added to the system via plowed-down red clover. While the standard N fertilization rate for potato in PEI is 155 kg N ha^{-1} (PEI Analytical Laboratories, Department of Agriculture and Fisheries, PEI), Jiang et al. (2019) suggested that the potential N supply from the plowed-down red clover can be comparable to total potato N uptake. Using field measurements, they estimate the total N accumulation in red clover biomass to be as high as 266 Kg N ha^{-1}. Liang et al. (2019) observed that the plowed-down red clover could add up to 311 Kg N h^{-1} to the soil. Jiang et al. (2011) considered a total N accumulation of 230 Kg N ha^{-1} in red clover based on empirical data and literature values. In their comparison of PBC and PSB rotations, Liang et al. (2019) found that plowed-down red clover resulted in the highest nitrogen loss through leaching compared to other cover crops. Azimi et al. (2022) further illustrated the significance of red clover by observing that the soil nitrate content of PBC plots before planting succeeding potato, was considerably was considerably higher than that of PSB, with values of 59 and 12.4 Kg N ha^{-1}, respectively. Following potato harvest, soil nitrate content was still significantly higher under PBC plots by 54%. Previous studies have consistently shown the inclusion of red clover in potato rotations can cause an excess of nitrogen accumulation in the subsequent growing season, increasing the potential for N leaching in the following potato crop.

Although field experiments have consistently suggested the significant N supply of red clover in PEI, the influence of red clover on nitrate loading at a watershed scale is still unclear. Knowing the influence is important for developing an integrated strategy for

mitigating water quality issues. Due to resource limitations, such as time and money, conducting field assessments of changes in land management techniques, like crop rotations, at a watershed scale is often not feasible. The SWAT model provides an alternative approach for assessing the influence of including red clover in potato rotations, among others, on nitrate loading at a watershed scale. The model has been used extensively for evaluating the effectiveness of BMPs in decreasing nitrate and other pollutant loads in watersheds (Akhavan et al. 2010; Haas et al. 2017; Lee et al. 2017; Liang 2020).

This study uses the semi-distributed SWAT model to model nitrogen loading dynamics at a watershed scale. Two key objectives are defined to better understand the impact of land use on nitrogen loading. A) To quantify the impact of nitrogen supply from red clover on nitrogen loading dynamics at the Dunk River Watershed. B) To assess the effectiveness of the PSB rotation, as a BMP, at a watershed scale in mitigating nitrate loading.

4.2 Methods

4.2.1 Study area

The Dunk River Watershed (DRW) represents a typical intensive farming watershed located in the central west part of PEI, with long-term records of surface and groundwater quality issues stemming from agricultural activities (Khan et al. 2003; Paradis et al. 2018; Roloson et al. 2021). of with a drainage area of 143 km^2. The DRW is an index basin with long-term hydrometric and surface water quality data. The watershed has a drainage area of 143 km^2 with elevation spanning from 138 m in its eastern region to -7.7 m near its outlet area, making the watershed relatively flat. The drainage area upstream of the gauging station near the watershed outlet is about 112 km^2 (Figure 4.1). Agricultural land comprises about 67% of the total area, with potato being the dominant crop cultivated in the watershed. The majority of agricultural land in the watershed is under potatoes rotated with forages and grains. Based on a 10-year average (2011-2021), about 20% of the

watershed has been under potato cultivation annually (

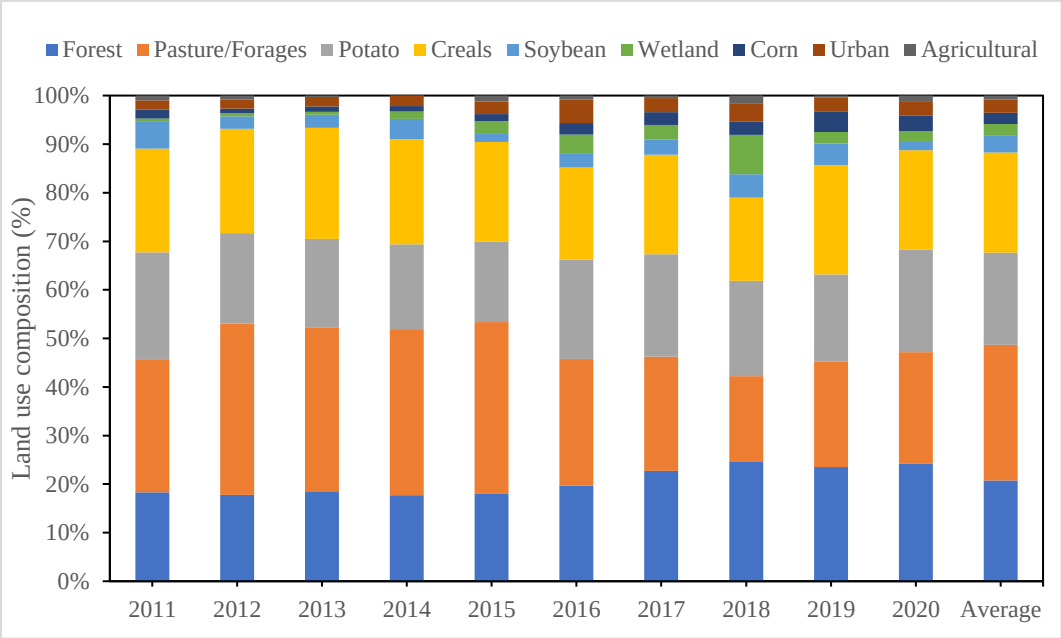

Figure 4.2). Following the introduction of modern farming practices to this area in the 1950s, synthetic fertilizers were widely adopted in the 1960s (Jiang and Somers, 2009). This region's environment is characterized as humid with as cool to moderate temperatures. The precipitation within the watershed ranged from 810 mm in 2006 and 1463 mm in 2002. The 20-year climate average (2002–2020) was 1265 mm, with the annual snowfall averaging 300 mm. (data accessed from Environment and Climate Change Canada: https://climate.weather.gc.ca/historical_data/search_historic_data_e.html).

The Alberry and Charlottetown (Orthic Humo-Ferric Podzol) series soils constitute the majority of the watershed, with the former accounting for 72% and the latter for 14%. Water extraction from the Charlottetown series is somewhat slow relative to supply since they are moderately coarse and well-drained. In the Alberry, coarse and well-drained series, water is readily but not quickly extracted from the soil. The overburden and rock formations of the basin have a relatively high hydraulic conductivity, which causes a quick response of the water table to precipitation and snowmelt events. There is approximately a

five-day lag between an increase in groundwater level and precipitation events (Liao et al. 2005; Paradis et al. 2006). Detailed description of soil types can be accessed from the soil database of the government of Canada (http://sis.agr.gc.ca/cansis/soils/pe/soils.html).

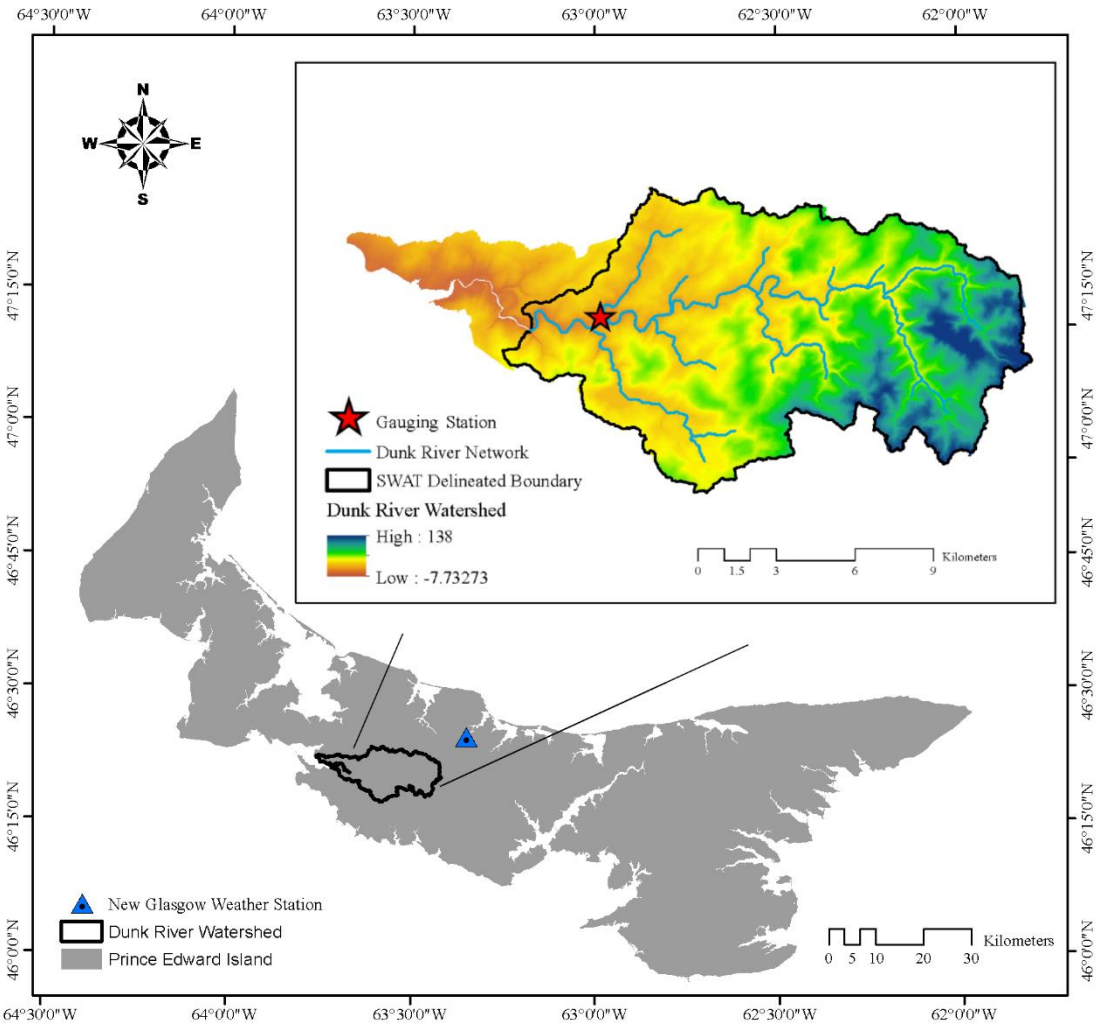

Figure 4.1. Location of the Dunk River Watershed.

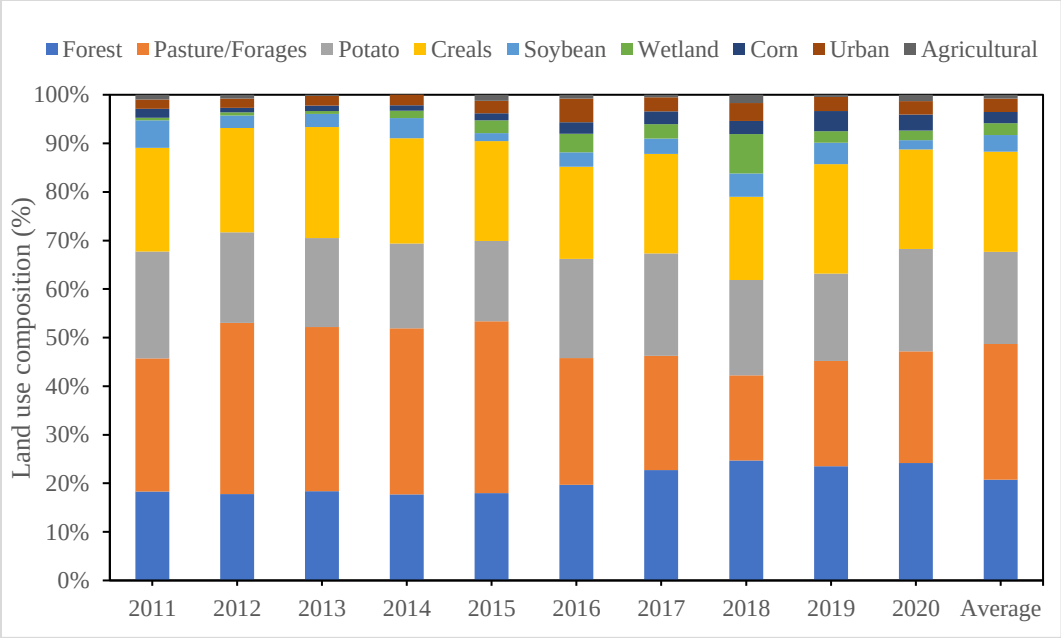

Figure 4.2. Land use composition of the Dunk River Watershed from 2011 to 2021.

A gauge station maintained by Environment and Climate Change Canada is located near the outlet of the watershed (Figure 4.1). Water level and associated discharge have been continuously monitored, and water samples have been taken at monthly or biweekly intervals in the growing-season period of the year, which is the period between May to October and monthly and at most twice over the non-growing season. Approximately 6–9 samples were taken for water quality analysis annually, with 5-9 samples taken over the growing season and 0 to 2 samples over the non-growing season. There were 75 water quality samples taken in total over the duration of study period, from which 65 samples were taken over the growing season and only 12 over the non-growing season. Minimum daily nitrate concentrate and nitrate load were 2.4 mg L^{-1} and 214 kg N $day^{-1,}$ respectively, and maxed at 5.9 mg L^{-1} and 1310 kg N day^{-1}, respectively, over the growing season. Minimum nitrate concentration and load over the non-growing season were 3.1 mg L^{-1} and

288 kg N day^{-1}, respectively. Maximum nitrate concentration and load over the non-growing season were 5 mg/l and 2043 kg N day^{-1}, respectively (Figure 4.3).

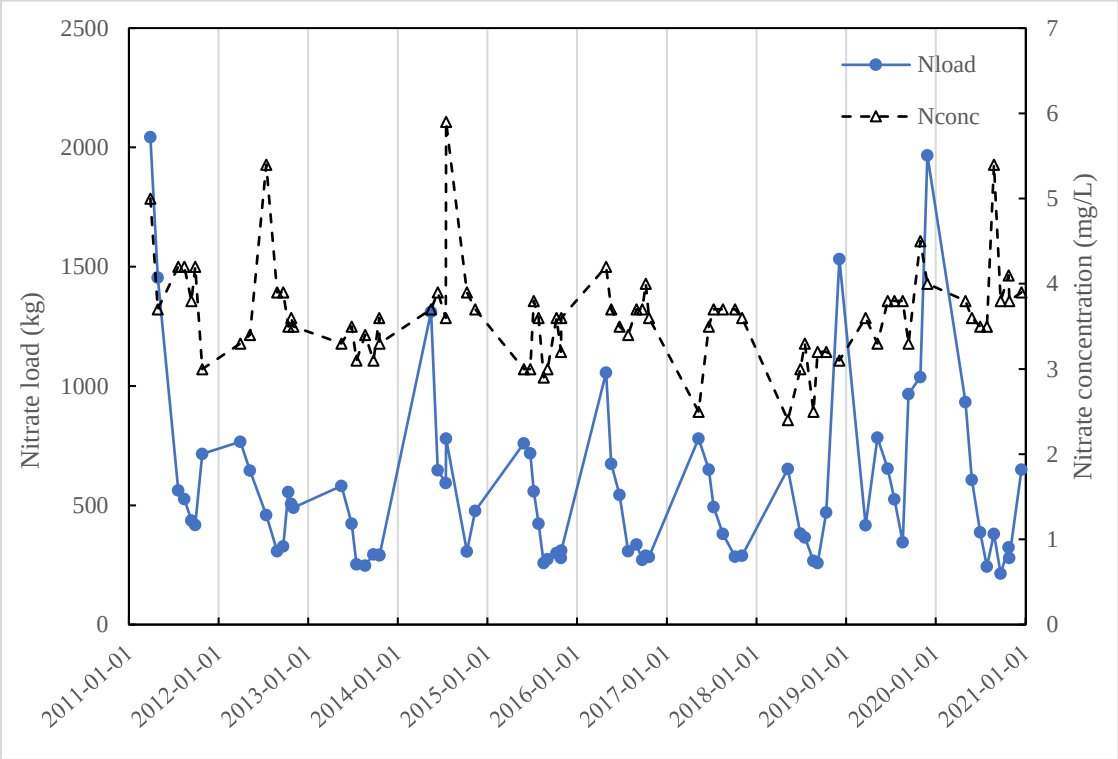

Figure 4.3. Nitrate concentration and relative nitrate load samples over the period of the study (2011-2020).

4.2.2 SWAT input data, setup, calibration, and validation

The Soil and Water Assessment Tool (SWAT) is a semi-distributed, physical-based hydrological model that was designed to simulate hydrological and water quality indicators (e.g., streamflow, sediment, nutrient and pesticide load) and crop growth at the watershed scale (Arnold and Fohrer 2005; Arnold et al. 1998; Gassman et al. 2007). The SWAT model has been used extensively for evaluating the effectiveness BMPs in reducing nitrate and

other pollutant loads from watersheds (Akhavan et al. 2010; Haas et al. 2017; Lee et al. 2017; Liang 2020).

SWAT requires soil, climate, land use, management practices, and topography input datasets. The New Glasgow station (46.41, 63.35), which is the nearest weather station (13 km northeast of the watershed), was accessed to provide weather information since no Environment Canada weather stations are located within the watershed. Soil data was obtained from the National Soil DataBase of Canada (NSDB). Annual land use data was retrieved from Agriculture and Agri-Food Canada's 2011-2021 Annual Crop Inventory maps (available at http://www.agr.gc.ca/atlas/aci/).

Single-year land use datasets have been widely used in SWAT experiments for model setup (El-Khoury et al. 2015; Sith et al. 2019; Yang et al. 2016). How well the model's land usage corresponds to temporal changes in land use impacts how reliable model predictions are (Pai and Saraswat 2011). Wang et al. (2018) suggested that the SWAT model configuration with dynamic land use can improve the prediction of total nitrogen and total phosphorus loads. The noncontinuous land use data input may not accurately reflect the actual watershed condition, reducing modeling accuracy (Pai and Saraswat 2011). Following the initial configuration of SWAT with 2011 land use data, we imported continuous land use data from 2011 to 2020 into the SWAT database. Since agricultural and forested terrain comprised most of the watershed (
Figure 4.2), the impact of septic systems was deemed minor.

The model divides a watershed into subbasins, subdivided into hydrologic response units (HRU) with homogenous land use, soil, and slope (Ullrich and Volk 2009). Hydrological and chemical parameters on the subbasin level are obtained from aggregation or area-averaged amounts of the HRUs as the primary calculation unit in the SWAT. The main channel and watershed outputs are calculated by implementing channel processes on the inputs to the channels. ArcGIS 10.5.1's ArcSWAT 2012 interface was used for model setup. The DRW was divided into 29 subbasins by SWAT and further separated into 707

HRUs based on the homogeneity of land use, soil, and slope classes using thresholds of 5%, 10%, and 15%, respectively.

4.2.3 Calibration procedure

Daily streamflow and nitrate load calibrations are carried out using the SUFI-2 algorithm in the Soil and Water Assessment Tool Calibration and Uncertainty Procedure (SWAT-CUP 2019) software package (Abbaspour 2015). The model was stabilized over a three-year warm-up period (2008–2010), calibrated from 2011–2017, and further verified from 2017–2020. The Global Sensitivity Analysis approach was used to conduct a sensitivity analysis of streamflow and nitrogen parameters to prioritize the sensitive parameters (Abbaspour et al. 2004). The present study employed the Global Sensitivity Analysis technique to determine the impact of changes in individual parameters on the objective function (Nash-Sutcliffe efficiency) while keeping other parameters constant (Equation 1).

$$g = \alpha + \sum_{i=1}^{m} \beta_i \times b_i \qquad \text{Equation (4.1)}$$

This method involves the use of regression coefficients (α and βi), calibration parameter (b_i), and the number of parameters considered (m). The advantage of this method is its speed and relative sensitivity evaluation, as opposed to absolute sensitivity. Two statistical measures were used in SWAT-CUP to assess sensitivity are the t-stat index, which indicates the extent of parameter sensitivity (larger absolute values signify greater sensitivity), and the p-value, which determines the most sensitive parameters ($p < 0.05$ in this study) (Abbaspour et al. 2004; Brighenti et al. 2019). The parameters for streamflow and nitrate load that were calibrated and fitted are listed in Supplementary Table 4.3.

4.2.4 Baseflow calibration

Baseflow can be a significant pathway of dissolved nutrient transport from watersheds. Various studies have highlighted that baseflow is the predominant delivery route for non-point source nitrogen to streams (Kang et al. 2008; Schilling and Zhang 2004; Schilling and Lutz 2004; Villarini et al. 2016). Groundwater is identified as the primary source of base flow for a typical stream in PEI during summer, contributing to nearly 100% of the stream flow and the relevant nitrate load (Francis 1989; Jiang et al. 2015; Jiang et al. 2004).

To emphasize the baseflow importance in our model, the separated baseflow was introduced to SWAT-CUP calibration along with the streamflow data. However, since SWAT does not report baseflow directly and the current baseflow separation methods provide estimations instead of relying on physical processes, a reliable sub-selection of the separated baseflow will be extracted for this purpose. The baseflow dataset represents the days inside summer (the critical period for nitrate loading) when the separated baseflow was equal to the streamflow (baseflow days). Calibrating for baseflow days ensures that: (a) the model does not over-estimate nitrate supply to compensate for and under-estimation in streamflow, and (b) the baseflow has the same value as the peak flows in the calibration process and prevents the peak flow from dominating the calibration processes (Abbaspour 2015). Baseflow separation was carried out using the Lyn and Hollick method (Lyne and Hollick 1979) using a recession factor of 0.98 obtained from the procedure explained earlier in Chapter 3. Supplementary Table 4.4 reports a summary of the selected pure baseflow days. SWAT-CUP utilizes an objective function to optimize the predictions and calibrate parameters. Each observed variable has a user-defined weight in the objective function that determines the importance of a specific variable in the calibration process. Streamflow and nitrate load were given an equal weight of 1. However, since the baseflow

prediction is not the primary goal of this simulation, it was given a lower weight of 0.7 in the objective function.

4.2.5 Statistical Analysis

The Nash-Sutcliffe efficiency (NS), percent bias (PBIAS), and coefficient of determination R^2 were used to assess the goodness-of-fit of the SWAT model simulations on streamflow and nitrate load. NS is a statistical metric frequently used to evaluate the goodness of fit of hydrologic models (Moriasi et al. 2007). The numeric scale (NS) spans from -∞ to 1, with 1 denoting a perfect correspondence between simulation and observation. PBIAS indicates the average tendency of simulated values to be greater than or less than observations. A PBIAS with a low magnitude indicates a superior simulation, with zero being the optimal value. Positive PBIAS values suggest model underestimation, and negative ones imply model overestimation (Gupta et al. 1999). R-squared (R^2) is a statistical measure representing the proportion of the variance in the dependent variable that is predictable from the independent variables. It is a value between 0 and 1, where a value of 1 indicates a perfect fit between the observed and predicted values (Neter et al. 1996).

$$NS = 1 - \frac{\sum_i (Q_m - Q_s)_i^2}{\sum_i (Q_{m,i} - Q_m)}$$ Equation 2.

$$PBIAS = 100 \times \frac{\sum_{i-1}^{n} (Q_m - Q_s)_i}{\sum_{i-1}^{n} Q_{m,i}}$$ Equation 3.

$$R^2 = \frac{\sum_i [(Q_{m,i} - Q_m)(Q_{s,i} - Q_s)]^2}{\sum_i (Q_{m,i} - Q_m)^2 \sum_i (Q_{s,i} - Q_s)^2}$$ Equation 4.

4.2.6 Log-transformation of streamflow

Often peak flow periods are associated with runoff events which may have significant importance in specific hydrological studies such as flood detection and sediment loading predictions. R2 and NS (Nash-Sutcliffe) are two commonly used statistical metrics to evaluate the performance of hydrological models in simulating streamflow. However, these metrics are sensitive to extreme values, such as peak flows caused by runoff events, and may not accurately represent the model performance during low-flow periods (Krause et al. 2005; Pushpalatha et al. 2012). As such, their use in calibration will be more influenced by high flow periods instead of the low flow periods as the main focus of this study. When calibrating a hydrological model, it can become essential to emphasize low-flow periods, which are often associated with limited water availability and significant ecological impacts. In PEI, the major concerning period for excessive nitrate loading is the low flow periods occurring during summer (Bugden et al. 2014; Jiang et al. 2015). Logarithmic transformation of streamflow values is a common approach to reduce the influence of runoff events on model evaluation and calibration. Gupta et al. (1998) suggested that the logarithmic transformation amplifies low flows and dampens high flows, allowing greater sensitivity to changes in low-flow conditions. Therefore, the log-transformed streamflow will be used in calibration and evaluation of the model to emphasize the importance of year-round low flow periods.

4.2.7 Red clover separation

Land use data is among the many inputs the SWAT model requires for simulating watershed processes. Including land use maps in the model makes it possible for

hydrologists to assess the impacts of various land use change scenarios. However, despite the importance of red clover in PEI as an industry-standard crop in rotation with potato, the annual crop inventory (2011-2019) does not distinguish legumes from pasture. The annual crop inventory generalized forages, legumes and pasture under the same category as pasture (Agriculture and Agri-Food Canada). The absence of red clover in the input data limits the SWAT model in assessing red clover role in the watershed. The pasture category, which includes legumes and other perennials, accounts for 26% of the DRW in the annual crop inventory. Therefore, the direct usage of annual crop inventory data in the SWAT model will inevitably lead to omitting a significant organic N source from legumes.

4.2.8 Separation procedure

In order to compensate for the absence of red clover in the input data, a rotation-based procedure will be implemented to distinguish red clover from other perennials. The land-use evolution of each pixel in the annual crop is expected to reflect the possibility of red clover rotated with potato. The algorithm will detect red clover based on the expected temporal alternations between potato and red clover in the PBC rotation system. In general, red clover is expected to be followed by potato according to the crop order in a PBC rotation. The algorithm will target all pasture cells; each cell with pasture land use followed by potato will be considered red clover. Additionally, rotation length analysis will be carried out to assess how well the separated clovers fit into potato rotation systems in PEI. It is noteworthy to mention that since a definite estimation of red clover cultivation is not possible, the assumptions will involve uncertainty. It should be noted that in some cases, the forages are a mix of red clover and perennial grass, such as timothy or rye. However, SWAT does not recognize underseeding and does not have a crop that can simulate a mix

of red clover and other forages. Therefore, the separated red clover here represents an "effective" forage crop, which only includes red clover for modeling purposes.

4.2.9 Plant N uptake adjustment

Previous research has emphasized that organic N is a significant contributor to the elevation of nitrate levels in agricultural watersheds in PEI, contributing up to 70% of the total annual nitrate loading (Danielescu and MacQuarrie 2011; Savard et al. 2010). Therefore, accurately accounting for the organic N added to the system can be as important as N fertilization determination. Our preliminary results showed that the default plant parameters in SWAT could produce unrealistic plant N accumulations in red clover, barley, and soybean. For instance, the nitrogen content of red clover can range from 100 to 700 Kg N ha^{-1} compared to the observed 311 Kg N ha^{-1} reported by Liang et al. (2019). The plant parameters for these three crops were adjusted to match the annual plan N uptake of the major crops in the watershed with reported values in the literature. The selected parameters that control for plant biomass and nitrogen uptake were Radiation-use efficiency or biomass-energy ratio (BIO_E), normal fraction of nitrogen in yield (CNYLD), normal fraction of nitrogen in plant biomass at emergence, 50% maturity, and maturity (PLTNFR_1, PLTNFR_2, PLTNFR_3). Table 4.1 reports the implemented plant parameters for red clover, barley, and soybean.

Table 4.1. Default and adjusted plant parameters for the major crops rotated with potato in the SWAT model.

		BIO_E	**CNYLD**	**PLTNFR_1**	**PLTNFR_2**	**PLTNFR_3**
	adjusted	**8**	**0.025**	**0.025**	**0.025**	**0.025**

Red clover	**default**	**25**	**0.065**	**0.065**	**0.028**	**0.024**
Barley	**adjusted**	**15**	**0.021**	**0.059**	**0.0226**	**0.0131**
	default	**35**	**0.021**	**0.059**	**0.0226**	**0.0131**
Soybean	**adjusted**	**15**	**0.06**	**0.03**	**0.03**	**0.03**
	default	**25**	**0.065**	**0.524**	**0.265**	**0.258**

4.2.10 Implementing the PSB rotation at the watershed scale

A land use change scenario will be implemented to simulate the effectiveness of an alternative potato rotation in mitigating nitrate loss from the DRW. The red clover will be replaced entirely with soybean in the annually updated land use maps to simulate the PSB rotation as one of the many BMPs.

4.3 Results and Discussion

4.3.1 Red clover separation

Red clover separation was carried out so that each pasture cell in the map was changed to red clover when it is in a single or two-year rotation with potato and is not directly followed by another red clover. Overall, 9.3% of the Dunk River Watershed was determined to be under red clover cultivation every year from 2011 to 2020. Subsequently, the average of other perennial land use (pasture) was reduced from 26% to 16.7%. Figure 4.4 demonstrates the annual summary of all red clover separation results. It was estimated that 7% of the watershed land use consisted of red clover in 2011, peaked at 11.8% in 2013, and continuedly reduced to its minimum in 2020 with 6.3% of the total area. Over the recent years, potato growers in PEI have shown less interest in rotating red clover with potato due to wireworm infestations associated with the forages such as red clover.

Buckwheat and brown mustard were introduced to replace red clover in 2016 when peak of wireworm population in this region was observed (personal communications with Christine Noronha, 2023). The decreasing trend of the detected red clover is in accordance with the decrease in planting red clover in PEI.

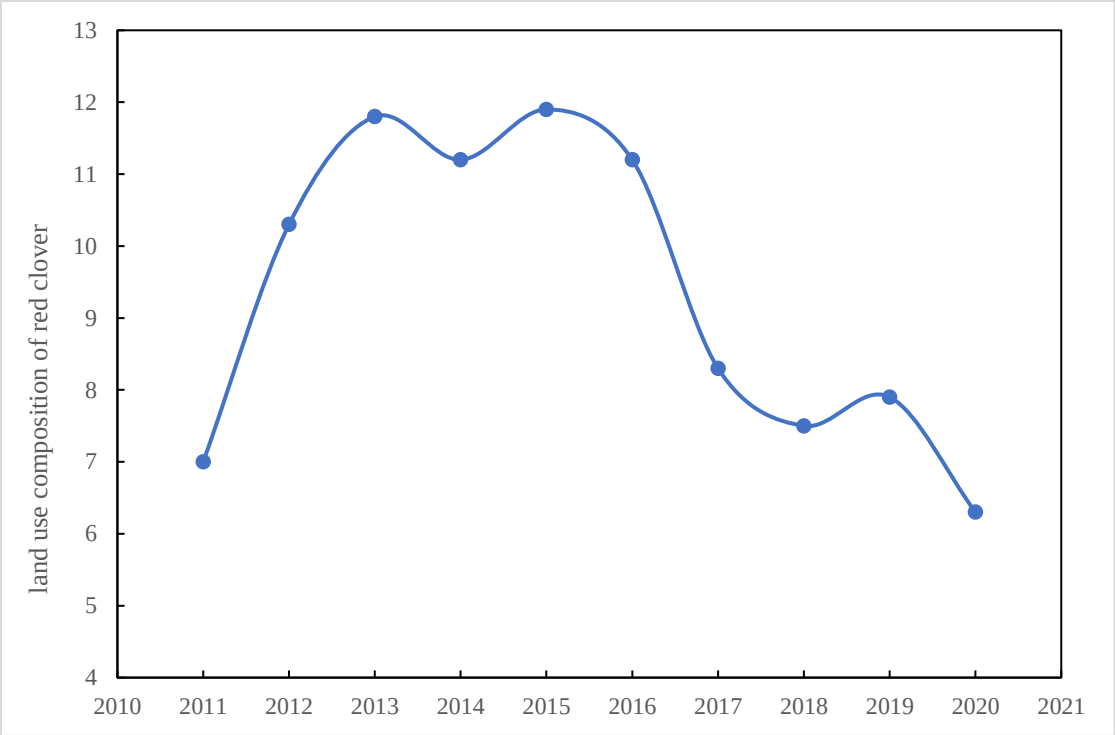

Figure 4.4. Annual variation of the separated red clover in the Dunk River Watershed.

Figure 4.5 demonstrates the inclusion of red clover in different lengths of potato rotations. Majority of the detected red clovers were in 3-year rotations with potato. On average, 75.4% of the separated red clovers were in a standard 3-year rotation with potato in which red clover is followed by potato. 20.3% were included in a less or more than 3-year rotation with potato with the condition that at least two occurrences of potato from 2011 to 2020 were observed in a particular cell of the map. 4.4% of the detected red clover was alternated

with potato only once over the period of the study. It should also be noted that the occurrence of potato fields not following the standard 3-yr rotation may be attributed to the accuracy of the maps caused by misclassification of the land use. However, since the algorithm does not represent a definite detection of red clover, all the detected clovers were kept to assess the importance of red clover at full extents.

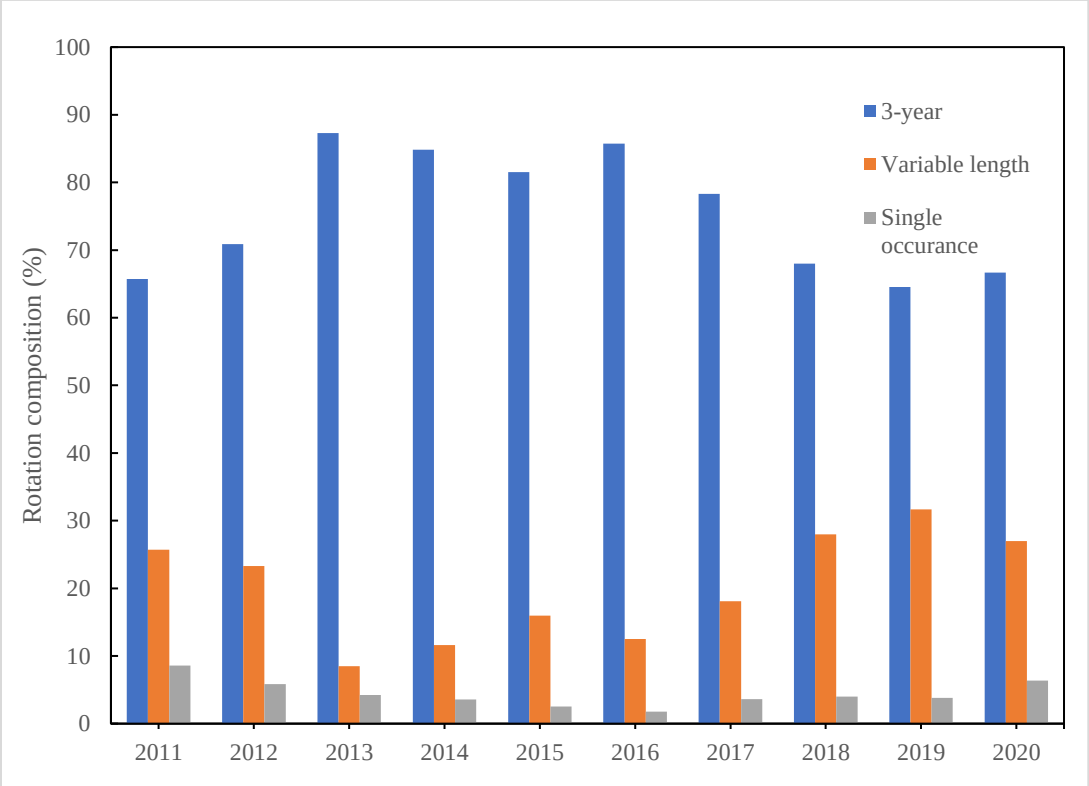

Figure 4.5. Proportion of separated red clover in various potato rotation patterns in the annual crop inventory.

4.3.2 SWAT model performance

4.3.2.1 Adjusted plant N uptake

In order to account for a more realistic representation of organic nitrogen input into the system, the plant parameters for some crops were needed to be adjusted manually. Figure 4.6 compares plant N uptake for various crops in the watershed using default and adjusted plant parameters. The plant N uptake of potato as the dominant crop in the watershed was obtained as 221 Kg N ha^{-1}. Barley, soybean and, red clover had plant N uptakes of 110, 339 and, 829 kg N ha^{-1}, respectively. While SWAT simulation of potato showed to match the expected N contents, red clover, soybean, and barley had significant discrepancies with the reference plant N uptake. The default parameters of red clover led to a massive plant N overestimation, four times larger than what is usually expected in PEI, and 160% larger than that of the field experiment (311 kg N ha^{-1}). Soybean simulated plant N content was 51% larger than the reference content with 224 kg N ha^{-1}. The model overpredicted the N content of barley by 26% compared to the reference 87.5 kg N ha^{-1}. The results indicate significant overestimation in calculating the N uptake of crops in rotation with potato. After parameter adjustments, plant N uptake by barley, soybean, and red clover was calculated as 87, 230, and 201 kg N ha^{-1}, respectively. The new plant N contents align more with the reference values obtained from the same experiment documented in Chapter 2 and other literature in PEI. It should be noted that the plant N uptakes obtained using adjusted parameters initially exactly matched the reference values. However, the calibration of flow and nitrate load inevitably influences the crop simulation as well as other processes in the watershed leading to a minor discrepancy between reference values and the simulation.

The default parameters resulted in an annual N uptake of 3070 t N yr^{-1} from the entire watershed. Whereas, after adjusting the parameters, the annual plant uptake in the watershed was 1642 t N yr-1. These results emphasize that using the default parameters

could lead to a significant overestimation in N uptake, as much as 86%. The excessive N uptake can later translate into excessive N input into the system when the crop residues return to the soil, causing an excessive N leached from the plant leftovers in the simulations. When calculating N loading from the watershed, different factors can compensate for the excessive N input (e.g., excessive denitrification, decreasing automated fertilization operation, ignoring legume N fixation). When these factors come into play, they inevitably cause a misrepresentation of the nitrogen balance components in the watershed, making the model unreliable for defining effective BMPs. The adjustment of plant parameters is a step that is commonly ignored in SWAT implementations. This is usually either because the organic N does not play a significant role in a specific watershed or simply trusting the SWAT model to perform a reasonable simulation of crops at the farm scale. Our results emphasize the importance of carefully accounting for Plant N uptake input to the watershed when organic N is a significant contributor to the N loading from the watershed.

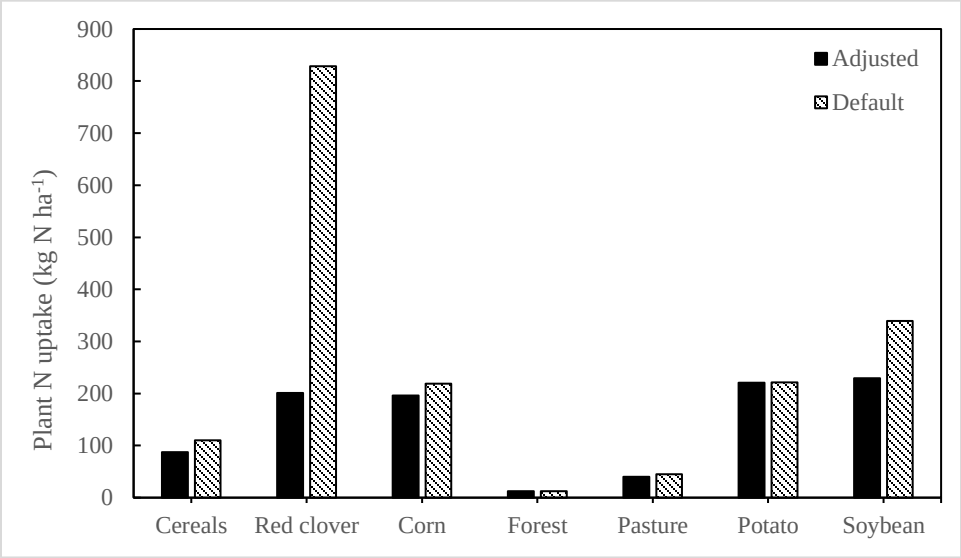

Figure 4.6. Nitrogen uptake of the major crops in the Dunk River Watershed using adjusted plant parameters.

It should be noted that adjustment of the plant parameters was carried out using random search constrained by the observed plant N uptakes and represent effective parameters. Therefore, the resulting plant simulation may not reflect the actual plant conditions precisely. This is because our goal was merely to reproduce documented annual nitrogen uptake in this region and not the actual plant growth and physiology. More research is needed to modify SWAT's plant growth in this region.

4.3.2.2 Streamflow and nitrate loading prediction

The model was calibrated for the streamflow, baseflow, and nitrate load variables. Figure 4.7, Figure 4.8, and Figure 4.9 compare the estimation and observation of the three variables at the gauging station during the calibration and validation periods. The results reveal that the SWAT model successfully predicted the daily streamflow, nitrate load, and baseflow based on the criteria outlined by Moriasi et al. (2007). Table 4.2 summarizes evaluative measures calculated for SWAT predictions of the streamflow, baseflow, and

nitrate load variables. During the calibration period, the model's performance in predicting streamflow was indicated by the NS, PBIAS, and R^2 values of 0.6, 17.4%, and 0.65, respectively. The model showed similar results during the validation period, with NS, PBIAS, and R^2 values of 0.59, 11%, and 0.61. During the calibration period, the model's prediction of baseflow was evaluated with a lower NS value of 0.43. However, PBIAS and R^2 were 8.6%, and 0.6, respectively, demonstrating a relatively good baseflow estimation. The performance of the model un baseflow estimation was improved during the validation period, with NS, PBIAS, and R^2 of 0.62, -5.6%, and 0.68, respectively. Over the calibration period, the model accurately predicted nitrate loads with NS, PBIAS, and R^2 of 0.71, 6.5%, and 0.7, respectively. Similar measures were obtained during the validation period with NS, PBIAS, and R^2 equaling 0.67, -5.5%, and 0.68. Moriasi et al. (2007) outlined that a model is considered to have a satisfactory performance if the monthly R^2 value is greater than 0.50, and the PBIAS falls within the range of ±25%. However, when a model is calibrated using daily time steps, its performance may be lower than that of a monthly time step model (White and Chaubey 2005). Wang et al. (2016) suggested that a model calibrated at a daily time step should have R^2 and NS values higher than 0.30 to be considered acceptable. The model produced relatively consistent statistical measures from the calibration period to validation as an indication of proper calibration. The lower NS value for baseflow days during calibration can be attributed to its smaller weight in the objective function compared to streamflow and N load, meaning that baseflow has lower importance in calibration. However, the small PBIAS values for baseflow estimation ensures that the model does not significantly overestimate or underestimate the streamflow during the dry periods when baseflow is the single delivery path of nitrate. Baseflow is

included to prevent the model from compensating for any nitrate load underestimations through overestimating nitrate supply. Similar changes of PBIAS from calibration to validation for both baseflow and nitrate load may be reflecting the correlation between baseflow and nitrate load over dry periods.

Table 4.2. Goodness-of-fit of the SWAT model simulations on streamflow, baseflow, and nitrate load.

	Period	R^2	NS	PBIAS (%)
Streamflow	**calibration**	**0.65**	**0.6**	**17.4**
	validation	**0.61**	**0.59**	**11**
Baseflow	**calibration**	**0.56**	**0.43**	**8.6**
	validation	**0.68**	**0.62**	**-5.6**
N load	**calibration**	**0.71**	**0.7**	**6.5**
	validation	**0.68**	**0.67**	**-5.5**

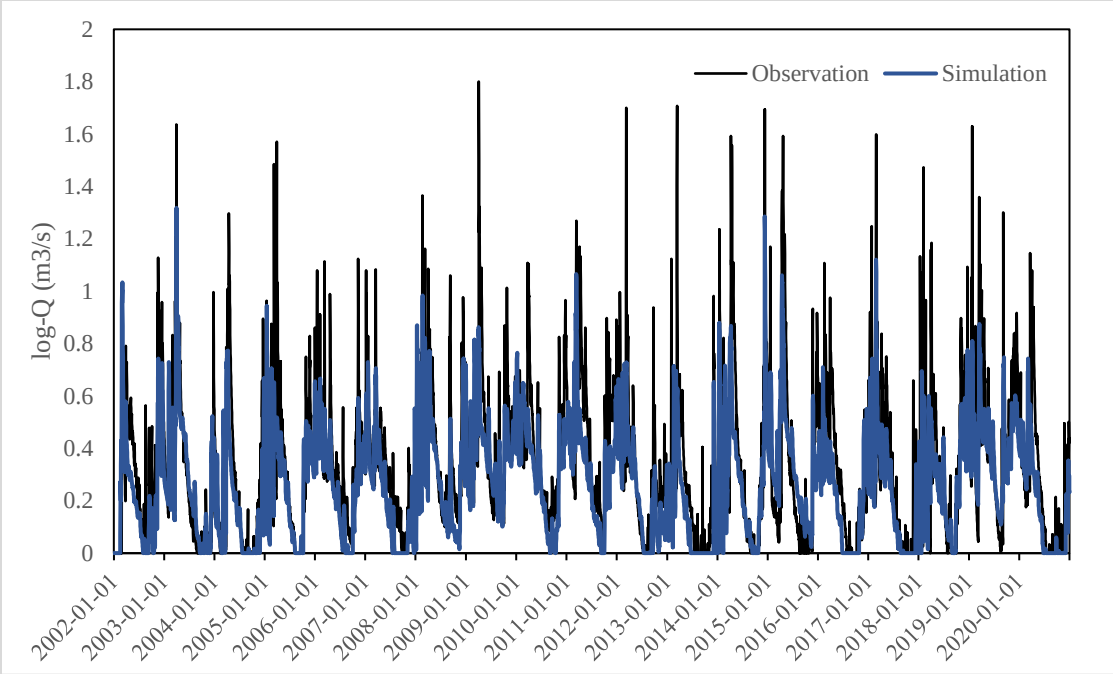

Figure 4.7. Daily log-transformed streamflow at the gauge station of Dunk River from 2011 to 2020.

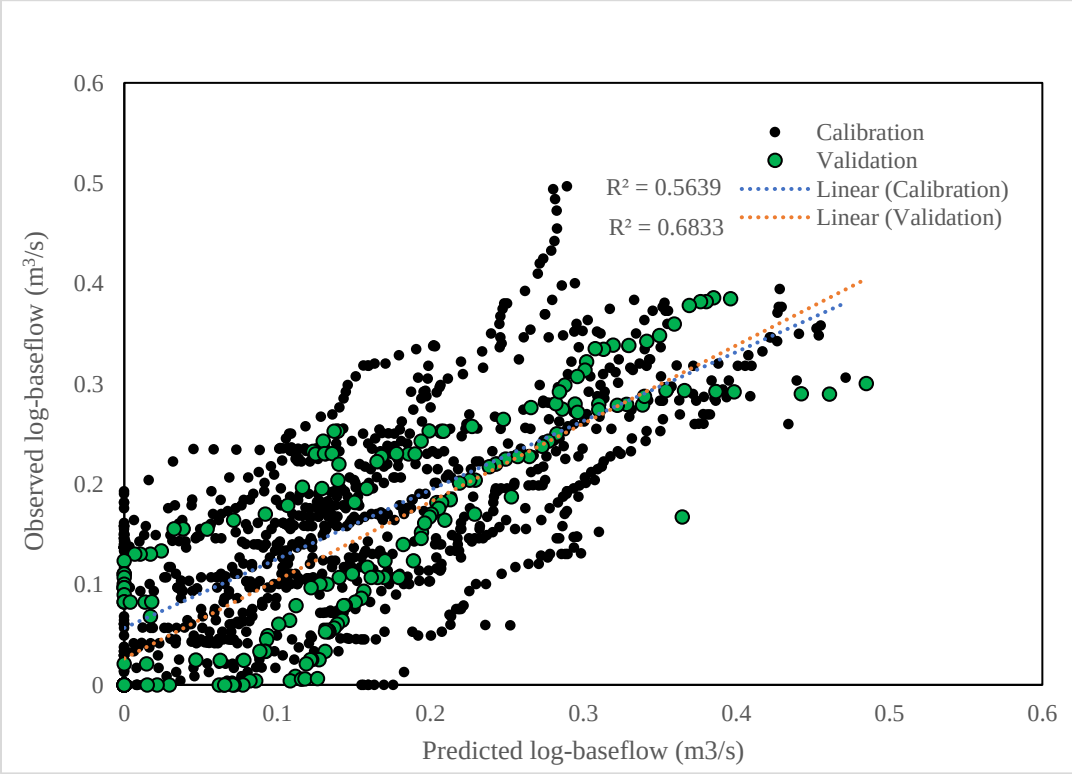

Figure 4.8. Daily baseflow at the gauge station of Dunk River from 2011 to 2020.

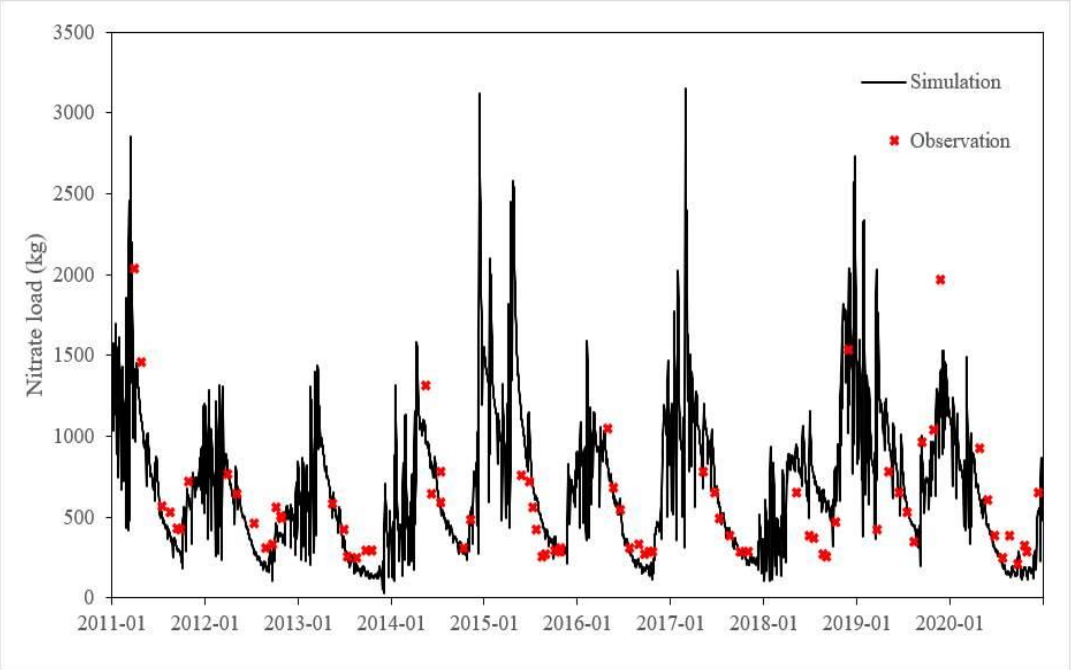

Figure 4.9. Daily nitrate load at the gauge station of Dunk River from 2011 to 2020.

4.3.3 Nitrate loading and leaching under different land use

4.3.3.1 Total N load contribution of each LU in the watershed

In total, 301 t N was loaded out of the watershed annually, with 38% (116 t N) belonging to growing season nitrate loading and 62% (186 t N) in the non-growing season. Potato land provided 157 t N yr^{-1} to the total nitrate loading out of the watershed. Cereals and red clover annual contributions were estimated as 70 and 49 t N yr^{-1}, respectively. 11, 6, and 4 t N yr^{-1} of the annual nitrate loading was sourced from pasture, forest, and soybean land use, respectively. Other land use, including corn and canola, provided 5 t N yr^{-1} in total.

The results of the total contribution of nitrate load by various land use categories indicate that potatoes were the largest exporter of nitrate during both the growing and non-growing seasons. As the most prominent crop by area (19%), potatoes provided 52.2% of the annual nitrate loading, 43.7% and 57.5% of nitrate during the growing and non-growing seasons,

respectively. Cereals had the second highest contribution to annual nitrate loading out of the watershed with 18%, followed by red clover with a 16% contribution. 30% (35 t N) and 18% (34 t N) of nitrate loading from the watershed were provided from cereal land use over the growing and non-growing seasons, respectively. Nitrate loading from red clover accounted for 15.7% (18.2 t N) of the growing season and 16.4% (31 t N) of the non-growing season nitrate loading of the watershed. The potato rotation (potatoes/red clover/cereals) contributed 82.5% and 89% of the total nitrate during the growing and non-growing seasons, respectively. This result is consistent with the findings of Jiang et al. (2015), who indicated that 75–98% of the nitrate loading of estuaries was derived from potato-rotated lands and underlined the need for more efficient N management under potato farming for water protection in Prince Edward Island. It is widely known that potato production systems are the primary source of nitrate leaching on Prince Edward Island due to the high amounts of nitrogen fertilizers used in potato cultivation (Benson et al. 2006; Jiang et al. 2015; Jiang et al. 2011; Liang et al. 2019; Zebarth et al. 2015). Figure 4.11 demonstrates the area coverage by different land use and their relative contribution to the annual N load. Our findings align with historical nitrate data from several PEI watersheds where low nitrate concentrations are frequently recorded during the dormant seasons (Jiang et al. 2015). Although nitrate concentrations were modest, intense flow caused a significant increase in the overall amount of nitrate exported from the watershed.

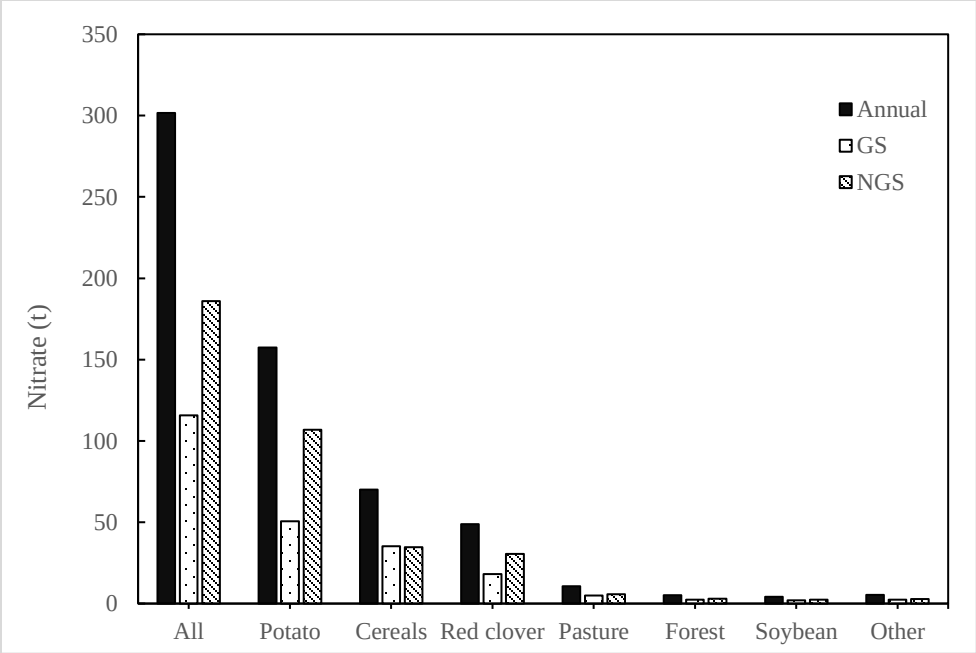

Figure 4.10. Average total nitrate load of different land use types from 2011 to 2020 in the watershed over annual, growing-season (GS), and non-growing season (NGS) periods.

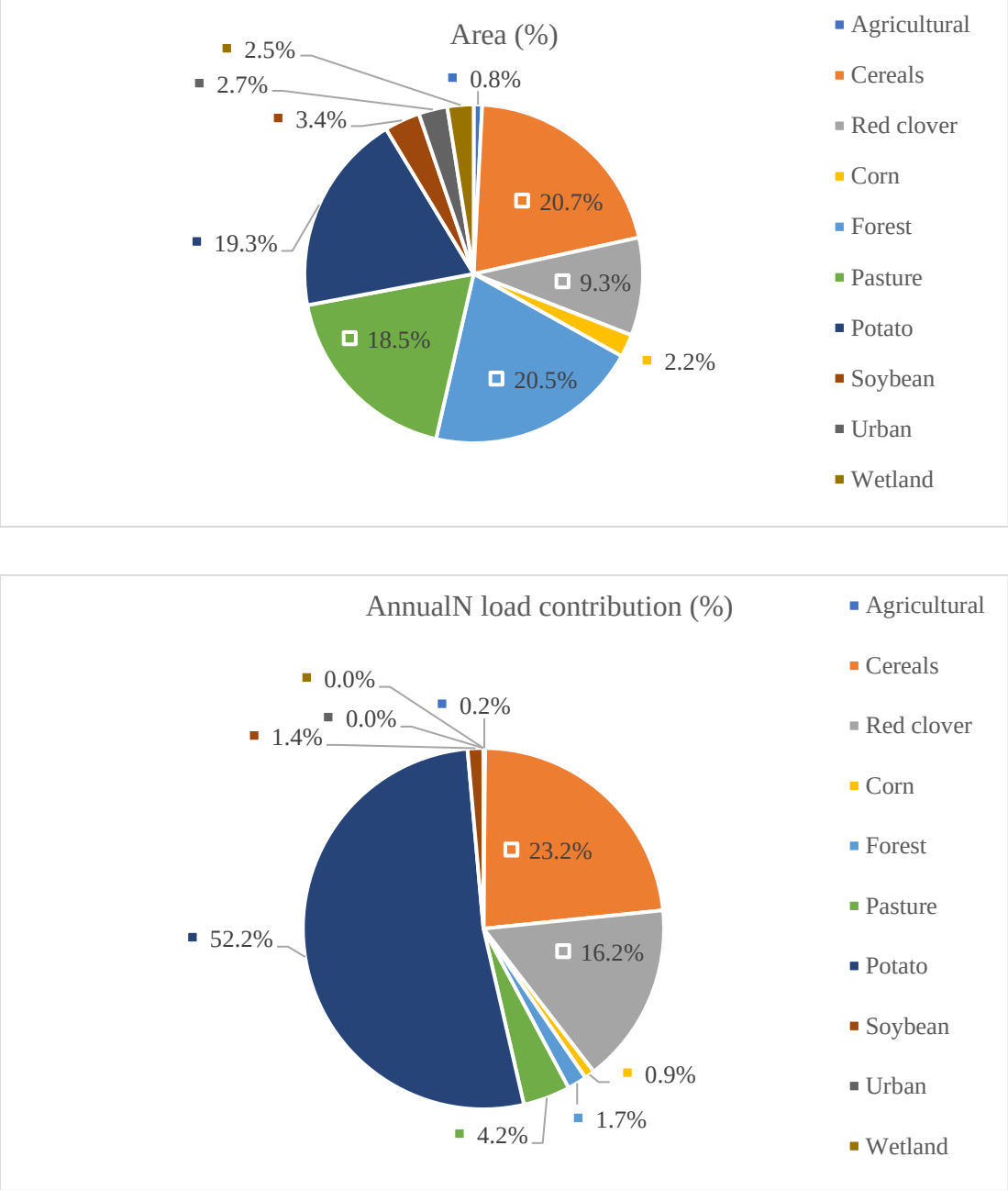

Figure 4.11. Average percentage area versus total annual nitrate load contribution of different land use types.

4.3.3.2 Source analysis of nitrate loading

In this study, groundwater was the principal source of nitrate loading. On an annual basis, the nitrate loading contribution of groundwater varied from 93.6% in forest land to 99% in cereal land. Over the growing season, groundwater nitrate delivery ranged from 96.2% in

potato to 98.9% for red clover and soybean. 91.3% and 99.5% of nitrate load were contributed by groundwater during non-growing season for forest and potato, respectively. Lateral flow demonstrated a minimal role in nitrate delivery out of HRUs, with a non-growing season range of 0.5% to 8.4% for potato and forest land, respectively. Lateral flow provided 1.1% to 3.8% of the total nitrate load for soybean and potato, respectively, during the growing season. Model simulations demonstrated neglectable nitrate loss via surface runoff under all land use types and different seasons. The absence of surface nitrate loss generally agrees with observations from multiple studies in PEI reporting low nitrate concentrations in surface runoff (Dunn et al. 2011; Jiang et al. 2015). In general, where the soil is saturated and has a good condition, the natural drainage will carry a predominant proportion of the nitrate to a depth where it will not be vulnerable to surface runoff (Baker 2001).

4.3.3.3 Average nitrate loading and leaching of each land use

Through utilizing the dynamic land use input feature of SWAT, we were able to determine the nitrate loading under different land use conditions. Nitrate loading was obtained from the output of SWAT HRU for each land use category to assess the effect of land use on water quality. The average annual nitrate load of forested land was the lowest among all land use categories, with 2.3 kg ha^{-1}. Agricultural land experienced significantly higher nitrate exports compared to forested land. On an annual basis, the nitrate load was found to be 46.5 kg N ha^{-1} for potatoes, 27.3 kg N ha^{-1} for cereal crops, 23.2 kg N ha^{-1} for red clover, 17.9 kg N ha^{-1} for soybean, 26.3 kg N ha^{-1} for corn, 3.2 kg N ha^{-1} for pastures/forages and 27 kg N ha^{-1} for canola. Similarly, average annual nitrate leaching was highest for potato and lowest for forest land, with 79.2 N ha^{-1} and 4.1 N ha^{-1},

respectively. Nitrate leaching from different land use was obtained as 60 kg N ha^{-1} yr^{-1} for red clover, 21.5 kg N ha^{-1} for cereal crops, 28.7 kg N ha^{-1} for soybean, 31.1 kg N ha^{-1} for corn and 26.9 kg N ha^{-1} for canola. The variation in nitrate loading and leaching between land use types highlights the significance of combining various land uses and preserving natural lands in maintaining the ecological sustainability of agricultural watersheds. Figure 4.12 compares average annual nitrate loading and leaching under different land uses. Our model findings support the commonly held belief that agricultural land is the principal contributor to nitrate pollution in the PEI's agricultural watersheds (Grizard et al. 2020; Jiang and Somers 2009; Liang et al. 2019). The results indicate that compared to forested land, agricultural land has a greater impact on water quality. This aligns with previous studies, such as Kandler et al. (2017), which suggest that agriculture is responsible for a high proportion of non-point source pollution. In fact, according to Kersebaum et al. (2003), agriculture has been estimated to be responsible for 55% of NPS pollution in the European Union. These findings align with previous studies by Haidary et al. (2013), who found a significant negative correlation between water pollution and forest land coverage, and Baker (2006), who found that undisturbed forests have a relatively minor impact on water quality compared to other land uses.

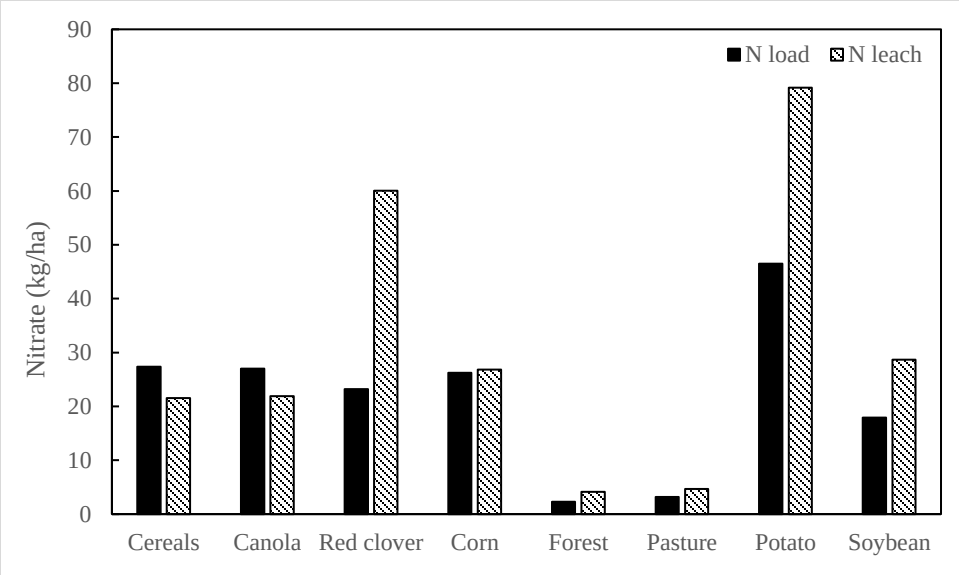

Figure 4.12. Nitrate loading and nitrate leaching variation under different land use.

4.3.3.4 Seasonal loading and leaching of each land use

The results from our model showed a marked variation in nitrate loading across different land use types between the growing and non-growing seasons. Figure 4.13 and Figure 4.14 demonstrate the variation in nitrate loading and leaching under different land uses over the growing season and non-growing season. Forest land had the lowest seasonal nitrate load among all land use types, with 1 kg N ha^{-1} in the growing season and 1.3 kg N ha^{-1} in the non-growing season. Potato, barley, and red clover had the largest nitrate loading during the growing season among dominant crops in the DRW, with 14.7, 13.3, and 8.9 kg N ha^{-1}, respectively. The non-growing season nitrate loading of potato, red clover, cereals, and soybean was 32.2, 14.2, 14, and 9.6 kg N ha^{-1}, respectively. Canola and corn showed to have equal non-growing season N loading with 14.4 kg N ha^{-1}. Pasture and forest land use had the lowest non-growing season loading with 1.3 and 1.7 kg N ha^{-1}, respectively. Non-growing season nitrate loading was notably larger than growing season for potato and red clover land, with 117% and 60% increase from the growing season, respectively. Other

agricultural land had a relatively similar average non-growing season to growing season N load ranging from a 5% increase for barley to a 20% increase for corn.

Unlike nitrate loading out of HRU into the main channel, the annual nitrate leaching process was dominated by the non-growing season. The non-growing season nitrate loading of potato, red clover, cereals, and soybean was estimated as 55.8, 55.2, 17.7, and 26.4 kg N ha^{-1}, respectively. The estimated non-growing season N leaching protentional was 18.7 kg N ha^{-1} for canola and 23.2 kg N ha^{-1} for corn. Pasture and forest land use had the lowest non-growing season loading with 4.1 and 3.6 kg N ha^{-1}, respectively. Non-growing season proportion of annual loading was highest for red clover and soybean, with 92.2% and 91.9%, respectively, and lowest for potato and barley, with 70% and 82% of their annual nitrate leaching, respectively. The higher growing season leaching in some agricultural land use (e.g., potato and barley) can be attributed to fertilizer application susceptible to leaching in the growing season. These findings align with several research suggesting nitrate leaching from agricultural lands in PEI, especially in potato lands, occurs predominantly during the non-growing season (Ballard et al. 2009; Jiang et al. 2011). The higher non-growing season leaching has been attributed to the significant nitrate availability from plant residues during winter when plant N uptake has stopped (Ballard et al. 2009; Liang et al. 2019; Somers et al. 2007).

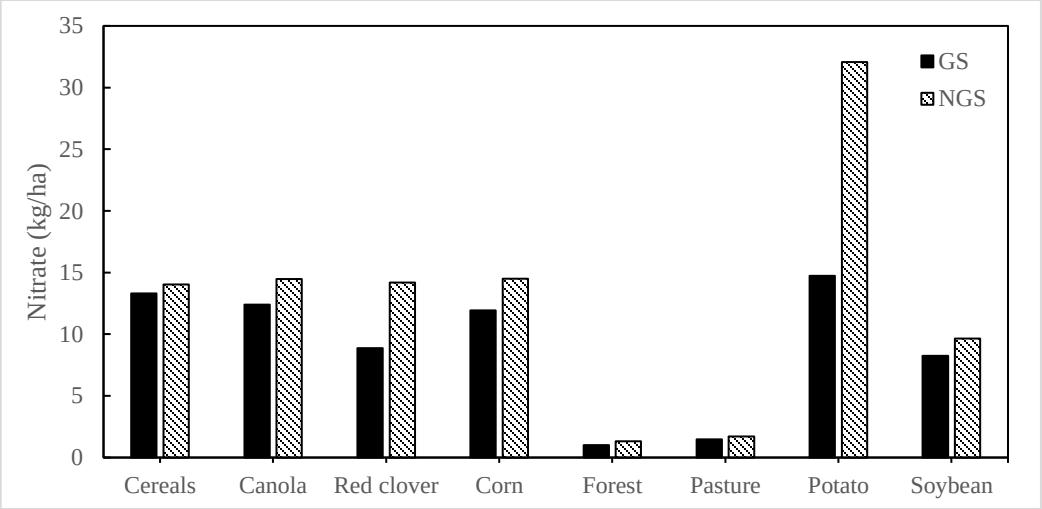

Figure 4.13. Average growing season (GS) and non-growing season (NGS) nitrate loading under different land use types during the study period.

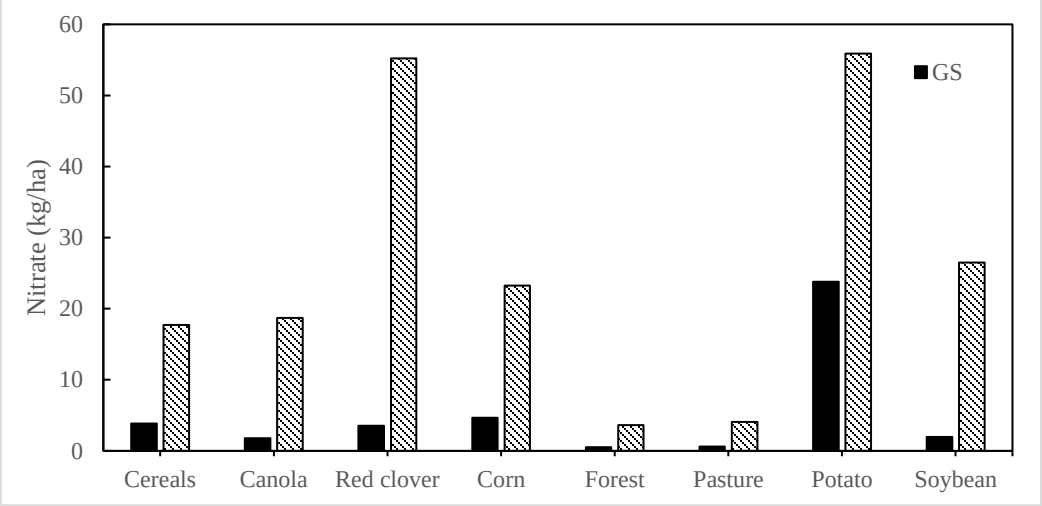

Figure 4.14. Average growing season (GS) and non-growing season (NGS) nitrate leaching under different land use types during the study period.

4.3.4 Significance of red clover in nitrate loading

The average nitrate loading of red clover (23.2 kg N ha^{-1}) was relatively similar to cereals (27.3 kg N ha^{-1}) and soybean (17.9 kg N ha^{-1}) as the crops commonly rotated with potato in PEI. However, they may not contribute equally to the total nitrate loading out of the watershed. The greater impact of red clover is also evident from its annual nitrate leaching results. In this study, red clover had the second highest nitrate leaching with 60 kg N ha^{-1}, whereas barley and soybean had 64% and 52% lower annual nitrate leached. Red clover is often used in potato rotations in PEI as their residue is a great addition to the soil organic matter and organic nitrogen due to their N fixation capacity. Red clover has a higher potential for nitrate leaching, particularly when incorporated during wet fall conditions. Masunga et al. (2016) pointed out that the high N mineralization potential of clover residue could result in significant environmental risks if not synchronized with crop demand. Liang et al. (2019a) discovered that clover presents a higher risk of nitrate leaching due to the slow decomposition of its residue and high N surplus during the non-growing season compared to other crops.

The plowed-down N from red clover may reside in the soil and transfer to the next growing season leading to an N surplus condition that increases leaching and loading from the crop following red clover. Nitrate leaching is thought to occur predominantly during the non-growing season, resulting in elevated nitrate levels in groundwater during the non-growing season (Jiang et al., 2011; Zebarth et al., 2015; Woli and Hoogenboom, 2018; Liang et al., 2019). However, a significant amount of leached nitrate may be trapped in the vadose zone after leaving the root zone, which leads to a prolonged nitrate travel time to groundwater, depending on the lithology of the vadose zone. This legacy N in the vadose zone may

function as a long-term source of contamination for both surface and groundwater, as noted by Van Meter et al. (2017, 2018) and Jiang et al. (2017). Consequently, the nitrate load in groundwater may result from the cumulative effects of land management practices over several years, including the direct effects of current land management and the carry-over effects from previous years. However, it should be noted that SWAT's ability to accurately simulate nitrate transport from in the vodose zone, and predict lateral and groundwater flow lag time may be limited, according to Ilampooranan et al. (2019). The magnitude of nitrate loading increase in other crops due to red clover in the DRW simulation will be demonstrated in the following sections.

4.3.5 Replacing red clover with soybean

Red clover land was completely replaced with soybean in model input data to assess the effectiveness of the alternative rotation PSB at a watershed scale. Total nitrate loading in DRW was 246 t N yr^{-1}. Nitrate loading over the growing season and non-growing season in the condition where soybean replaces red clover was obtained as 94 t N $yr^{-1}$and 152 t N yr^{-1}. These results indicate that replacing soybean with red clover alone reduced annual loading from 301 kg N y^{-1} by 18.4%. Average growing season and non-growing season nitrate loading of the watershed observed similar reductions with 18.7% and 18.2% decrease in loading compared to the initial situation where potato is rotated with red clover (PBC). Figure 4.15 compares nitrate loading from the watershed under red clover and soybean potato rotations. The reduction was not solely sourced from red clover replacement with soybean. Other land use types that were previously in rotation with red clover underwent considerable decrease in their nitrate loading. Figure 4.16 compares the contribution of different land use to the total nitrate loading of the watershed under red

clover and soybean potato rotations. Cereals, potato and, soybean, provided 63, 130 and, 33 t N yr^{-1}. Forest land and pasture/forages contributed 5.2 and 10 tons of nitrate to the annual loading out of the watershed. Other agricultural land use had minimal contribution due to their insignificant area in the DRW. The replaced soybean area generated 29.7 t N yr^{-1}, representing a 39% reduction from the red clover with 48.7 t N yr^{-1}. Nitrate loading from potato and cereals experienced reductions of 17.4% and 10%, respectively. The replaced PSB potato rotation (potatoes/soybean/cereals) lands generated 222.5 t N yr^{-1} nitrate loading representing a 19.4% decrease from that of the previous PBC (potato/red clover/cereals) rotation lands with an annual contribution of 276 t N yr^{-1}. Forest and pasture/forage lands experienced the least change in their loading, with 5.6% and 0.2% reduction. The lack of sensible change in nitrate loading from pasture land use demonstrates that the algorithm was fairly reliable in separating red clover from pastures not rotated with agricultural land use. Red clover and soybean were the only crops with nitrogen fixating capabilities. The average annual fixation rate for red clover and soybean was 134.5 kg N ha^{-1} and 193.2 kg N ha^{-1}, respectively. Red clover and soybean had similar plant N uptake with 229 kg N ha^{-1} and 201 kg N ha^{-1}, respectively. However, most of the soybean's N content is harvested from the field as soybean grains, while the commonly adopted practice for red clover cultivation is plowing down the entirety of the plant. The difference in the N returned as the residue is expected to reduce nitrate loading on a field and watershed scale.

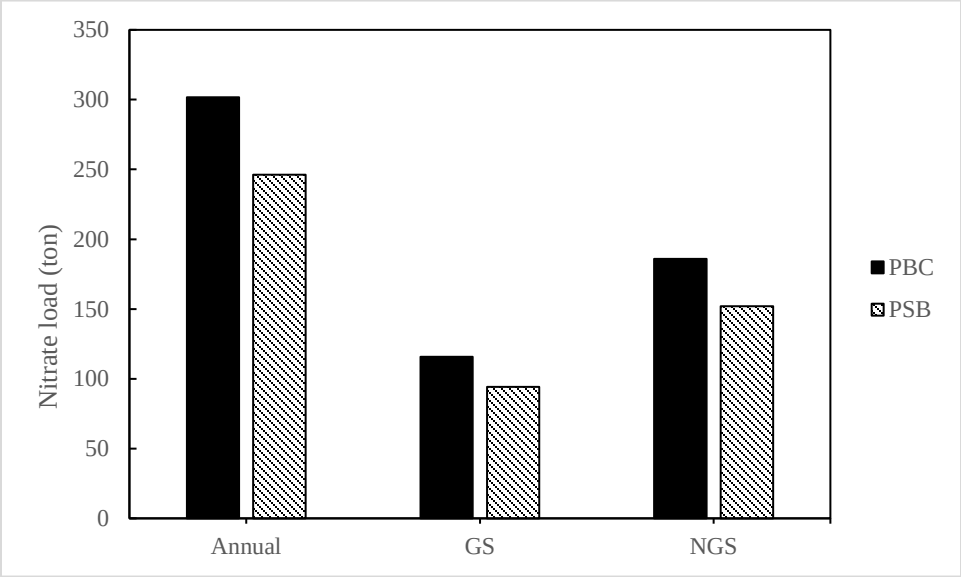

Figure 4.15. Nitrate loading from watershed under PSB and PBC rotations over annual, growing, and non-growing seasons.

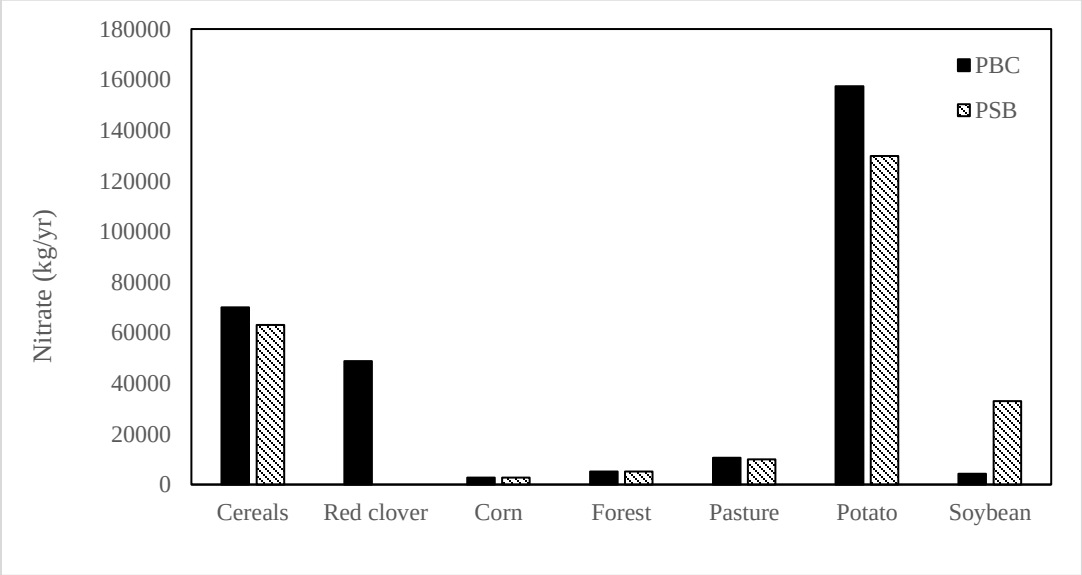

Figure 4.16. Nitrate load contribution of various land use to total nitrate load from watershed under PSB and PBC scenarios.

4.4 Conclusion

This study was carried out to assess the importance of red clover on nitrate loading from Dunk River Watershed and evaluate the mitigating impact of an alternative potato rotation using the SWAT model. Furthermore, several insights are provided on challenges in accurately modeling nitrogen loading dynamics in agriculturally dominated watersheds of Atlantic Canada.

1. The results of the SWAT model reveal that controlling for nitrogen input from crop residue is of great importance in the accurate modeling of nitrate loading. Red clover residue is a significant source of additional nitrogen to the soil due to its high biological nitrogen fixation rates. The SWAT model predicted an average nitrogen fixation rate of 134 kg N ha^{-1} for red clover. Despite the presence of red clover in the standard three-year potato rotation in PEI, the annual crop inventory does not separate red clover from pasture and forages. Through the implementation of an alternative algorithm, red clover was estimated to constitute 9.3% of the watershed. The separated red clover area fixed 282 t N annually in the watershed. These observations demonstrate that the absence of separated red clover in the original land use data can significantly underestimate organic nitrogen input into the watershed.

2. Furthermore, SWAT overestimated plant nitrogen uptake of several crops using its default plant parameters. Plant N uptake of barley, red clover, and soybean was overestimated by 26, 51, and 160%, respectively, compared to the average expected plant N contents in the Atlantic region. Therefore, the plant parameters of these crops were adjusted to match the expected plant N uptake. Annual plant N uptake in the watershed using default parameters was 1424 t N larger than adjusted parameters

representing an 86% overestimation of the total annual N uptake. It is likely that the absence of red clover-fixated nitrogen may be compensated by overestimation of N uptake in barley, soybean, and other crops when using default plant parameters, therefore producing a model that does not respect actual nitrogen dynamics in the watershed. These observations indicate that much care needs to be taken into account when defining organic N input into the watershed as a significant contributor to nitrate loading from the watershed.

3. Red clover biomass is completely returned to the soil as a common practice in PEI with the expectation that the returned organic N in the biomass enriches soil nutrients for the following potato year. However, a number of studies in PEI have argued that the organic N in red clover residue may lead to an excessive N supply and reduce potato yield while significantly increasing nitrate leaching from farms under potato rotation (Azimi et al. 2022; Jiang et al. 2019; Liang et al. 2019; Nyiraneza et al. 2015). Annual nitrogen uptake of red clover was estimated as 201 kg N $ha^{-1,}$ which is completely returned to the soil as residue. Annual nitrate loading from red clover into the main reach of the watershed was calculated as 23.2 kg N ha^{-1}, accounting for 15.7% of the growing season and 16.4% of the non-growing season nitrate loading of the watershed. Nitrate leaching from red clover was obtained as 60 kg N ha^{-1}, as second highest among potato rotation crops, followed by soybean and barley with 28.7 and 21.5 kg N ha^{-1}, respectively.

4. Alternative crop rotations are recognized as effective best management practices in mitigating nitrate leaching from farms. Previous studies have reported the alternative potato-soybean-barley rotation to reduce nitrate leaching compared to the conventional

at the farm scale. Using the SWAT model to assess the alternative rotation at the watershed scale revealed that replacing red clover with soybean remarkably reduced nitrate loading from the dunk river watershed by 18%. In addition, the results indicated that the alternative PSB rotation caused the other potato rotation crops to undergo considerable nitrate loading reduction. After replacing red clover with soybean in the land use maps, potato and cereals average nitrate loading was reduced by 17.4 and 10%, respectively. While soybean has shown to be effective, other BMPs, such as different termination methods, plowing timing of red clover, and other alternative rotation crops, may be selected based on what the landowners decide. Here we only assess soybean replacement as one of the many BMPs. Other management scenarios can be evaluated following a similar approach.

This study assessed the importance of potato rotation crops in nitrate loading from the Dunk River Watershed. The results revealed that the organic nitrogen from the plowed-down red clover residues as a standard rotation crop in PEI immensely contributes to nitrate loading at the watershed scale. SWAT simulations indicated that implementing BMPs, such as crop rotation, can effectively mitigate nitrate loading from watersheds with intensive potato cultivation. This study further demonstrated important considerations for modelling nitrate loading in this region; (1) using local experimental data to constraint plant N uptake parameters is of great importance; (2) accounting for N input using accurate land use information (e.g., red clover) is critical. The findings of this study can be of great importance for watershed management planning. separation) in combination with local empirical agronomic information is important.

Bibliography

Abbaspour, K.C. 2015. SWAT-CUP: SWAT calibration and uncertainty programs—a user manual, *Eawag: Dübendorf, Switzerland*: 16-70.

Abbaspour, K.C., C. Johnson, and M.T. Van Genuchten. 2004. Estimating uncertain flow and transport parameters using a sequential uncertainty fitting procedure, *Vadose zone journal*, 3: 1340-52.

Akhavan, S., J. Abedi-Koupai, S.-F. Mousavi, M. Afyuni, S.-S. Eslamian, and K.C. Abbaspour. 2010. Application of SWAT model to investigate nitrate leaching in Hamadan–Bahar Watershed, Iran, *Agriculture, ecosystems & environment*, 139: 675-88.

Arnold, J.G., and N. Fohrer. 2005. SWAT2000: current capabilities and research opportunities in applied watershed modelling, *Hydrological Processes: An International Journal*, 19: 563-72.

Arnold, J.G., R. Srinivasan, R.S. Muttiah, and J.R. Williams. 1998. Large area hydrologic modeling and assessment part I: model development 1, *JAWRA Journal of the American Water Resources Association*, 34: 73-89.

Azimi, M.A., Y. Jiang, F.-R. Meng, and K. Liang. 2022. Yield responses of four common potato cultivars to an industry standard and alternative rotation in Atlantic Canada, *American Journal of Potato Research*: 1-11.

Baker, J.L. 2001. Limitations of improved nitrogen management to reduce nitrate leaching and increase use efficiency, *TheScientificWorldJOURNAL*, 1: 10-16.

Baker, L.A. 1992. Introduction to nonpoint source pollution in the United States and prospects for wetland use, *Ecological Engineering*, 1: 1-26.

Ballard, J., D. Paradis, R. Lefebvre, and M. Savard. 2009. Numerical modeling of the dynamics of multisource nitrate generation and transfer, PEI, Paper 210, GeoHalifax'09. In *62th Canadian Geotechnical Conference and 10th Joint CGS/IAH Conference*.

Benson, V.S., J.A. VanLeeuwen, J. Sanchez, I.R. Dohoo, and G.H. Somers. 2006. Spatial analysis of land use impact on ground water nitrate concentrations, *Journal of environmental quality*, 35: 421-32.

Bernard, G., S. Asiedu, and P. Boswall. 1993. Atlantic Canada potato guide, *Atlantic Provinces Agriculture Services Coordinating Committee publication*, 1300: 93.

Brighenti, T.M., N.B. Bonumá, F. Grison, A. de Almeida Mota, M. Kobiyama, and P.L.B. Chaffe. 2019. Two calibration methods for modeling streamflow and suspended sediment with the swat model, *Ecological Engineering*, 127: 103-13.

Bugden, G., Y. Jiang, M. van den Heuvel, H. Vandermeulen, K. MacQuarrie, C. Crane, and B. Raymond. 2014. Nitrogen loading criteria for estuaries in Prince Edward Island. (Fisheries and Oceans Canada= Pêches et océans Canada).

Danielescu, S., and K.T. MacQuarrie. 2011. Nitrogen loadings to two small estuaries, Prince Edward Island, Canada: a 2-year investigation of precipitation, surface water and groundwater contributions, *Hydrological Processes*, 25: 945-57.

Danielescu, S., and K.T. MacQuarrie. 2013. Nitrogen and oxygen isotopes in nitrate in the groundwater and surface water discharge from two rural catchments: implications for nitrogen loading to coastal waters, *Biogeochemistry*, 115: 111-27.

De Notaris, C., J. Rasmussen, P. Sørensen, and J.E. Olesen. 2018. Nitrogen leaching: A crop rotation perspective on the effect of N surplus, field management and use of catch crops, *Agriculture, ecosystems & environment*, 255: 1-11.

Dunn, A., G. Julien, W. Ernst, A. Cook, K. Doe, and P. Jackman. 2011. Evaluation of buffer zone effectiveness in mitigating the risks associated with agricultural runoff in Prince Edward Island, *Science of the Total Environment*, 409: 868-82.

El-Khoury, A., O. Seidou, D. Lapen, Z. Que, M. Mohammadian, M. Sunohara, and D. Bahram. 2015. Combined impacts of future climate and land use changes on discharge, nitrogen and phosphorus loads for a Canadian river basin, *Journal of environmental management*, 151: 76-86.

Environment-Canada. 2011. Water quality status and trends of nutrients in major drainage areas in Canada. Technical Summary.

Francis, R.M. 1989. Hydrogeology of the Winter River Basin-Prince Edward Island. (Water Resources Branch, Department of the Island, Prince Edward Island).

Gassman, P.W., M.R. Reyes, C.H. Green, and J.G. Arnold. 2007. The soil and water assessment tool: historical development, applications, and future research directions, *Transactions of the ASABE*, 50: 1211-50.

Giri, S., A.P. Nejadhashemi, and S.A. Woznicki. 2016. Regulators' and stakeholders' perspectives in a framework for bioenergy development, *Land Use Policy*, 59: 143-53.

Giri, S., and Z. Qiu. 2016. Understanding the relationship of land uses and water quality in twenty first century: a review, *Journal of environmental management*, 173: 41-48.

Goolsby, D.A., and W.A. Battaglin. 2001. Long-term changes in concentrations and flux of nitrogen in the Mississippi River Basin, USA, *Hydrological Processes*, 15: 1209-26.

Green, P.A., C.J. Vörösmarty, M. Meybeck, J.N. Galloway, B.J. Peterson, and E.W. Boyer. 2004. Pre-industrial and contemporary fluxes of nitrogen through rivers: a global assessment based on typology, *Biogeochemistry*, 68: 71-105.

Grizard, P., K.T. MacQuarrie, and Y. Jiang. 2020. Land-use based modeling approach for determining freshwater nitrate loadings from small agricultural watersheds, *Water Quality Research Journal*, 55: 278-94.

Gupta, H.V., S. Sorooshian, and P.O. Yapo. 1998. Toward improved calibration of hydrologic models: Multiple and noncommensurable measures of information, *Water Resources Research*, 34: 751-63.

Gupta, H.V., S. Sorooshian, and P.O. Yapo. 1999. Status of automatic calibration for hydrologic models: Comparison with multilevel expert calibration, *Journal of Hydrologic Engineering*, 4: 135-43.

Haas, M.B., B. Guse, and N. Fohrer. 2017. Assessing the impacts of Best Management Practices on nitrate pollution in an agricultural dominated lowland catchment considering environmental protection versus economic development, *Journal of environmental management*, 196: 347-64.

Hua, B., J. Yang, F. Liu, G. Zhu, B. Deng, and J. Mao. 2018. Characterization of dissolved organic matter/nitrogen by fluorescence excitation-emission matrix spectroscopy and X-ray photoelectron spectroscopy for watershed management, *Chemosphere*, 201: 708-15.

Jabbar, F.K., and K. Grote. 2019. Statistical assessment of nonpoint source pollution in agricultural watersheds in the Lower Grand River watershed, MO, USA, *Environmental Science and Pollution Research*, 26: 1487-506.

Jiang, S., Q. Zhang, A. Werner, C. Wellen, S. Jomaa, Q. Zhu, O. Büttner, G. Meon, and M. Rode. 2019a. Effects of stream nitrate data frequency on watershed model performance and prediction uncertainty, *Journal of Hydrology*, 569: 22-36.

Jiang, Y., P. Nishimura, M.R. van den Heuvel, K.T. MacQuarrie, C.S. Crane, Z. Xing, B.G. Raymond, and B.L. Thompson. 2015. Modeling land-based nitrogen loads from groundwater-dominated agricultural watersheds to estuaries to inform nutrient reduction planning, *Journal of Hydrology*, 529: 213-30.

Jiang, Y., J. Nyiraneza, M. Khakbazan, X. Geng, and B.J. Murray. 2019b. Nitrate leaching and potato yield under varying plow timing and nitrogen rate, *Agrosystems, Geosciences & Environment*, 2: 1-14.

Jiang, Y., and G. Somers. 2009. Modeling effects of nitrate from non-point sources on groundwater quality in an agricultural watershed in Prince Edward Island, Canada, *Hydrogeology Journal*, 17: 707-24.

Jiang, Y., G. Somers, and J. Mutch. 2004. Application of numerical modeling to groundwater assessment and management in Prince Edward Island.

Jiang, Y., B. Zebarth, and J. Love. 2011. Long-term simulations of nitrate leaching from potato production systems in Prince Edward Island, Canada, *Nutrient Cycling in Agroecosystems*, 91: 307-25.

Kang, S., H. Lin, W.J. Gburek, G.J. Folmar, and B. Lowery. 2008. Baseflow nitrate in relation to stream order and agricultural land use, *Journal of environmental quality*, 37: 808-16.

Krause, P., D.P. Boyle, and F. Bäse. 2005. Comparison of different efficiency criteria for hydrological model assessment, *Advances in geosciences*, 5: 89-97.

Lee, S., A.M. Sadeghi, I.-Y. Yeo, G.W. McCarty, and W.D. Hively. 2017. Assessing the impacts of future climate conditions on the effectiveness of winter cover crops in reducing nitrate loads into the Chesapeake Bay watersheds using the SWAT model, *Transactions of the ASABE*, 60: 1939-55.

Liang, K. 2020. 'Enhancing understanding of BMP effectiveness and land use change impacts on water quality, water quantity, and potato production in Atlantic Canada', University of New Brunswick.

Liang, K., Y. Jiang, J. Nyiraneza, K. Fuller, D. Murnaghan, and F.-R. Meng. 2019. Nitrogen dynamics and leaching potential under conventional and alternative potato rotations in Atlantic Canada, *Field Crops Research*, 242: 107603.

Liang, K., Y. Jiang, J. Qi, K. Fuller, J. Nyiraneza, and F.-R. Meng. 2020. Characterizing the impacts of land use on nitrate load and water yield in an agricultural watershed in Atlantic Canada, *Science of the Total Environment*, 729: 138793.

Liao, S.L., M. Savard, G. Somers, D. Paradis, and Y. Jiang. 2005. Preliminary results from water-isotope characterization of groundwater, surface water, and precipitation in the Wilmot River watershed, Prince Edward Island. (Natural Resources Canada, Geological Survey of Canada).

Lyne, V., and M. Hollick. 1979. Stochastic time-variable rainfall-runoff modelling. In *Institute of Engineers Australia National Conference*, 89-93. Institute of Engineers Australia Barton, Australia.

Moriasi, D.N., J.G. Arnold, M.W. Van Liew, R.L. Bingner, R.D. Harmel, and T.L. Veith. 2007. Model evaluation guidelines for systematic quantification of accuracy in watershed simulations, *Transactions of the ASABE*, 50: 885-900.

Myrbeck, Å. 2014. Soil tillage influences on soil mineral nitrogen and nitrate leaching in Swedish arable soils.

Neter, J., M.H. Kutner, C.J. Nachtsheim, and W. Wasserman. 1996. Applied linear statistical models.

Noori, N., L. Kalin, and S. Isik. 2020. Water quality prediction using SWAT-ANN coupled approach, *Journal of Hydrology*, 590: 125220.

Nyiraneza, J., R.D. Peters, V.A. Rodd, M.G. Grimmett, and Y. Jiang. 2015. Improving productivity of managed potato cropping systems in Eastern Canada: crop rotation and nitrogen source effects, *Agronomy Journal*, 107: 1447-57.

Ouyang, W., X. Hao, L. Wang, Y. Xu, M. Tysklind, X. Gao, and C. Lin. 2019. Watershed diffuse pollution dynamics and response to land development assessment with riverine sediments, *Science of the Total Environment*, 659: 283-92.

Pai, N., and D. Saraswat. 2011. SWAT2009_LUC: A tool to activate the land use change module in SWAT 2009, *Transactions of the ASABE*, 54: 1649-58.

Paradis, D., J. Ballard, M. Savard, R. Lefebvre, Y. Jiang, G. Somers, S. Liao, and C. Rivard. 2006. Impact of agricultural activities on nitrates in ground and surface water in the

Wilmot Watershed, PEI, Canada. In *59th Canadian Geotechnical Conference and the 7th joint CGS/IAH-CNC Conference, Vancouver*, 1-4.

Pellerin, B.A., B.A. Bergamaschi, R.J. Gilliom, C.G. Crawford, J. Saraceno, C.P. Frederick, B.D. Downing, and J.C. Murphy. 2014. Mississippi River nitrate loads from high frequency sensor measurements and regression-based load estimation, *Environmental Science & Technology*, 48: 12612-19.

Peralta, J.M.a., and C.O. Stockle. 2002. Dynamics of nitrate leaching under irrigated potato rotation in Washington State: a long-term simulation study, *Agriculture, ecosystems & environment*, 88: 23-34.

Prunty, L., and R. Greenland. 1997. Nitrate leaching using two potato-corn N-fertilizer plans on sandy soil, *Agriculture, ecosystems & environment*, 65: 1-13.

Pushpalatha, R., C. Perrin, N. Le Moine, and V. Andréassian. 2012. A review of efficiency criteria suitable for evaluating low-flow simulations, *Journal of Hydrology*, 420: 171-82.

Qi, J., S. Li, C.P.-A. Bourque, Z. Xing, and F.-R. Meng. 2018. Developing a decision support tool for assessing land use change and BMPs in ungauged watersheds based on decision rules provided by SWAT simulation, *Hydrology and Earth System Sciences*, 22: 3789-806.

Romanelli, A., D.X. Soto, I. Matiatos, D.E. Martínez, and S. Esquius. 2020. A biological and nitrate isotopic assessment framework to understand eutrophication in aquatic ecosystems, *Science of the Total Environment*, 715: 136909.

Savard, M.M., D. Paradis, G. Somers, S. Liao, and E. van Bochove. 2007. Winter nitrification contributes to excess NO3− in groundwater of an agricultural region: A dual-isotope study, *Water Resources Research*, 43.

Savard, M.M., G. Somers, A. Smirnoff, D. Paradis, E. van Bochove, and S. Liao. 2010. Nitrate isotopes unveil distinct seasonal N-sources and the critical role of crop residues in groundwater contamination, *Journal of Hydrology*, 381: 134-41.

Schilling, K., and Y.-K. Zhang. 2004. Baseflow contribution to nitrate-nitrogen export from a large, agricultural watershed, USA, *Journal of Hydrology*, 295: 305-16.

Schilling, K.E., and D.S. Lutz. 2004. RELATION OF NITRATE CONCENTRATIONS TO BASEFLOW IN THE RACCOON RIVER, IOWA 1, *JAWRA Journal of the American Water Resources Association*, 40: 889-900.

Sith, R., A. Watanabe, T. Nakamura, T. Yamamoto, and K. Nadaoka. 2019. Assessment of water quality and evaluation of best management practices in a small agricultural watershed adjacent to Coral Reef area in Japan, *Agricultural Water Management*, 213: 659-73.

Somers, G., M.M. Savard, and D. Paradis. 2007. Mass balance calculations to estimate nitrate proportions from various sources in the agricultural Wilmot watershed of Prince Edward Island. In *The 60th Canadian Geotechnical Conference and 8th Joint GCS/IAH-CNC Groundwater Conference, Ottawa*, 112-18.

Torstensson, G., H. Aronsson, and L. Bergström. 2006. Nutrient use efficiencies and leaching of organic and conventional cropping systems in Sweden, *Agronomy Journal*, 98: 603-15.

Ullrich, A., and M. Volk. 2009. Application of the Soil and Water Assessment Tool (SWAT) to predict the impact of alternative management practices on water quality and quantity, *Agricultural Water Management*, 96: 1207-17.

Villarini, G., C.S. Jones, and K.E. Schilling. 2016. Soybean area and baseflow driving nitrate in Iowa's Raccoon River, *Journal of environmental quality*, 45: 1949-59.

Vörösmarty, C.J., P.B. McIntyre, M.O. Gessner, D. Dudgeon, A. Prusevich, P. Green, S. Glidden, S.E. Bunn, C.A. Sullivan, and C.R. Liermann. 2010. Global threats to human water security and river biodiversity, *Nature*, 467: 555-61.

Vos, J., C. Van Loon, and G. Bollen. 2012. Effects of Crop Rotation on Potato Production in the Temperate Zones: Proceedings of the International Conference on Effects of Crop Rotation on Potato Production in the Temperate Zones, held August 14–19, 1988, Wageningen, The Netherlands. (Springer Science & Business Media).

Wade, A., C. Neal, P. Whitehead, and N. Flynn. 2005. Modelling nitrogen fluxes from the land to the coastal zone in European systems: a perspective from the INCA project, *Journal of Hydrology*, 304: 413-29.

Wang, C., R. Jiang, L. Boithias, S. Sauvage, J.-M. Sánchez-Pérez, X. Mao, Y. Han, A. Hayakawa, K. Kuramochi, and R. Hatano. 2016. Assessing potassium environmental losses from a dairy farming watershed with the modified SWAT model, *Agricultural Water Management*, 175: 91-104.

Wang, Q., R. Liu, C. Men, L. Guo, and Y. Miao. 2018. Effects of dynamic land use inputs on improvement of SWAT model performance and uncertainty analysis of outputs, *Journal of Hydrology*, 563: 874-86.

White, K.L., and I. Chaubey. 2005. Sensitivity analysis, calibration, and validations for a multisite and multivariable SWAT model 1, *JAWRA Journal of the American Water Resources Association*, 41: 1077-89.

Xiang, C., Y. Wang, and H. Liu. 2017. A scientometrics review on nonpoint source pollution research, *Ecological Engineering*, 99: 400-08.

Yang, X., Q. Liu, G. Fu, Y. He, X. Luo, and Z. Zheng. 2016. Spatiotemporal patterns and source attribution of nitrogen load in a river basin with complex pollution sources, *Water Research*, 94: 187-99.

Zebarth, B., C. Drury, N. Tremblay, and A. Cambouris. 2009. Opportunities for improved fertilizer nitrogen management in production of arable crops in eastern Canada: A review, *Canadian Journal of Soil Science*, 89: 113-32.

Zebarth, B.J., S. Danielescu, J. Nyiraneza, M.C. Ryan, Y. Jiang, M. Grimmett, and D.L. Burton. 2015. Controls on nitrate loading and implications for BMPs under intensive potato production systems in Prince Edward Island, Canada, *Groundwater Monitoring & Remediation*, 35: 30-42.

Zhang, X., X. Liu, M. Zhang, R.A. Dahlgren, and M. Eitzel. 2010. A review of vegetated buffers and a meta-analysis of their mitigation efficacy in reducing nonpoint source pollution, *Journal of environmental quality*, 39: 76-84.

4.5 Supplementary documents

Supplementary Table 4.3. Parameters used for streamflow and nitrate load calibration in SWAT and parameter sensitivity analysis.

Category	Parameter	Minimum	Maximum	t-stat	p	Fitted Values
Streamflow	**r__CN2.mgt**	**-0.27**	**-0.20**	**-1.58**	**0.12**	**-0.26**
	r__OV_N.hru	**0.09**	**0.18**	**-2.27**	**0.02**	**0.17**
	r__SOL_AWC().sol	**-0.06**	**0.08**	**-3.07**	**0.00**	**-0.01**
	r__SOL_BD().sol	**-0.10**	**0.00**	**1.71**	**0.09**	**-0.01**
	r__SOL_K().sol	**-0.27**	**-0.11**	**-1.64**	**0.10**	**-0.19**
	v__CANMX.hru	**1.37**	**3.27**	**-0.57**	**0.57**	**1.57**
	v__CH_COV1.rte	**-0.05**	**0.19**	**0.37**	**0.71**	**0.05**
	v__CH_K1.sub	**58.99**	**152.77**	**-0.84**	**0.40**	**142.41**
	v__CH_K2.rte	**244.80**	**322.08**	**1.69**	**0.09**	**263.70**
	v__CH_N1.sub	**0.10**	**0.12**	**-0.27**	**0.78**	**0.12**
	v__CH_N2.rte	**0.21**	**0.30**	**0.14**	**0.89**	**0.24**
	v__EPCO.bsn	**0.09**	**0.35**	**-0.72**	**0.47**	**0.30**
	v__ESCO.bsn	**0.07**	**0.19**	**0.55**	**0.58**	**0.15**
	v__GW_DELAY.gw	**82.06**	**142.70**	**6.84**	**0.00**	**133.51**
	v__GW_REVAP.gw	**0.04**	**0.05**	**-4.88**	**0.00**	**0.04**
	v__GWQMN.gw	**0.00**	**501.46**	**1.77**	**0.08**	**175.26**
	v__RCHRG_DP.gw	**0.07**	**0.09**	**1.21**	**0.23**	**0.09**
	v__REVAPMN.gw	**38.77**	**116.34**	**-1.19**	**0.24**	**92.41**
	v__SFTMP.bsn	**-4.48**	**-3.40**	**1.03**	**0.30**	**-3.43**
	v__SHALLST.gw	**0.00**	**650.03**	**0.29**	**0.77**	**376.69**
	v__SMFMN.bsn	**6.00**	**9.92**	**2.18**	**0.03**	**7.77**
	v__SMFMX.bsn	**3.21**	**5.07**	**1.71**	**0.09**	**4.19**

	v__SMTMP.bsn	**-0.44**	**1.39**	**-0.45**	**0.65**	**0.17**
	v__SURLAG.bsn	**9.82**	**15.97**	**0.72**	**0.47**	**10.04**
	v__TIMP.bsn	**0.59**	**0.84**	**0.97**	**0.33**	**0.83**
Nitrate load	**v__CMN.bsn**	**0.00**	**0.00**	**-0.18**	**0.85**	**0.00**
	v__DECR_MIN.bsn	**0.00**	**0.03**	**-1.26**	**0.21**	**0.01**
	v__HLIFE_NGW.gw	**183.91**	**300.00**	**0.74**	**0.46**	**277.54**
	v__N_UPDIS.bsn	**20.92**	**62.76**	**0.81**	**0.42**	**28.43**
	v__NPERCO.bsn	**0.01**	**0.07**	**0.35**	**0.73**	**0.02**
	v__RCN.bsn	**1.33**	**5.62**	**-1.54**	**0.12**	**4.67**
	v__RSDCO.bsn	**0.03**	**0.05**	**-2.15**	**0.03**	**0.04**
	v__SDNCO.bsn	**0.70**	**1.00**	**0.18**	**0.86**	**0.93**
	v__ANION_EXCL.sol	**0.57**	**0.80**	**1.19**	**0.24**	**0.60**
	v__SOL_NO3().chm	**63.51**	**91.09**	**0.26**	**0.80**	**70.72**
	v__SPCON.bsn	**0.00**	**0.01**	**0.30**	**0.77**	**0.00**

Supplementary Table 4.4. Summary of selected baseflow dataset.

Year	**Count**	**Avg bfQ (m^3/s)**	**Max bfQ (m^3/s)**	**Min bfQ (m^3/s)**
2002	**68**	**1.4**	**2.2**	**0.9**
2003	**76**	**1.5**	**2.3**	**1.0**
2004	**77**	**1.2**	**1.9**	**0.8**
2005	**70**	**1.3**	**2.1**	**0.8**
2006	**50**	**1.5**	**1.8**	**1.2**
2007	**73**	**1.6**	**2.2**	**1.3**
2008	**66**	**1.5**	**2.4**	**1.3**
2009	**59**	**1.7**	**2.4**	**1.3**
2010	**63**	**1.5**	**2.0**	**1.2**

2011	**69**	**1.9**	**3.1**	**1.4**
2012	**60**	**1.1**	**1.5**	**0.8**
2013	**67**	**1.2**	**1.7**	**0.8**
2014	**69**	**1.5**	**2.4**	**1.0**
2015	**72**	**1.6**	**2.5**	**1.0**
2016	**65**	**1.3**	**1.8**	**0.9**
2017	**72**	**1.5**	**2.5**	**0.9**
2018	**57**	**1.4**	**1.9**	**1.0**
2019	**75**	**1.6**	**2.4**	**1.0**
2020	**56**	**1.2**	**1.8**	**0.6**
Total	**1264**	**1.4**	**3.1**	**0.6**

bfQ represents baseflow (m^3/s).

Chapter 5: Conclusions and Future Research

5.1 Major Outcomes and Conclusions

5.1.1 Alternative PSB rotation could reduce soil mineral nitrogen content while increase potato yields compared to the conventional PBC rotation

Over the past few decades, crop rotation has been widely used as a BMP to reduce the adverse impacts of potato production on the environment and preserve soil productivity. Crop rotation systems that include both non-legumes and legumes can combine the advantages of N preservation and green manure production. Two potato rotations (potato-barley-red clover (PBC)) and potato-soybean-barley (PSB)) experiments were conducted from 2014 to 2017 to understand the effects of different rotation crops and rotation systems on soil mineral nitrogen contents and yield of four potato cultivars.

While soil mineral N content before potato planting was significantly higher under the PBC rotation by 79%, the PSB rotation produced significantly higher yields compared to PBC by 19.5%. The lower yield despite higher N contents in PBC could be an indication of excessive N supply from the plowed-down red clover. The alternative PSB rotation had a greater impact on the yield of russet cultivars, with Gold Rush being the most susceptible, followed by Russet Burbank and Prospect cultivars. However, Shepody showed less sensitivity, experiencing only a 3% decline in yield under the PBC rotation. Russet Burbank achieved the highest yield under both PBC and PSB rotations.

Furthermore, our preliminary economic analysis revealed that the additional income from soybeans in the PSB rotation and the average increase in potato yield could increase the gross income of a rotation cycle up to 30%. The adverse influence of excessive nitrogen supply from red clover organic matter on potato yield had been previously documented in

PEI conditions (Jiang et al. 2019; Nyiraneza et al. 2015). Soil nitrate supply in the cool, humid Atlantic region is predominated by the mineralization occurring over the growing season (Ojala et al. 1990; Sharifi et al. 2007; Zebarth and Rosen 2007; Zebarth et al. 2004). However, the timing and amount of this mineralization are highly uncertain (Nyiraneza et al. 2012; Sharifi et al. 2007). Therefore, the poor connection between tuber production and pre-planting N measurements might be caused by the indefinite amount of soil N supply from the preceding legume's growing season mineralization (Bélanger et al. 2000, 2001). This study demonstrated significant environmental and economic benefits of an alternative rotation and investigated the responses of four common potato cultivars to this rotation.

5.1.2 Groundwater level data can be used in parameter optimization of digital filter methods when separating baseflow from streamflow.

Automated techniques for separating baseflow are widely used for diverse watersheds that exhibit significant spatial and temporal variations. In this study, we implemented three low-pass filter methods using different recommended and alternative standard parameterization schemes. Our objective was to assess their effectiveness and identify the most appropriate methods and parameters for the hydrogeological conditions in PEI. Given the absence of calibration data such as conductivity, we proposed a new approach to evaluate the performance of each method. This approach incorporates two criteria: (a) the linear correlation between the daily separated baseflow and relevant groundwater levels, and (b) the ability of each method to accurately predict maximum baseflow during dry periods when streamflow relies solely on baseflow. The results indicated that both the recommended and alternative parameterization of the Eckhardt method exhibited

unsatisfactory performance, consistently leading to significant underestimation of baseflow during periods characterized by low streamflow and dominance of baseflow.

In contrast, the Lyne and Hollick method proved to be highly effective, consistently achieving near-1 baseflow index (BFI) values during dry periods as well as exhibiting solid correlation with groundwater level. Furthermore, a novel approach was proposed that utilizes evaluative measures to narrow the range of uncertain parameters and improve the process of baseflow separation. The objective was to optimize each method by maximizing the relevant evaluative criteria. Both the LH and EK methods yielded a BFI of 0.68, and their evaluative measure values were nearly identical after selecting optimum parameters. The LH and EK methods using recommended parameters estimated BFI as 0.77 and 0.62, respectively, demonstrating underestimation and overestimation of BFI compared to the BFI using optimum parameters (0.68).

Baseflow separation is of critical importance in various hydrological studies. The study showcased how readily available data (e.g., groundwater level) can be used to identify inaccuracies in estimating baseflow caused by improper parameterization. Additionally, it highlighted the possibility of optimizing baseflow separation using groundwater level data in cases where direct calibration data for baseflow separation is unavailable.

5.1.3 Importance of red clover in nitrate loading mitigation and effectiveness of PSB Rotation rotation

Various experiments in Atlantic Canada have observed red clover to increase soil nitrogen contents and nitrate leaching from potato fields (Azimi et al. 2022; Jiang et al. 2019; Liang et al. 2019). The SWAT model was utilized to assess the influence of red clover and the alternative PSB rotation at a watershed scale. Despite the significance of red clover, the

available annually updated land use map does not recognize red clover and groups all perennial crops as pasture. An alternative algorithm was implanted to detect red clover based on annual land use alternations of each cell in the map. Red clover was estimated to consist of 9.3% of the Dunk River Watershed during the period of study from 2011 to 2020. Red clover was capable of introducing 134 kg N ha^{-1} into the watershed through nitrogen fixation, which is comparable to the average recommended potato fertilization rates (180 kg N ha^{-1}). The nitrogen content in red clover biomass accumulated to 201 kg N $ha^{-1,}$ which is thoroughly returned to the soil as a common red cover cultivation practice in PEI. Red clover contributed to 16% of the total nitrate loading in the Dunk River Watershed, as estimated by the SWAT model. The alternative PSB rotation was assessed by replacing red clover with soybean in the annually updated land use data. The results indicated that the alternative PSB rotation effectively reduced nitrate loading in the Dunk River Watershed by 18%. Simulating the alternative rotation further revealed that red clover not only directly possesses a significant proportion of the nitrate loading but also increases nitrate loading from other rotation crops in the subsequent years. Nitrate loading from potato and cereal was decreased by 17.4 and 10% after replacing red clover with soybean.

The significance of potato rotation crops in nitrate loading from the Dunk River Watershed was evaluated. The findings showed that the organic nitrogen from the red clover residues significantly impacts the nitrate loading at the watershed scale. Crop rotation is an efficient BMP for reducing nitrate loading from watersheds under intense potato cultivation. The study presents critical information on modeling nitrogen loading by revealing the importance of accurately accounting for organic nitrogen input to the system. While the omission of red clover will remove a relatively large source of fixated nitrogen, the lack of

nitrogen may be compensated for by overestimating plant N uptake in other crops. It was observed that using the default plant parameters, SWAT overpredicted nitrogen uptake in the watershed by up to 86%. Based on these observations, we recommend adjusting the plant parameters to obtain a rough estimation of the annual nitrogen uptake for various crops in the watershed.

5.2 Limitations and future work

In Chapter 2, the assessment of N balance in rotating systems is subject to uncertainties. Applications of organic amendments as nitrogen supply are significantly more complex than mineral fertilizers (Masunga et al. 2016). The uncertainties in predicting soil N supply as influenced by soil organic matter and the plowed-down residues significantly complicate potato field N management. From an economic standpoint, the potato producers would be hesitant to reduce N input since uncertainties associated with soil N supplies may compromise crop yield and quality. Insights into the soil N and potato yield of four cultivars relating to the traditional PBC and alternative PSB rotation systems were obtained from the field experiment from 2014 to 2017. Nutrient dynamics of organic amendments are influenced by various factors, including time, management practices, soil conditions, moisture content, texture, and microbial community. Therefore, long-term and comprehensive studies are also required to evaluate the impacts of rotation and cultivar with respect to varying factors influencing nutrient dynamics. In addition, despite the clear numerical difference between yields of different cultivars, and rotations within each cultivar, the differences were not statistically different. This is likely due to relatively small sample sizes compared to the variation in the dependent variables, suggesting future experiments with more repetitions to approve the results further.

In the absence of environmental tracer measurements to calibrate baseflow separation methods, chapter 3 demonstrated the benefits of using daily correlation with groundwater level as a new metric to evaluate and optimize baseflow separation. However, the evaluative measures and optimization procedure for baseflow separation were attained based on dry periods where measured streamflow is assumed to equal baseflow. Although a strong linear correlation existed between baseflow and groundwater level over the summer, the same linear relationship may not pertain over wet periods. Therefore, the performance of different baseflow separation methods over the periods outside the summer season may not be directly addressed using the currently available data. Obtaining continuous tracer-based baseflow estimations is needed to assess the reliability of the proposed optimization method over the non-growing season and wet periods.

There were several limitations in Chapter 3 when implementing the SWAT model to assess the importance of red clover and soybean as the alternative cover crop.

(1) Separating red clover from pasture in land use data involves uncertainty since it was carried out solely on crop rotation assumptions. To accurately estimate red clover in the watershed, collecting land use data that directly categorize red clover is needed.

(2) The alternative rotation, red clover was replaced with soybean. However, the replacement does not produce the correct potato-soybean-barley sequence since red clover is followed by potato in the conventional potato-barley-red clover rotation. In addition, incorporating multiple land use change scenarios with different percentages of red clover

replacement will be beneficial to provide supportive information for the mitigation strategies.

(3) The SWAT model was calibrated and validated using water quality data, mainly collected over the growing season. Therefore, the calculated statistical measures are primarily influenced by growing season observations. Additional nitrate samples over the non-growing season will be needed to verify further the model's performance in predicting nitrate loading.

(4) In studying nitrate loading, groundwater plays a key role as the single dominant source of transportation. In this study, baseflow estimation was carried out using signal processing theory and only partially used during dry periods. By obtaining reliable baseflow measurements (e.g., environmental tracer methods), the model can be calibrated for baseflow separately using all year-round data.

(5) SWAT incorporates simple conceptual groundwater equations and does not necessarily reflect the actual groundwater processes. Therefore, temporal changes in nitrate load over the study period or projected into the future were not assessed due to the complexity of groundwater nitrate mitigation in PEI (Jiang and Somers 2009; Paradis et al. 2018). Coupling the SWAT model with groundwater flow and nutrient transport models such as MODFLOW and RT3D will be necessary to identify accurate temporal changes in nitrate loading and groundwater nitrate concentration (Bailey et al. 2017; Conan et al. 2003; Galbiati et al. 2006; Narula and Gosain 2013; Wei et al. 2019).

Bibliography

Abbaspour, K.C. 2015. SWAT-CUP: SWAT calibration and uncertainty programs—a user manual, *Eawag: Dübendorf, Switzerland*: 16-70.

Abbaspour, K.C., C. Johnson, and M.T. Van Genuchten. 2004. Estimating uncertain flow and transport parameters using a sequential uncertainty fitting procedure, *Vadose zone journal*, 3: 1340-52.

Akhavan, S., J. Abedi-Koupai, S.-F. Mousavi, M. Afyuni, S.-S. Eslamian, and K.C. Abbaspour. 2010. Application of SWAT model to investigate nitrate leaching in Hamadan–Bahar Watershed, Iran, *Agriculture, ecosystems & environment*, 139: 675-88.

Alberto, A., A. St-Hilaire, S.C. Courtenay, and M.R. Van Den Heuvel. 2016. Monitoring stream sediment loads in response to agriculture in Prince Edward Island, Canada, *Environmental monitoring and assessment*, 188: 1-15.

Arnold, J., P. Allen, R. Muttiah, and G. Bernhardt. 1995. Automated base flow separation and recession analysis techniques, *Groundwater*, 33: 1010-18.

Arnold, J.G., and P.M. Allen. 1999. Automated methods for estimating baseflow and ground water recharge from streamflow records 1, *JAWRA Journal of the American Water Resources Association*, 35: 411-24.

Arnold, J.G., and N. Fohrer. 2005. SWAT2000: current capabilities and research opportunities in applied watershed modelling, *Hydrological Processes: An International Journal*, 19: 563-72.

Arnold, J.G., R. Srinivasan, R.S. Muttiah, and J.R. Williams. 1998. Large area hydrologic modeling and assessment part I: model development 1, *JAWRA Journal of the American Water Resources Association*, 34: 73-89.

Azimi, M.A., Y. Jiang, F.-R. Meng, and K. Liang. 2022. Yield responses of four common potato cultivars to an industry standard and alternative rotation in Atlantic Canada, *American Journal of Potato Research*: 1-11.

Bailey, R., H. Rathjens, K. Bieger, I. Chaubey, and J. Arnold. 2017. SWATMOD-Prep: Graphical user interface for preparing coupled SWAT-MODFLOW simulations, *JAWRA Journal of the American Water Resources Association*, 53: 400-10.

Baker, J.L. 2001. Limitations of improved nitrogen management to reduce nitrate leaching and increase use efficiency, *TheScientificWorldJOURNAL*, 1: 10-16.

Baker, L.A. 1992. Introduction to nonpoint source pollution in the United States and prospects for wetland use, *Ecological Engineering*, 1: 1-26.

Ballard, J., D. Paradis, R. Lefebvre, and M. Savard. 2009. Numerical modeling of the dynamics of multisource nitrate generation and transfer, PEI, Paper 210, GeoHalifax'09. In *62th Canadian Geotechnical Conference and 10th Joint CGS/IAH Conference*.

Bartlett, G.L. 2014. Quantifying the temporal variability of discharge and nitrate loadings for intertidal springs in two Prince Edward Island estuaries. (MScE Thesis, Department of Civil Engineering, University of New Brunswick …).

Beck, H.E., A.I. van Dijk, D.G. Miralles, R.A. De Jeu, L.S. Bruijnzeel, T.R. McVicar, and J. Schellekens. 2013. Global patterns in base flow index and recession based on

streamflow observations from 3394 catchments, *Water Resources Research*, 49: 7843-63.

Bélanger, G., J. Walsh, J. Richards, P. Milburn, and N. Ziadi. 2000. Yield response of two potato culivars to supplemental irrigation and N fertilization in New Brunswick, *American Journal of Potato Research*, 77: 11-21.

Bélanger, G., J. Walsh, J. Richards, P. Milburn, and N. Ziadi. 2001. Predicting nitrogen fertilizer requirements of potatoes in Atlantic Canada with soil nitrate determinations, *Canadian Journal of Soil Science*, 81: 535-44.

Benson, V.S., J.A. VanLeeuwen, J. Sanchez, I.R. Dohoo, and G.H. Somers. 2006. Spatial analysis of land use impact on ground water nitrate concentrations, *Journal of environmental quality*, 35: 421-32.

Brighenti, T.M., N.B. Bonumá, F. Grison, A. de Almeida Mota, M. Kobiyama, and P.L.B. Chaffe. 2019. Two calibration methods for modeling streamflow and suspended sediment with the swat model, *Ecological Engineering*, 127: 103-13.

Bugden, G., Y. Jiang, M. van den Heuvel, H. Vandermeulen, K. MacQuarrie, C. Crane, and B. Raymond. 2014. Nitrogen loading criteria for estuaries in Prince Edward Island. (Fisheries and Oceans Canada= Pêches et océans Canada).

Cartwright, I., B. Gilfedder, and H. Hofmann. 2014. Contrasts between estimates of baseflow help discern multiple sources of water contributing to rivers, *Hydrology and Earth System Sciences*, 18: 15-30.

Cartwright, I., and M.P. Miller. 2021. Temporal and spatial variations in river specific conductivity: Implications for understanding sources of river water and hydrograph separations, *Journal of Hydrology*, 593: 125895.

Cartwright, I., and U. Morgenstern. 2018. Using tritium and other geochemical tracers to address the “old water paradox” in headwater catchments, *Journal of Hydrology*, 563: 13-21.

Chapman, T. 1999. A comparison of algorithms for stream flow recession and baseflow separation, *Hydrological Processes*, 13: 701-14.

Chapman, T.G. 1991. Comment on “Evaluation of automated techniques for base flow and recession analyses” by RJ Nathan and TA McMahon, *Water Resources Research*, 27: 1783-84.

Conan, C., F. Bouraoui, N. Turpin, G. de Marsily, and G. Bidoglio. 2003. Modeling flow and nitrate fate at catchment scale in Brittany (France), *Journal of environmental quality*, 32: 2026-32.

Danielescu, S., and K.T. MacQuarrie. 2011. Nitrogen loadings to two small estuaries, Prince Edward Island, Canada: a 2-year investigation of precipitation, surface water and groundwater contributions, *Hydrological Processes*, 25: 945-57.

Danielescu, S., and K.T. MacQuarrie. 2013. Nitrogen and oxygen isotopes in nitrate in the groundwater and surface water discharge from two rural catchments: implications for nitrogen loading to coastal waters, *Biogeochemistry*, 115: 111-27.

De Notaris, C., J. Rasmussen, P. Sørensen, and J.E. Olesen. 2018. Nitrogen leaching: A crop rotation perspective on the effect of N surplus, field management and use of catch crops, *Agriculture, ecosystems & environment*, 255: 1-11.

Devito, K., A. Hill, and N. Roulet. 1996. Groundwater-surface water interactions in headwater forested wetlands of the Canadian Shield, *Journal of Hydrology*, 181: 127-47.

Duncan, H.P. 2019. Baseflow separation–A practical approach, *Journal of Hydrology*, 575: 308-13.

Dunn, A., G. Julien, W. Ernst, A. Cook, K. Doe, and P. Jackman. 2011. Evaluation of buffer zone effectiveness in mitigating the risks associated with agricultural runoff in Prince Edward Island, *Science of the Total Environment*, 409: 868-82.

Eckhardt, K. 2005. How to construct recursive digital filters for baseflow separation, *Hydrological Processes: An International Journal*, 19: 507-15.

Eckhardt, K. 2008. A comparison of baseflow indices, which were calculated with seven different baseflow separation methods, *Journal of Hydrology*, 352: 168-73.

Eckhardt, K. 2012. Analytical sensitivity analysis of a two parameter recursive digital baseflow separation filter, *Hydrology and Earth System Sciences*, 16: 451-55.

Edwards, L., J.R. Burney, M. Brimacombe, and A.H. MacRae. 2008. Potato Land Use and Nitrate Runoff Characteristics of Two Subcatchments of the Wilmot River Watershed, Prince Edward Island (PEI), Canada, *Water Quality Research Journal*, 43: 121-28.

El-Khoury, A., O. Seidou, D. Lapen, Z. Que, M. Mohammadian, M. Sunohara, and D. Bahram. 2015. Combined impacts of future climate and land use changes on discharge, nitrogen and phosphorus loads for a Canadian river basin, *Journal of environmental management*, 151: 76-86.

Environment-Canada. 2011. Water quality status and trends of nutrients in major drainage areas in Canada. Technical Summary.

FitzHugh, T.W., and D. Mackay. 2000. Impacts of input parameter spatial aggregation on an agricultural nonpoint source pollution model, *Journal of Hydrology*, 236: 35-53.

Francis, R.M. 1989. Hydrogeology of the Winter River Basin-Prince Edward Island. (Water Resources Branch, Department of the Island, Prince Edward Island).

Furey, P.R., and V.K. Gupta. 2001. A physically based filter for separating base flow from streamflow time series, *Water Resources Research*, 37: 2709-22.

Galbiati, L., F. Bouraoui, F. Elorza, and G. Bidoglio. 2006. Modeling diffuse pollution loading into a Mediterranean lagoon: development and application of an integrated surface–subsurface model tool, *Ecological Modelling*, 193: 4-18.

Gassman, P.W., M.R. Reyes, C.H. Green, and J.G. Arnold. 2007. The soil and water assessment tool: historical development, applications, and future research directions, *Transactions of the ASABE*, 50: 1211-50.

Giri, S., A.P. Nejadhashemi, and S.A. Woznicki. 2016. Regulators' and stakeholders' perspectives in a framework for bioenergy development, *Land Use Policy*, 59: 143-53.

Giri, S., and Z. Qiu. 2016. Understanding the relationship of land uses and water quality in twenty first century: a review, *Journal of environmental management*, 173: 41-48.

Goolsby, D.A., and W.A. Battaglin. 2001. Long-term changes in concentrations and flux of nitrogen in the Mississippi River Basin, USA, *Hydrological Processes*, 15: 1209-26.

Graszkiewicz, Z., R. Murphy, P. Hill, and R. Nathan. 2011. Review of techniques for estimating the contribution of baseflow to flood hydrographs. In *Proceedings of the 34th World Congress of the International Association for HydroEnvironment Research and Engineering: 33rd Hydrology and Water Resources Symposium and 10th Conference on Hydraulics in Water Engineering. Engineers Australia*, 138.

Green, P.A., C.J. Vörösmarty, M. Meybeck, J.N. Galloway, B.J. Peterson, and E.W. Boyer. 2004. Pre-industrial and contemporary fluxes of nitrogen through rivers: a global assessment based on typology, *Biogeochemistry*, 68: 71-105.

Grizard, P. 2013. 'Modeling nitrate loading from watersheds to coastal waters of the Northumberland Strait', University of New Brunswick.

Grizard, P., K.T. MacQuarrie, and Y. Jiang. 2020. Land-use based modeling approach for determining freshwater nitrate loadings from small agricultural watersheds, *Water Quality Research Journal*, 55: 278-94.

Gupta, H.V., S. Sorooshian, and P.O. Yapo. 1998. Toward improved calibration of hydrologic models: Multiple and noncommensurable measures of information, *Water Resources Research*, 34: 751-63.

Gupta, H.V., S. Sorooshian, and P.O. Yapo. 1999. Status of automatic calibration for hydrologic models: Comparison with multilevel expert calibration, *Journal of Hydrologic Engineering*, 4: 135-43.

Guzmán, P., O. Batelaan, M. Huysmans, and G. Wyseure. 2015. Comparative analysis of baseflow characteristics of two Andean catchments, Ecuador, *Hydrological Processes*, 29: 3051-64.

Haas, M.B., B. Guse, and N. Fohrer. 2017. Assessing the impacts of Best Management Practices on nitrate pollution in an agricultural dominated lowland catchment considering environmental protection versus economic development, *Journal of environmental management*, 196: 347-64.

Hagedorn, B. 2020. Hydrograph separation through multi objective optimization: Revealing the importance of a temporally and spatially constrained baseflow solute source, *Journal of Hydrology*, 590: 125349.

Howcroft, W., I. Cartwright, and D.I. Cendón. 2019. Residence times of bank storage and return flows and the influence on river water chemistry in the upper Barwon River, Australia, *Applied Geochemistry*, 101: 31-41.

Hua, B., J. Yang, F. Liu, G. Zhu, B. Deng, and J. Mao. 2018. Characterization of dissolved organic matter/nitrogen by fluorescence excitation-emission matrix spectroscopy and X-ray photoelectron spectroscopy for watershed management, *Chemosphere*, 201: 708-15.

Huyck, A.A., V.R. Pauwels, and N.E. Verhoest. 2005. A base flow separation algorithm based on the linearized Boussinesq equation for complex hillslopes, *Water Resources Research*, 41.

Jabbar, F.K., and K. Grote. 2019. Statistical assessment of nonpoint source pollution in agricultural watersheds in the Lower Grand River watershed, MO, USA, *Environmental Science and Pollution Research*, 26: 1487-506.

Jackson, W., L. Asmussen, E. Hauser, and A. White. 1973. Nitrate in surface and subsurface flow from a small agricultural watershed. In.: Wiley Online Library.

Jemison Jr, J.M., and R.H. Fox. 1994. Nitrate leaching from nitrogen-fertilized and manured corn measured with zero-tension pan lysimeters. In.: Wiley Online Library.

Jha, M.K., K. Schilling, P.W. Gassman, and C. Wolter. 2010. Targeting land-use change for nitrate-nitrogen load reductions in an agricultural watershed, *Journal of soil and water conservation*, 65: 342-52.

Jiang, Y., P. Nishimura, M.R. van den Heuvel, K.T. MacQuarrie, C.S. Crane, Z. Xing, B.G. Raymond, and B.L. Thompson. 2015. Modeling land-based nitrogen loads from groundwater-dominated agricultural watersheds to estuaries to inform nutrient reduction planning, *Journal of Hydrology*, 529: 213-30.

Jiang, Y., J. Nyiraneza, M. Khakbazan, X. Geng, and B.J. Murray. 2019. Nitrate leaching and potato yield under varying plow timing and nitrogen rate, *Agrosystems, Geosciences & Environment*, 2: 1-14.

Jiang, Y., J. Nyiraneza, B. Murray, S. Chapman, A. Malenica, and B. Parker. 2017. Vadose zone processes delay groundwater nitrate reduction response to BMP implementation as observed in paired cultivated vs. uncultivated potato rotation fields, *Journal of Hydrology*, 555: 760-76.

Jiang, Y., M. Ramsay, F. Meng, and T. Stetson. 2021. Characterizing potato yield responses to water supply in Atlantic Canada's humid climate using historical yield and weather data: Implications for supplemental irrigation, *Agricultural Water Management*, 255: 107047.

Jiang, Y., and G. Somers. 2009. Modeling effects of nitrate from non-point sources on groundwater quality in an agricultural watershed in Prince Edward Island, Canada, *Hydrogeology Journal*, 17: 707-24.

Jiang, Y., and G. Somers. 2011. Watershed evaluation of beneficial management practices (WEBs) in the Souris River Watershed, Prince Edward Island: Site hydrogeology.

In *Proceedings of Joint Conference of the Canadian Quaternary Association (CANQUA)*. Canadian Chapter of the International Association of Hydrogeologists Quebec City.

Jiang, Y., G. Somers, and J. Mutch. 2004. Application of numerical modeling to groundwater assessment and management in Prince Edward Island.

Jiang, Y., B. Zebarth, and J. Love. 2011. Long-term simulations of nitrate leaching from potato production systems in Prince Edward Island, Canada, *Nutrient Cycling in Agroecosystems*, 91: 307-25.

Kang, S., H. Lin, W.J. Gburek, G.J. Folmar, and B. Lowery. 2008. Baseflow nitrate in relation to stream order and agricultural land use, *Journal of environmental quality*, 37: 808-16.

Khan, F., T. Husain, and A. Lumb. 2003. Water quality evaluation and trend analysis in selected watersheds of the Atlantic region of Canada, *Environmental monitoring and assessment*, 88: 221-48.

Krause, P., D.P. Boyle, and F. Bäse. 2005. Comparison of different efficiency criteria for hydrological model assessment, *Advances in geosciences*, 5: 89-97.

Ladson, A.R., R. Brown, B. Neal, and R. Nathan. 2013. A standard approach to baseflow separation using the Lyne and Hollick filter, *Australasian Journal of Water Resources*, 17: 25-34.

Lamb, K.J., K.T. MacQuarrie, K.E. Butler, S. Danielescu, E. Mott, M. Grimmet, and B.J. Zebarth. 2019. Hydrogeophysical monitoring reveals primarily vertical movement of an applied tracer across a shallow, sloping low-permeability till interface: Implications for agricultural nitrate transport, *Journal of Hydrology*, 573: 616-30.

Lee, S., A.M. Sadeghi, I.-Y. Yeo, G.W. McCarty, and W.D. Hively. 2017. Assessing the impacts of future climate conditions on the effectiveness of winter cover crops in reducing nitrate loads into the Chesapeake Bay watersheds using the SWAT model, *Transactions of the ASABE*, 60: 1939-55.

Leon, L., E. Soulis, N. Kouwen, and G. Farquhar. 2001. Nonpoint source pollution: a distributed water quality modeling approach, *Water Research*, 35: 997-1007.

Li, L., H.R. Maier, D. Partington, M.F. Lambert, and C.T. Simmons. 2014. Performance assessment and improvement of recursive digital baseflow filters for catchments with different physical characteristics and hydrological inputs, *Environmental Modelling & Software*, 54: 39-52.

Liang, K. 2020. 'Enhancing understanding of BMP effectiveness and land use change impacts on water quality, water quantity, and potato production in Atlantic Canada', University of New Brunswick.

Liang, K., Y. Jiang, J. Nyiraneza, K. Fuller, D. Murnaghan, and F.-R. Meng. 2019. Nitrogen dynamics and leaching potential under conventional and alternative potato rotations in Atlantic Canada, *Field Crops Research*, 242: 107603.

Liang, K., Y. Jiang, J. Qi, K. Fuller, J. Nyiraneza, and F.-R. Meng. 2020. Characterizing the impacts of land use on nitrate load and water yield in an agricultural watershed in Atlantic Canada, *Science of the Total Environment*, 729: 138793.

Liao, S.L., M. Savard, G. Somers, D. Paradis, and Y. Jiang. 2005. Preliminary results from water-isotope characterization of groundwater, surface water, and precipitation in the Wilmot River watershed, Prince Edward Island. (Natural Resources Canada, Geological Survey of Canada).

Lin, K., S. Guo, W. Zhang, and P. Liu. 2007. A new baseflow separation method based on analytical solutions of the Horton infiltration capacity curve, *Hydrological Processes: An International Journal*, 21: 1719-36.

Logan, T., D. Eckert, and D. Beak. 1994. Tillage, crop and climatic effects of runoff and tile drainage losses of nitrate and four herbicides, *Soil and Tillage Research*, 30: 75-103.

Lott, D.A., and M.T. Stewart. 2016. Base flow separation: A comparison of analytical and mass balance methods, *Journal of Hydrology*, 535: 525-33.

Lyne, V., and M. Hollick. 1979. Stochastic time-variable rainfall-runoff modelling. In *Institute of Engineers Australia National Conference*, 89-93. Institute of Engineers Australia Barton, Australia.

Lyu, H., C. Xia, J. Zhang, and B. Li. 2020. Key challenges facing the application of the conductivity mass balance method: a case study of the Mississippi River basin, *Hydrology and Earth System Sciences*, 24: 6075-90.

Masunga, R.H., V.N. Uzokwe, P.D. Mlay, I. Odeh, A. Singh, D. Buchan, and S. De Neve. 2016. Nitrogen mineralization dynamics of different valuable organic amendments commonly used in agriculture, *Applied Soil Ecology*, 101: 185-93.

Mau, D.P., and T.C. Winter. 1997. Estimating ground-water recharge from streamflow hydrographs for a small mountain watershed in a temperate humid climate, New Hampshire, USA, *Groundwater*, 35: 291-304.

McCallum, J.L., P.G. Cook, P. Brunner, and D. Berhane. 2010. Solute dynamics during bank storage flows and implications for chemical base flow separation, *Water Resources Research*, 46.

Moriasi, D.N., J.G. Arnold, M.W. Van Liew, R.L. Bingner, R.D. Harmel, and T.L. Veith. 2007. Model evaluation guidelines for systematic quantification of accuracy in watershed simulations, *Transactions of the ASABE*, 50: 885-900.

Müller, K., M. Deurer, H. Hartmann, M. Bach, M. Spiteller, and H.-G. Frede. 2003. Hydrological characterisation of pesticide loads using hydrograph separation at different scales in a German catchment, *Journal of Hydrology*, 273: 1-17.

Myrbeck, Å. 2014. Soil tillage influences on soil mineral nitrogen and nitrate leaching in Swedish arable soils.

Narula, K.K., and A. Gosain. 2013. Modeling hydrology, groundwater recharge and non-point nitrate loadings in the Himalayan Upper Yamuna basin, *Science of the Total Environment*, 468: S102-S16.

Nathan, R.J., and T.A. McMahon. 1990. Evaluation of automated techniques for base flow and recession analyses, *Water Resources Research*, 26: 1465-73.

Nejadhashemi, A.P., A. Shirmohammadi, and H.J. Montas. 2003. Evaluation of streamflow partitioning methods. In *2003 ASAE Annual Meeting*, 1. American Society of Agricultural and Biological Engineers.

Neter, J., M.H. Kutner, C.J. Nachtsheim, and W. Wasserman. 1996. Applied linear statistical models.

Noori, N., L. Kalin, and S. Isik. 2020. Water quality prediction using SWAT-ANN coupled approach, *Journal of Hydrology*, 590: 125220.

Nyiraneza, J., R.D. Peters, V.A. Rodd, M.G. Grimmett, and Y. Jiang. 2015. Improving productivity of managed potato cropping systems in Eastern Canada: crop rotation and nitrogen source effects, *Agronomy Journal*, 107: 1447-57.

Nyiraneza, J., N. Ziadi, B.J. Zebarth, M. Sharifi, D.L. Burton, C.F. Drury, S. Bittman, and C.A. Grant. 2012. Prediction of soil nitrogen supply in corn production using soil chemical and biological indices, *Soil Science Society of America Journal*, 76: 925-35.

Ojala, J., J. Stark, and G. Kleinkopf. 1990. Influence of irrigation and nitrogen management on potato yield and quality, *American potato journal*, 67: 29-43.

Ouyang, W., X. Hao, L. Wang, Y. Xu, M. Tysklind, X. Gao, and C. Lin. 2019. Watershed diffuse pollution dynamics and response to land development assessment with riverine sediments, *Science of the Total Environment*, 659: 283-92.

Pai, N., and D. Saraswat. 2011. SWAT2009_LUC: A tool to activate the land use change module in SWAT 2009, *Transactions of the ASABE*, 54: 1649-58.

Paradis, D., J.-M. Ballard, R. Lefebvre, and M.M. Savard. 2018. Multi-scale nitrate transport in a sandstone aquifer system under intensive agriculture, *Hydrogeology Journal*, 26: 511-31.

Paradis, D., J. Ballard, M. Savard, R. Lefebvre, Y. Jiang, G. Somers, S. Liao, and C. Rivard. 2006. Impact of agricultural activities on nitrates in ground and surface water in the Wilmot Watershed, PEI, Canada. In *59th Canadian Geotechnical Conference and the 7th joint CGS/IAH-CNC Conference, Vancouver*, 1-4.

Paradis, D., H. Vigneault, R. Lefebvre, M.M. Savard, J.-M. Ballard, and B. Qian. 2016. Groundwater nitrate concentration evolution under climate change and agricultural adaptation scenarios: Prince Edward Island, Canada, *Earth System Dynamics*, 7: 183-202.

Pellerin, B.A., B.A. Bergamaschi, R.J. Gilliom, C.G. Crawford, J. Saraceno, C.P. Frederick, B.D. Downing, and J.C. Murphy. 2014. Mississippi River nitrate loads from high frequency sensor measurements and regression-based load estimation, *Environmental Science & Technology*, 48: 12612-19.

Peralta, J.M.a., and C.O. Stockle. 2002. Dynamics of nitrate leaching under irrigated potato rotation in Washington State: a long-term simulation study, *Agriculture, ecosystems & environment*, 88: 23-34.

Piggott, A.R., S. Moin, and C. Southam. 2005. A revised approach to the UKIH method for the calculation of baseflow/Une approche améliorée de la méthode de l'UKIH pour le calcul de l'écoulement de base, *Hydrological sciences journal*, 50.

Prunty, L., and R. Greenland. 1997. Nitrate leaching using two potato-corn N-fertilizer plans on sandy soil, *Agriculture, ecosystems & environment*, 65: 1-13.

Pushpalatha, R., C. Perrin, N. Le Moine, and V. Andréassian. 2012. A review of efficiency criteria suitable for evaluating low-flow simulations, *Journal of Hydrology*, 420: 171-82.

Qi, J., S. Li, C.P.-A. Bourque, Z. Xing, and F.-R. Meng. 2018. Developing a decision support tool for assessing land use change and BMPs in ungauged watersheds based on decision rules provided by SWAT simulation, *Hydrology and Earth System Sciences*, 22: 3789-806.

Rammal, M., P. Archambeau, S. Erpicum, P. Orban, S. Brouyère, M. Pirotton, and B. Dewals. 2018. An Operational Implementation of Recursive Digital Filter for Base Flow Separation, *Water Resources Research*, 54: 8528-40.

Ramos, C. 1996. 'Effect of agricultural practices on the nitrogen losses to the environment.' in, *Fertilizers and environment* (Springer).

Raymond, B.G., C.S. Crane, and D.K. Cairns. 2002. Nutrient and chlorophyll trends in Prince Edward Island estuaries, *Can. Tech. Rep. Fish. Aquat. Sci./Rapp. Tech. Can. Sci. Halieut. Aquat.*: 142-53.

Roloson, S.D., M.R. Coffin, K.M. Knysh, and M.R. van den Heuvel. 2021. Movement of non-native rainbow trout in an estuary with periodic summer hypoxia, *Hydrobiologia*, 848: 4001-16.

Romanelli, A., D.X. Soto, I. Matiatos, D.E. Martínez, and S. Esquius. 2020. A biological and nitrate isotopic assessment framework to understand eutrophication in aquatic ecosystems, *Science of the Total Environment*, 715: 136909.

Rutledge, A.T. 1998. Computer programs for describing the recession of ground-water discharge and for estimating mean ground-water recharge and discharge from streamflow records: Update. (US Department of the Interior, US Geological Survey).

Saraiva Okello, A.M.L., S. Uhlenbrook, G.P. Jewitt, I. Masih, E.S. Riddell, and P. Van der Zaag. 2018. Hydrograph separation using tracers and digital filters to quantify runoff components in a semi-arid mesoscale catchment, *Hydrological Processes*, 32: 1334-50.

Savard, M.M., D. Paradis, G. Somers, S. Liao, and E. van Bochove. 2007. Winter nitrification contributes to excess NO3− in groundwater of an agricultural region: A dual-isotope study, *Water Resources Research*, 43.

Savard, M.M., G. Somers, A. Smirnoff, D. Paradis, E. van Bochove, and S. Liao. 2010. Nitrate isotopes unveil distinct seasonal N-sources and the critical role of crop residues in groundwater contamination, *Journal of Hydrology*, 381: 134-41.

Schein, A., S.C. Courtenay, C.S. Crane, K.L. Teather, and M.R. van den Heuvel. 2012. The role of submerged aquatic vegetation in structuring the nearshore fish community within an estuary of the southern Gulf of St. Lawrence, *Estuaries and Coasts*, 35: 799-810.

Schilling, K., and Y.-K. Zhang. 2004. Baseflow contribution to nitrate-nitrogen export from a large, agricultural watershed, USA, *Journal of Hydrology*, 295: 305-16.

Schilling, K.E., and D.S. Lutz. 2004. RELATION OF NITRATE CONCENTRATIONS TO BASEFLOW IN THE RACCOON RIVER, IOWA 1, *JAWRA Journal of the American Water Resources Association*, 40: 889-900.

Schwartz, S.S. 2007. Automated Algorithms for Heuristic Base-Flow Separation 1, *JAWRA Journal of the American Water Resources Association*, 43: 1583-94.

Sharifi, M., B.J. Zebarth, D.L. Burton, C.A. Grant, G.A. Porter, J.M. Cooper, Y. Leclerc, G. Moreau, and W.J. Arsenault. 2007. Evaluation of laboratory-based measures of soil mineral nitrogen and potentially mineralizable nitrogen as predictors of field-based indices of soil nitrogen supply in potato production, *Plant and Soil*, 301: 203-14.

Sith, R., A. Watanabe, T. Nakamura, T. Yamamoto, and K. Nadaoka. 2019. Assessment of water quality and evaluation of best management practices in a small agricultural watershed adjacent to Coral Reef area in Japan, *Agricultural Water Management*, 213: 659-73.

Sloto, R.A., and M.Y. Crouse. 1996. HYSEP: A computer program for streamflow hydrograph separation and analysis, *Water-resources investigations report*, 96: 4040.

Smakhtin, V.U. 2001. Low flow hydrology: a review, *Journal of Hydrology*, 240: 147-86.

Somers, G., M.M. Savard, and D. Paradis. 2007. Mass balance calculations to estimate nitrate proportions from various sources in the agricultural Wilmot watershed of Prince Edward Island. In *The 60th Canadian Geotechnical Conference and 8th Joint GCS/IAH-CNC Groundwater Conference, Ottawa*, 112-18.

Stewart, M., J. Cimino, and M. Ross. 2007. Calibration of base flow separation methods with streamflow conductivity, *Groundwater*, 45: 17-27.

Sujono, J., S. Shikasho, and K. Hiramatsu. 2004. A comparison of techniques for hydrograph recession analysis, *Hydrological Processes*, 18: 403-13.

Tallaksen, L. 1995. A review of baseflow recession analysis, *Journal of Hydrology*, 165: 349-70.

Tan, S.B., E.Y.-M. Lo, E.B. Shuy, L.H. Chua, and W.H. Lim. 2009. Hydrograph separation and development of empirical relationships using single-parameter digital filters, *Journal of Hydrologic Engineering*, 14: 271-79.

Torstensson, G., H. Aronsson, and L. Bergström. 2006. Nutrient use efficiencies and leaching of organic and conventional cropping systems in Sweden, *Agronomy Journal*, 98: 603-15.

Ullrich, A., and M. Volk. 2009. Application of the Soil and Water Assessment Tool (SWAT) to predict the impact of alternative management practices on water quality and quantity, *Agricultural Water Management*, 96: 1207-17.

Van de Poll, H. 1981. Report on the geology of Prince Edward Island, *PEI Department of Tourism, Industry and Energy, Charlottetown, PEI, Canada*.

Villarini, G., C.S. Jones, and K.E. Schilling. 2016. Soybean area and baseflow driving nitrate in Iowa's Raccoon River, *Journal of environmental quality*, 45: 1949-59.

Vörösmarty, C.J., P.B. McIntyre, M.O. Gessner, D. Dudgeon, A. Prusevich, P. Green, S. Glidden, S.E. Bunn, C.A. Sullivan, and C.R. Liermann. 2010. Global threats to human water security and river biodiversity, *Nature*, 467: 555-61.

Vos, J., C. Van Loon, and G. Bollen. 2012. Effects of Crop Rotation on Potato Production in the Temperate Zones: Proceedings of the International Conference on Effects of Crop Rotation on Potato Production in the Temperate Zones, held August 14–19, 1988, Wageningen, The Netherlands. (Springer Science & Business Media).

Voutchkova, D.D., S.N. Miller, and K.G. Gerow. 2019. Parameter sensitivity of automated baseflow separation for snowmelt-dominated watersheds and new filtering procedure for determining end of snowmelt period, *Hydrological Processes*, 33: 876-88.

Wade, A., C. Neal, P. Whitehead, and N. Flynn. 2005. Modelling nitrogen fluxes from the land to the coastal zone in European systems: a perspective from the INCA project, *Journal of Hydrology*, 304: 413-29.

Wang, C., R. Jiang, L. Boithias, S. Sauvage, J.-M. Sánchez-Pérez, X. Mao, Y. Han, A. Hayakawa, K. Kuramochi, and R. Hatano. 2016. Assessing potassium environmental losses from a dairy farming watershed with the modified SWAT model, *Agricultural Water Management*, 175: 91-104.

Wang, Q., R. Liu, C. Men, L. Guo, and Y. Miao. 2018. Effects of dynamic land use inputs on improvement of SWAT model performance and uncertainty analysis of outputs, *Journal of Hydrology*, 563: 874-86.

Ward, M.H., T.M. DeKok, P. Levallois, J. Brender, G. Gulis, B.T. Nolan, and J. VanDerslice. 2005. Workgroup report: drinking-water nitrate and health—recent findings and research needs, *Environmental health perspectives*, 113: 1607-14.

Wei, X., R.T. Bailey, R.M. Records, T.C. Wible, and M. Arabi. 2019. Comprehensive simulation of nitrate transport in coupled surface-subsurface hydrologic systems using the linked SWAT-MODFLOW-RT3D model, *Environmental Modelling & Software*, 122: 104242.

Werner, A.D., M.R. Gallagher, and S.W. Weeks. 2006. Regional-scale, fully coupled modelling of stream–aquifer interaction in a tropical catchment, *Journal of Hydrology*, 328: 497-510.

Whitaker, A.C., S.N. Chapasa, C. Sagras, U. Theogene, R. Veremu, and H. Sugiyama. 2022. Estimation of baseflow recession constant and regression of low flow indices in eastern Japan, *Hydrological sciences journal*, 67: 191-204.

White, K.L., and I. Chaubey. 2005. Sensitivity analysis, calibration, and validations for a multisite and multivariable SWAT model 1, *JAWRA Journal of the American Water Resources Association*, 41: 1077-89.

Xiang, C., Y. Wang, and H. Liu. 2017. A scientometrics review on nonpoint source pollution research, *Ecological Engineering*, 99: 400-08.

Xie, J., X. Liu, K. Wang, T. Yang, K. Liang, and C. Liu. 2020. Evaluation of typical methods for baseflow separation in the contiguous United States, *Journal of Hydrology*, 583: 124628.

Yang, X., Q. Liu, G. Fu, Y. He, X. Luo, and Z. Zheng. 2016. Spatiotemporal patterns and source attribution of nitrogen load in a river basin with complex pollution sources, *Water Research*, 94: 187-99.

Yu, Z., and F.W. Schwartz. 1999. Automated calibration applied to watershed-scale flow simulations, *Hydrological Processes*, 13: 191-209.

Zebarth, B., C. Drury, N. Tremblay, and A. Cambouris. 2009. Opportunities for improved fertilizer nitrogen management in production of arable crops in eastern Canada: A review, *Canadian Journal of Soil Science*, 89: 113-32.

Zebarth, B., and C. Rosen. 2007. Research perspective on nitrogen BMP development for potato, *American Journal of Potato Research*, 84: 3-18.

Zebarth, B., G. Tai, R.d. Tarn, H. De Jong, and P. Milburn. 2004. Nitrogen use efficiency characteristics of commercial potato cultivars, *Canadian Journal of Plant Science*, 84: 589-98.

Zebarth, B.J., S. Danielescu, J. Nyiraneza, M.C. Ryan, Y. Jiang, M. Grimmett, and D.L. Burton. 2015. Controls on nitrate loading and implications for BMPs under intensive potato production systems in Prince Edward Island, Canada, *Groundwater Monitoring & Remediation*, 35: 30-42.

Zhang, J., Y. Zhang, J. Song, and L. Cheng. 2017. Evaluating relative merits of four baseflow separation methods in Eastern Australia, *Journal of Hydrology*, 549: 252-63.

Zhang, R., Q. Li, T.L. Chow, S. Li, and S. Danielescu. 2013. Baseflow separation in a small watershed in New Brunswick, Canada, using a recursive digital filter calibrated with the conductivity mass balance method, *Hydrological Processes*, 27: 2659-65.

Zhang, X., X. Liu, M. Zhang, R.A. Dahlgren, and M. Eitzel. 2010. A review of vegetated buffers and a meta-analysis of their mitigation efficacy in reducing nonpoint source pollution, *Journal of environmental quality*, 39: 76-84.

Curriculum Vitae

Candidate's Full Name: Mohammad Amir Azimi

M.Sc. in Environmental Management, University of New Brunswick, Canada (2020-2023)

B.Sc. in Water Engineering, Razi University of Kermanshah, Iran (2012-2016)

Publications:

1. Azimi, M.A., Y. Jiang, F.-R. Meng, and K. Liang. 2022. Yield responses of four common potato cultivars to an industry standard and alternative rotation in Atlantic Canada, American Journal of Potato Research: 1-11.
2. Azimi, M.A., M.J. Manshti, A.G. Motahari, A. Karami, and K. Roshtami. 2015. Determining Hourly Evaporation Measurement Accuracy of Small Pans in Comparison with Class-A Pan, Asian Journal of Applied Sciences, 3.